

**DESIGNING A BIOREACTOR FOR  
REGENERATING HIGH ASPECT RATIO TISSUES**

By

**MAMATHA DEVARAPALLI**

Masters of Science in Chemical Engineering

Oklahoma State University

Stillwater, Oklahoma

2008

Submitted to the Faculty of the  
Graduate College of the  
Oklahoma State University  
in partial fulfillment of  
the requirements for  
the Degree of  
**MASTER OF SCIENCE**  
December, 2008

**DESIGNING A BIOREACTOR FOR  
REGENERATING HIGH ASPECT RATIO TISSUES**

Thesis Approved:

Dr. Sundararajan V. Madihally

---

Thesis Adviser

Dr. Heather Fahlenkamp

---

Dr. Gary L. Foutch

---

Dr. A. Gordon Emslie

---

Dean of the Graduate College

## **ACKNOWLEDGMENTS**

I would like to express my gratitude to all those who gave me the possibility to complete this thesis. I want to thank my advisor Dr. Sundararajan V. Madihally, Edward E. Bartlett Chair and Former Head of the department Dr. R. Russell Rhinehart, Amoco Chair and the current head of the department Dr. Khaled A.M. Gasem for giving me the opportunity to convert from non thesis to thesis student and do this research work.

I am deeply indebted to my advisor Dr. Sundararajan V. Madihally whose help, stimulating suggestions and encouragement not only helped me in carrying this research working successfully but also helped me in writing this thesis. I would also like to thank my thesis committee members Dr. Heather Fahlenkamp and Dr. Gary L. Foutch for their valuable suggestions while writing this thesis.

I want to thank my former colleagues Dr. Benjamine J. Lawrence for his help, support and valuable hints.

Lastly, and most importantly, I wish to thank my parents, Venkata Rao and Shiva Parvathi for their love and support which encouraged me to do my best in all matters of life. To them I dedicate this thesis.

## TABLE OF CONTENTS

Chapter	Page
I. INTRODUCTION.....	1
1.1 Need for Tissue Engineering .....	1
1.2 Importance of Bioreactor Design.....	3
1.3 Objectives .....	5
II. REVIEW OF LITERATURE.....	8
2.1 Tissue Engineering.....	8
2.2 Porous Templates.....	9
2.3 Bioreactors for Tissue Engineering .....	13
2.4 CFD Modeling .....	19
III. FLOW DYNAMICS IN CIRCULAR BIOREACTORS CONTAINING TISSUE ENGINEERING SCAFFOLDS.....	23
3.1 Introduction.....	23
3.2 Materials and Methods.....	24
3.2.1 Sources of Material .....	24
3.2.2 Obtaining RTD function using CFD.....	24
3.2.3 Obtaining RTD function from experimental set up .....	27
3.2.4 Preparation of porous structure.....	29
3.2.5 Simulation including the porous structure .....	30
3.3 Results.....	32
3.3.1 Steady State profile in the reactor without porous structure.....	32
3.3.2 Transient profile in reactor without porous structure .....	32
3.3.3 RTD without porous structure .....	33
3.3.4 Effect of porous structure on flow distribution.....	36
3.3.5 Effect of changing pore sizes of the porous structure on the pressure drop and shear stress .....	38
3.3.6 Effect of changing porosity of the porous structure on the pressure drop and shear stresses.....	42
3.4 Discussion.....	43

<b>Chapter</b>	<b>Page</b>
IV. OPTIMIZATION OF BIOREACTOR FOR TISSUE ENGINEERING: NUTRIENT CONSUMPTIONS .....	47
4.1 Introduction.....	47
4.2 Materials and Methods.....	50
4.2.1 Reactor Designs .....	50
4.2.2 Simulating fluid flow in the porous structure .....	53
4.2.3 Simulating reaction in the porous region of the reactor.....	53
4.2.4 Determination of Michaelis-Menten parameters from literature .....	55
4.3 Results.....	56
4.3.1 Effect of inlet and outlet shape on pressure drop and shear stress.....	56
4.3.2 Effect of flow rate on pressure drop and shear stress .....	60
4.3.3 Effect of permeability on pressure drop and shear stress .....	62
4.3.4 Steady State concentration profile of nutrients.....	64
4.3.5 Influence of RTD on Oxygen consumption for SMCs .....	66
4.3.6 Effect of varying cell density on Oxygen consumption.....	70
4.4 Discussion .....	71
V. CONCLUSION AND RECOMMENDATIONS.....	76
5.1 Conclusions.....	76
5.2 Recommendations.....	78
REFERENCES .....	81
APPENDICES .....	87
A.    CFX Manual.....	87
B.    Determination of RTD for circular reactor using CFX simulations (Sample calculations).....	98
C.    COMSOL Manual.....	109

## LIST OF TABLES

Table	Page
1. Effect of pore size and pore number on pressure drop and shear stress .....	39
2. Effect of reduced pore size with constant pore number on pressure drop and shear stress .....	42
3. Kinetic parameters for different cell types.....	55
4. Pressure drop and shear stress within the reaction simulations at a variety of different flow rates 85 $\mu\text{m}$ , 120 pores/ $\text{mm}^2$ and 154 $\mu\text{m}^2$ .....	61
5. Pressure drop and shear stress within the reaction simulation for decreasing pore size in circular reactor at 0.1ml/min .....	63
6. Effect of cell density on pressure drop, shear stress and outlet oxygen concentration at 85 $\mu\text{m}$ , 120 pores/ $\text{mm}^2$ and 154 $\mu\text{m}^2$ .....	71

## LIST OF FIGURES

Figure	Page
1. In-vitro Tissue Engineering .....	9
2. Petri Dish for tissue culture.....	14
3. Stirred tank reactor.....	16
4. Slow turning lateral vessel .....	17
5. High aspect ratio vessel .....	17
6. Parallel plate reactor .....	18
7. Schematic of reactor designs utilized in the study showing major dimensions in millimeters.....	25
8. Reactor set up used in experimentation .....	28
9. Chitosan porous structure pictures.....	30
10. Steady State Streamline profile and contour plots in different reactors simulated with flow rate of 20 mL/min.....	34
11. Concentration profiles at reactor outlet for different times at 20ml/min	35
12. RTD of tracer at 156 mL/min and 20mL/min	36
13. Effect of flow rate and porous structure on the RTD of tracer .....	37
14. Effect of pore size and pore number on pressure drop and maximum shear stress.....	40
15. Shear stress distribution with the porous structure for the case with 85 $\mu\text{m}$ , 120 pores/ $\text{mm}^2$ .....	41
16. Schematics of the reactor designs .....	52
17. Pressure distribution across the cross section in all the six designs .....	58
18. Shear Stress distribution across the cross section in all the six designs .....	59
19. Oxygen concentration profile across the circular reactor for different cell types and at different flow rates .....	65
20. Glucose concentration profile across the circular reactor for different cell types and at different flow rates.....	66
21. Comparison of oxygen outlet concentration and shear stress distribution in Design 1 and Design 6 .....	68
22. Effect of cell density on Oxygen consumption.....	71

# **CHAPTER I**

## **INTRODUCTION**

### **1.1 NEED FOR TISSUE ENGINEERING**

According to the United Network Organ Sharing (UNOS) the number of patients waiting for organ transplantation in the United States was around 40,000 in 1998 and this number raised to nearly 100,000 in 2008. However, the number of donors has not increased in these years and is only 8000 in 2008. Hence the patients in need of organ transplantation are increasing steadily when compared to the number of organ donors present, which is the fundamental reason for increased interest in the field of tissue engineering. Tissue engineering gives the hope of regenerating needed tissues by using biomaterials that are biodegradable.

Tissue engineering is an interdisciplinary subject which deals with improving the patient care by replacing the damaged part of organs/tissues with regenerated tissue, using concepts from life sciences and engineering. There are many requirements that a biomaterial need to satisfy in order to be used as a scaffold for the cells to grow on them (Freyman T 2001), unlike traditional prosthetic devices. Prosthesis is a technique in which the damaged part (say a part of the limb, hand or bone) in the body is replaced with a biocompatible material which does not support the cell growth but does the functionality of that particular part (Kannan et al. 2005). Whereas, in tissue engineering the tissue is regenerated using a biodegradable material in the form of a scaffold.

Scaffolds are prepared in the shape that the tissue to be regenerated and replaced (Lisa Christenson 1997). Scaffolds are generated from biomaterials that promote cell adhesion and cell growth, in addition to being biocompatible, non-toxic and strong enough to support the cells until the cells produce their own extra cellular matrix (ECM)(Lawrence and Madihally 2008).

Many natural and synthetic polymers, like chitosan, polycaprolactone (PCL), poly lactic-co-glycolic acid (PLGA), gelatin are used in generating tissue engineering scaffolds. Small intestinal submucosa(SIS) is a natural matrix that was and is being used successfully in regenerating the tissue for bladder implants. However, the reproducibility and repeatability of the results from natural matrices is of major concern as the properties of the natural matrix vary depending on the location, age and gender of the animal. Hence, there is a growing interest in developing new matrices that are obtained from synthetic polymers. There have been significant research and development in polymer processing technology for the past few decades (Hayashi 1994; Raghunath et al. 2007; Sarasam et al. 2006). Blending synthetic and natural polymers has been an approach to develop new biomaterials with wide range of physicochemical properties and biological interactions. There are many scaffolding techniques developed to improve the quality of the materials used for tissue engineering purposes (Blan and Birla 2008; Bonfield 2006; Freed et al. 1994; Salerno et al. 2007).

Two types of tissue engineering techniques, “unseeded” and “seeded” are investigated for their effectiveness in tissue regeneration. The unseeded technique involves the direct implementation of a biodegradable scaffold into the human body encouraging the natural process of regeneration to occur. The optimum environmental

conditions such as temperature, pH, and sufficient amount of nutrients required for the cells to grow are maintained inside the body. In contrast, there are many tissues that need to be grown *in vitro* first and then transplanted to replace the damaged part in the patient's body. Seeded techniques utilize *in vitro* seeding of cells from the tissue to be developed on to porous matrices, establishing cell-composite grafts that are implanted *in vivo*. In this case, the cells are to be grown in a system where the nutrients supply is replenished and the optimum conditions are maintained similar to the way that they are maintained in the human body. Since a significant number of cells are required to colonize a three dimensional porous structures, bioreactors are used to provide a continuous supply of essential nutrients (i.e., amino acids, glucose, oxygen) and regulate the pH and temperature as the cell seeded matrix matures.

## **1.2 IMPORTANCE OF BIOREACTOR DESIGN**

Bioreactors of different configurations and flow systems have been widely utilized for regenerating tissues *in vitro*. Bioreactors help in maintaining the specific conditions like pH, temperature and allows for replenishment of the nutrients (Martin and Vermette 2005). For growing tissues like skin and bladder, the tissues need to be regenerated on scaffolds with a high aspect ratio where the surface area is significantly high compared to the thickness. Fluid flow is also utilized as a way to introduce hydrodynamic stresses on to cells. Some cells change their structure and composition to meet the functional demands by responding to the mechanical stresses (Chen et al. 1999; Gray et al. 1988; Jeong et al. 2005). A popular bioreactor configuration involves growing cell seeded constructs in microgravity (Marolt et al. 2006). However, for

growing large aspect ratio tissues, microgravity reactor would deform the structure due to bending and rolling while tumbling through the growth medium, creating a random stress pattern within the developing material. Hence, microgravity reactors may not be suitable for regenerating thin cross-sectional tissues. Among all the reactors that are currently being studied the parallel plate construct (Lawrence et al. 2008; Lawrence BJ 2008) has the following advantages over the other systems:

- (a) gives good support to the scaffold
- (b) prevents deformation of the scaffold
- (c) shear induced by the fluid flow
- (d) continuous flow replenishes the nutrients

Unlike the traditional rectangular reactor (Huang et al. 2005a; Macario et al. 2007), a circular reactor has curvature effects which reduce the dead spaces at the edges when the rectangular reactor is scaled up. Therefore, it is more practical to use a circular reactor for growing large tissues clinically.

Flow and nutrient consumption patterns within bioreactors containing large porous structures with high aspect ratios have not been studied. Channeling and dead zones are the two main factors for the non-ideal fluid distribution conditions within a bioreactor when it is scaled up. Channeling would not allow the fluid to disperse within the reactor and the dead zones would end up with low supply of nutrients and hence damaging the tissue in that region. Sometime dead zone can lead to necrosis. Non-uniform flow patterns lead to (i) poor distribution of nutrients and (ii) non-uniform shear stress distribution. These factors affect cellular colonization and the assembly of ECM elements, which affects the quality of regenerated tissues. Thus, in a scaled up system,

the residence time distribution studies play a major role in reactor design for tissue engineering purposes. Further, tissue regeneration is a dynamic process where the porous characteristics change due to proliferation of cells, *de novo* deposition of matrix components, and degradation of the porous architecture. These changes affect the transport characteristics. There is a lack of understanding on the influence of these factors.

### **1.3 OBJECTIVES**

This study utilized a circular parallel plate reactor and evaluated the design requirements for regenerating tissues with high aspect ratio. Further, the effects of changing porous characteristics during tissue regeneration attributed to *de novo* synthesis of matrix elements and cell colonization were also evaluated. The two main objectives of this study are:

***Specific aim 1: Characterize the flow dynamics of a circular bioreactor containing porous structures.***

The non-ideal fluid distribution is characterized using the residence time distribution (RTD). The RTD measures the amount of time different molecules present in the fluid spend within the reactor, allowing for consumption by the cellular components. Understanding these characteristics is important in designing the reactor shape and optimizing the location of the inlets and outlets. The RTD analysis was done using Solid Works simulation software CFX 11 (ANSYS Inc, Canonsburg, PA.) and/or Comsol Multiphysics 3.4 (COMSOL, Inc., Burlington, MA), the flow dynamics of the

system was analyzed by considering that the Brinkman equation holds good in the porous region and the Navier-Stokes equation holds in the non porous region. The steady state results were used for the initial values and a tracer fluid was applied as a step input to understand fluid distribution. The simulation produced a RTD that was validated using bioreactors fabricated in-house from polycarbonates. RTDs were obtained experimentally by introducing a red food dye as a step change into the reactor containing porous structures. The simulations and experiments had similar concentration and RTD profiles, showing that methodology is a valid approach to analyze flow properties in the reactor systems. In this study, apart from the pressure, shear stress distribution throughout the reactor with the porous structure in COMSOL Multiphysics 3.4 was also analyzed.

***Specific aim 2: Understand the consumption patterns in the bioreactor; the relationship between residence time distribution and the consumption patterns***

The RTD analysis is independent of the metabolic reactions, although the total consumption of nutrients is determined by the residence time. To understand the nutrient distribution with consumption, simulations were performed by incorporating the reaction systems in COMSOL Multiphysics along with the Brinkman equation. Metabolic consumption for both oxygen and glucose was included using a Michaelis-Menten kinetic rate law derived from literature for three different cell types namely chondrocytes, smooth muscle cells and hepatocytes to understand the effect of cell type on the nutrients flow rate requirements for the cells to grow. Based on the shear stress profiles, first reactor was reconfigured to place the inlets and outlets away from the porous structure.

Initially the reactor shape, inlet and outlet positions were optimized. Later on, it was found from the shear stress distribution analysis and residence time distribution analysis that the shear stresses were higher at the inlet and outlet. To avoid high shear stresses within the porous region, the inlet and outlet were moved away from the porous region. Six different circular reactors with extended inlets and outlets of different shape were designed. The simulations were done in AnSYS 11.0 without the porous structure. The pressure, shear stress distribution was analyzed in six designs and one was chosen as the best design for further analysis in COMSOL3.4. The modified design with improved extensions had better shear stress distribution in the absence of porous structure. Further, the comparison of the outlet oxygen concentration and the minimum oxygen concentration indicated that the modified design has better nutrient distribution compared to the design where the inlet and outlet are on the porous structure.

## CHAPTER II

### REVIEW OF LITERATURE

#### 2.1 TISSUE ENGINEERING

The field of Tissue Engineering provides the promise of generating functionally replaceable tissue parts. The technology is based on using biodegradable scaffolds as a guide and support for the in-growth of cells during tissue regeneration. The two principal techniques being used in Tissue Engineering for repairing the damaged organ/tissue are

- (i) tissue regeneration *in situ* and
- (ii) implantation of tissues grown on the scaffolds *in vitro*

The first technique involves use of a scaffold *in situ* to regenerate the tissue. This approach has been used in the regeneration of supporting tissues such as cartilage. In the second technique the tissue regeneration process takes place *in vitro* prior to implantation (**Figure 2.1**). The tissue regenerated *in vitro* should have good mechanical properties, should not create any host tissue reaction due to immunogenicity and the scaffold used should degrade completely prior to the transplantation. Unlike in the *in vivo* transplantation of the disintegrated cells and the scaffolds, the *in vitro* process gives a chance to engineer the tissue before the transplantation thus, allowing improvement of the cell grafting and survival.

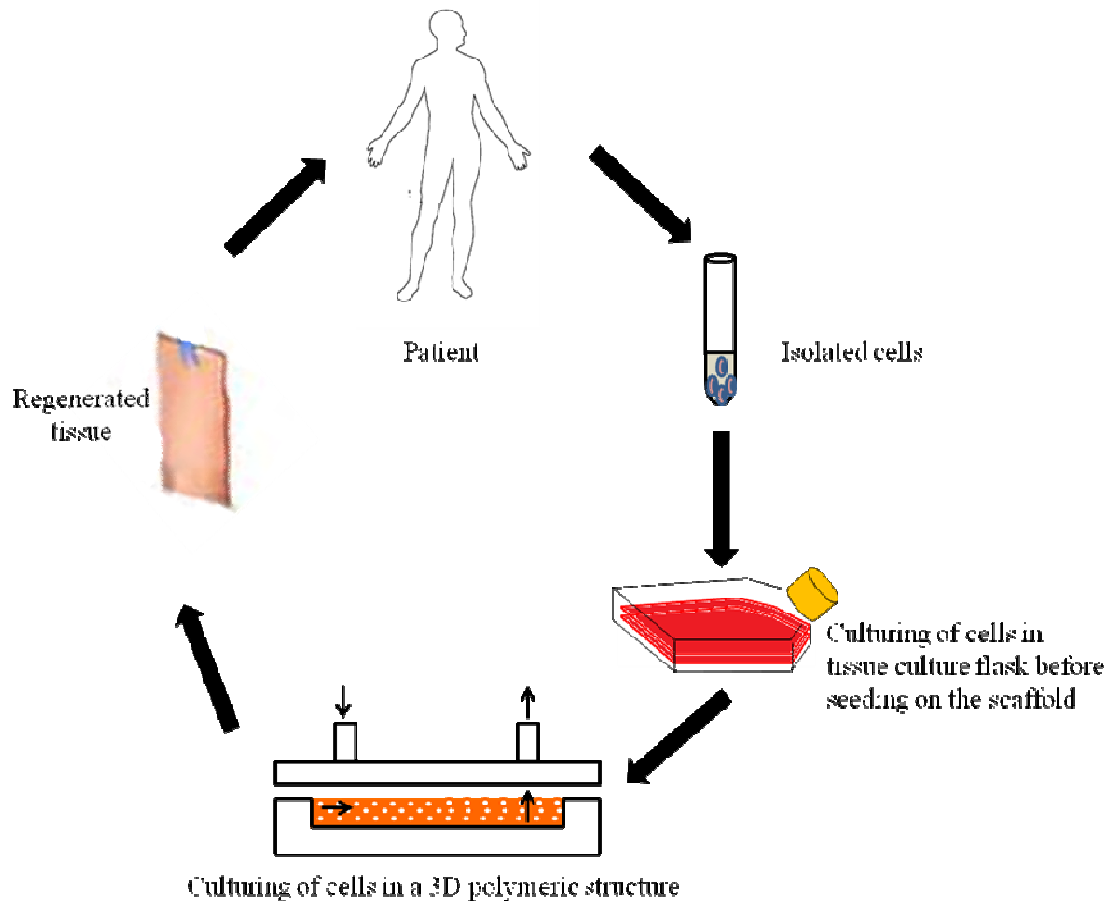


**Figure 2.1:** *In vitro* Tissue Engineering

## 2.2 POROUS TEMPLATES

A tissue in reality is composed of different cells arranged in an orderly manner. When they are disengaged and grown to form large structures, the cells need a support system which gives temporary mechanical support and degrades once the tissue is regenerated (Lisa Christenson 1997). Porous templates made of biomaterials that are degradable and promote cell growth are utilized as a support system (Chandy and Sharma 1990; Hayashi 1994). These are also called as scaffolds.

Some of the natural and synthetic polymers being used as scaffolds are chitosan, polycaprolactone (PCL), poly lactic-co-glycolic acid (PLGA), and gelatin. These are either used independently or mixed together to form a composite that serves the purpose of growing a specific tissue. Chitosan is a natural polymer derived from chitin, the primary structural polymer obtained mainly from exoskeletons of shrimp and crab shells. It is a relatively an inexpensive natural polymer that is widely used in the biomedical industry for different purposes such as wound healing and drug delivery systems (Olteanu and Enescu 2007; Prabakaran 2008). In this project, chitosan was used as a scaffold, since, the fabrication techniques of the chitosan scaffolds are well developed in the laboratory.

***Fabrication of porous structure:*** Advances have been made in synthesizing porous structures from various polymers. Gas foaming, fiber extrusion and bonding, three-dimensional printing, phase separation, emulsion freeze-drying, porogen leaching and electro spinning are some of the methods used in preparation of a scaffold (Blan and Birla 2008; Hollister 2006; Raghunath et al. 2007; Salerno et al. 2007). Although each technique has advantages and disadvantages, controlled rate freezing and lyophilization technique (CRFLT) is the method of choice while forming porous structures from natural polymers such as chitosan and collagen, which dissolve in acidic water. CRFLT generates open pore structures, suitable for guiding cell in-growth. CRFLT is carried out at low temperatures and avoids the concern associated with the loss of biological activity of proteins due to thermal denaturation. CRFLT is a method used in this study as the chitosan scaffold fabricated by using these techniques have been extensively studied in the laboratory (Huang et al. 2005a; Madihally and Matthew 1999; Tillman et al. 2006b).

In controlled rate freezing, a polymer solution is used to generate a scaffold. The solution is then cooled below the melting point of the solvent which is subsequently removed leaving the polymer with interconnected pores. For example, the Chitosan solution is prepared in acidic water and is frozen in a refrigerator maintained at -80 °C for 4 – 5 h or until the solution is completely frozen. Then the sample is freeze dried in a lyophilizer. The direction in which the chitosan fibers align depends on the direction in which the heat transfer takes place. If there is a uniform cooling from all the directions then the scaffold obtained would be having uniform pores. The alignment of the pores would be in the direction from which the cooling of the sample takes place. The water molecules in between the polymeric fibers get vaporized resulting in pores, and providing a porous structure.

To regenerate a tissue that is practically useful in the surgical purposes for implantation it is necessary to provide a three dimensional environment that replicates the normal physiological conditions observed in the body (Bonfield 2006). Thus, it is important to understand the 3D characteristics of the porous material. Many *in vitro* experiments have shown that cells respond differently in attachment, morphology, migration, and proliferation on 3D scaffolds unlike traditional 2D tissue culture. Some of these that affect the cell colonization in 3D environment was recently reviewed by Madihally *et al* (Lawrence and Madihally 2008).

**Porosity:** High porosity supports cell growth. The higher the porosity the higher is the supply of the nutrients. Porosity also plays an important role in cell adhesion and migration as high porosity helps in providing large surface area for the cellular

interaction and extra cellular regeneration (Freed et al. 1994; Ishaug-Riley et al. 1998; Marois et al. 1999).

**Pore size:** Pore size affects the cell binding, morphology and cell growth. The pore size depends on the way the biomaterial is processed into a scaffold. Appropriate pore size helps in spreading the cells uniformly. Small pore size may hinder the supply of the nutrients and on the other hand reducing the pore size improves the extra cellular matrix retention (Grad et al. 2004; S Grad 2004). Thus, it is necessary to have an optimal pore size that supports the cell growth. The optimal pore size that promotes cell growth for majority of the cell types such as hepatocytes found in liver, smooth muscle cells present in various tissues, and chondrocytes present in cartilage is around 50 - 150 $\mu$ m(Yannas et al. 1989). As the cells grow the pore size decreases (Griffon et al. 2006; Thomson et al. 1995).

**Topography:** Topography is the surface characteristics of the scaffold and dictates the type of cell adhesion, migration, growth and spreading which further influences the cell behavior. Surface roughness increases the cell migration area. Smooth muscle cells and chondrocytes showed improved adhesion and growth when the roughness of the polymer scaffold is increased. In a study (Sarasam and Madihally 2005; Sarasam et al. 2006) when Polycaprolactone (PCL) and chitosan are blended, the antibacterial properties of the material were minimized but the surface roughness of the composite scaffold increased. Thus, allowing the fibroblasts to proliferate and spread in a much better way than before.

**Mechanotransduction:** Many parts of the body are exposed to stresses either due to the weight they carry (such as bone), the function they perform (such as bladder and

cartilage) or due to the flow of fluid (lung and blood vessels). Thus, it is important to grow the cells outside the body by exposing them to the same conditions that they are exposed to within the body. Mechanotransduction is the term used for the responses that cells generate to mechanical stresses during the tissue regeneration process. The two ways in which stresses can be applied on the cells are hydrodynamic and mechanical. The hydrodynamic stresses are due to the fluid flow in the system and mechanical stresses are due to the external forces applied on the scaffold. The *in vitro* studies indicate that the flow through the scaffold would dictate the micro structural shear stresses and the shear stresses initiate signal transduction cascades that lead to altered gene expression profiles (Chen et al. 1999; Gray et al. 1988; Huang et al. 2005a; Jeong et al. 2005; Papadaki et al. 1999). For example, some cell types like endothelial cells present in the lumen of blood vessels, and chondrocytes align themselves in the direction of the flow when cultured in flow through systems (Gray et al. 1988; Huang et al. 2005a; Takahashi and Berk 1996). The presence of flow within the system in which the cells are grown on the scaffold also affects the production of extracellular matrix elements (ECMs). Apart from the bulk stresses due to fluid flow the cells even experience the stresses due to some material resistance to movement during migration and adhesion.

### **2.3 BIOREACTORS IN TISSUE ENGINEERING:**

Bioreactors are widely utilized in tissue engineering as a way to distribute nutrients within the biodegradable porous structures and to provide physical forces required by the developing tissue (Gooch et al. 2001; Gray et al. 1988; Huang et al. 2005a; Martin and Vermette 2005). Bioreactors are described as systems in which the

biological processes of growing cells takes place under closely monitored operating conditions like temperature, pressure, pH, and nutrient supply (Jaasma et al. 2008). The efficient supply of nutrients along with mechanical stresses that support the cellular proliferation and differentiation on a 3D scaffold is an important step towards the development of functional grafts that replace the damaged part or tissue of the body (Butler et al. 2000). The requirements for 3D culture of cells are much different from that on a monolayer or 2D cultures (Cukierman et al. 2001). Thus there is a need for development of models to understand these nutrients and other physiochemical requirements.

Traditionally, cells are cultured in petri dishes (**Figure 2.2**) with a certain amount of medium containing necessary factors. In a petri dish, cells get attached to the bottom of the plastic and the nutrient supply was maintained by replenishing the medium in a timely fashion (Martin and Vermette 2005). This static cell culture is limited by the number of cells that can be grown with extra cellular matrix formation at the center of the construct (Botchwey et al. 2003; Goldstein et al. 2001; Phillips et al. 2006). It was



**Figure 2.2:** Petri Dish for tissue culture

observed that the thickness of the tissue grown was around 0.5mm for bone tissue and 0.18mm for cardiac tissue, which was not comparable with the thickness of the actual tissue. Hence, there was a need for further improvements.

Controlled flow systems such as spinner flasks, rotary vessels, and flow-through perfusion systems are being used to increase the proliferation for different cell types (Hoerstrup et al. 2000; Lichtenberg et al. 2005). Cells respond to hydrodynamic stress by remodeling their surrounding extracellular matrix elements and change the tissue composition to meet the functional demands. Some of the bioreactors utilized in tissue engineering are discussed below in brief:

***Stirred tank reactor:*** The stirred tank reactor is similar to the regular continuous stirred tank reactor (CSTR) seen in any chemical industry (Martin and Vermette 2005). The scaffold along with the cells seeded on it, is suspended in the medium (**Figure 2.3**) and the medium is rotated with the help of a magnetic stirrer. There was a poor balance between the increasing mass transfer and the shear stress which is to be maintained at optimum levels because of which there was tissue damage and the thickness of the tissue grown was around 0.3mm. There was not much improvement in the quality of the tissue generated from this stirred tank reactor.

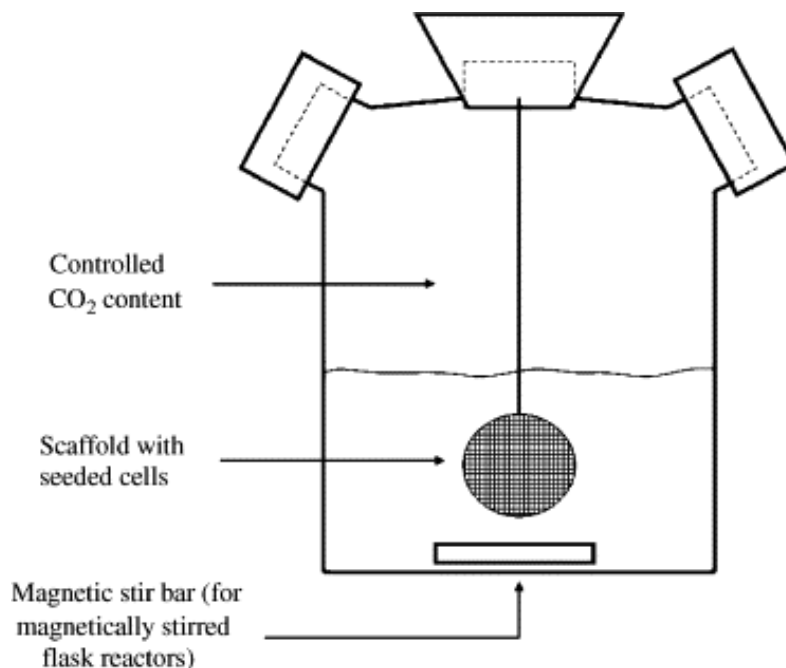


**Figure 2.3:** Stirred tank reactor (Courtesy: Martin Y, Vermette P. 2005. Bioreactors for tissue mass culture: Design, characterization, and recent advances. *Biomaterials* 26(35):7481-7503)

*Slow turning lateral vessel (STLV):* The stirred tank reactor was further modified to a slow turning lateral vessel in which two concentric cylinders (**Figure 2.4**) were rotated independent of each other (Martin and Vermette 2005). The continuous flow loop allows the replenishment of the nutrients and the gas exchange is provided by the inner concentric cylinder. The cells are seeded on micro carrier beads which attach together to form larger tissues. Though the tissue thickness reported in this case is much higher than the other two cases, the tissue grown was not of uniform thickness, the tissue was thick at the edges and thinner at the center. This kind of a problem encountered while generating a tissue is called as necrosis.

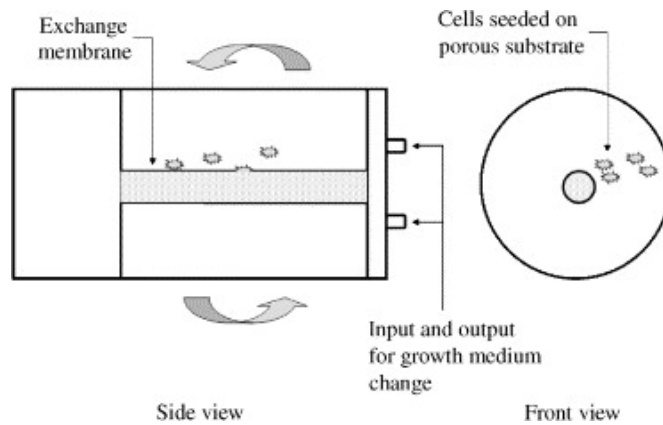


**Figure 2.4:** Slow turning lateral vessel reactor. (Courtesy: Martin Y, Vermette P. 2005. Bioreactors for tissue mass culture: Design, characterization, and recent advances. Biomaterials. 26(35):7481-7503).

**High aspect ratio vessel (HARV):** The high aspect ratio vessel reactor is similar to slow turning lateral vessel reactor (Figure 2.5) except for the fact that the length and the speed of the reactor has been reduced (Martin and Vermette 2005). The speed has been reduced to 12-15rpm unlike in a slow turning lateral vessel where the speed was around 15-30rpm. The disadvantage of this reactor is that as the tissue grows the terminal velocity increases and the tissue starts hitting the bottom thus hindering the supply of the nutrients.

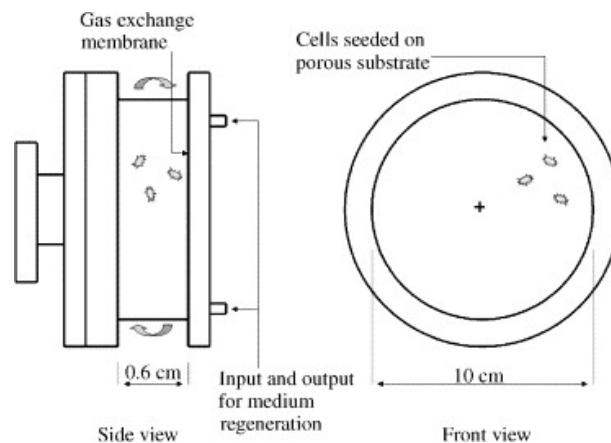


**Figure 2.5:** High aspect ratio vessel (Courtesy: Martin Y, Vermette P. 2005. Bioreactors for tissue mass culture: Design, characterization, and recent advances. Biomaterials. 26(35):7481-7503)

**Parallel plate reactors:** One of the ways to increase the diffusion of the nutrients through the scaffold is by using a flow-through perfusion (**Figure 2.6**) bioreactor system.

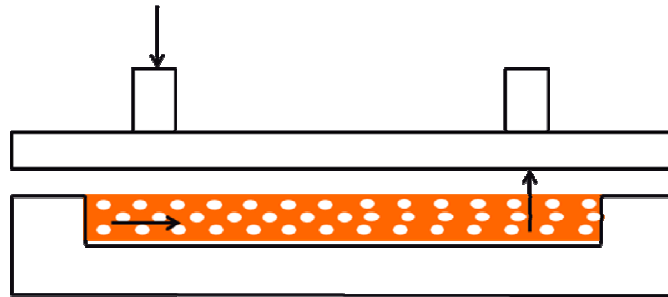


**Figure 2.6:** Parallel plate reactor

Parallel plate bioreactors have been used for growing and maintaining of primary cell for cellular therapy purposes of different cell types (Koller et al. 1993; Palsson et al. 1993). Apart from improving the diffusion of the nutrients and replenishing the medium, the flow-through bioreactor stimulates mechanical stresses induced due to the nutrient flow which improves the proliferation, attachment and activity of some of the cell types (Botchwey et al. 2003; Goldstein et al. 2001; Jeong et al. 2005; Phillips et al. 2006; Sikavitsas et al. 2003; Sikavitsas et al. 2005). Flow rate through the scaffold micro architecture dictates the local shear stresses experienced by the cells. While the scaffold is subjected to the bulk forces supplied by the tissue and fluid flow, the cells experience the micromechanical properties of the individual fibers and local shear stresses within the porous structure.

Using bioreactors, an improvement in the quality of the regenerated tissue is observed in some studies (Niklason et al. 1999). However, other studies show deterioration in the quality of the tissue (Heydarkhan-Hagvall et al. 2006). Flow of growth medium improves nutrient and waste transport, but alterations in the synthesis of matrix elements induced by shear stresses could deteriorate the tissues (Gooch et al.

2001). Additionally, shear stress affects the scaffold architecture as well as cellular alignment within the structures (Gray et al. 1988; Huang et al. 2005a).

## **2.4 CFD MODELING:**

Computational fluid dynamics (CFD) is a tool used in many areas of chemical engineering and biomedical engineering to simulate flows of gases and liquids, heat and mass transfer, moving bodies, multiphase physics, and chemical reactions. To better understand the effect of fluid flow in bioreactors, a number of studies have been performed using CFD (Brown A 2007; Brown and Meenan 2007; Cioffi et al. 2006; Hutmacher and Singh 2008; Porter et al. 2005a; Porter B 2005; Sander and Nauman 2003; Sander EA 2003; Williams et al. 2002). Some analysis has been carried out on how the shear stresses affect the cellular activity and growth, but these studies depended on two dimensional fluid flow and the mass transfer related to the fluid flow was described in a two dimensional mathematical model. Palsson *et al* studied the effect of bioreactor geometry on the fluid flow and on the concentration distribution utilizing the Navier Stokes equations (Palsson 1996). However, this study did not account for the presence of a porous structure within the flow domain. Hence, findings from these studies are only useful in conditions where no porous structures are present. In other studies (Chung et al. 2007), porosity based permeability was used to understand the fluid dynamics in a perfusion system. However, the porosity could change either by decrease in number of pores or by decrease in the pore diameter. Hence, it may not reflect the true regeneration.

In majority of these studies small scale cylindrical scaffolds were utilized, which focus on only the wall shear stresses (Bilgen B 2007; Williams KA 2002) and the flow characteristics were analyzed using either Darcy's or Navier Stokes equation (Capuani et al. 2003). These studies assess the flow patterns and shear stresses either within the bioreactor or around the porous construct. Some studies do not account for porosity or transport through the scaffold (Timmins et al. 2007; Williams et al. 2002). Flow characteristics are analyzed using either Darcy's equation (Boschetti et al. 2006), or the Brinkman equation which is considered as an extension of Darcy's equation (Chung et al. 2007). The Brinkman equation accounts for both viscous and drag forces in the porous medium and reduces to either the Navier-Stokes equation or Darcy's law if either force becomes dominant (Capuani et al. 2003). Brinkman equation is the only fluid flow equation that accounts for both the viscous and drag forces in the porous medium and reduces to either Navier's or Darcy's equation when one of the forces become dominant. In our study, to mimic the tissue regeneration process, we used Brinkman equation to study the flow dynamics within the porous structure and calculated the permeability based on the pore size keeping the number of pores constant. However, porous characteristics change during tissue regeneration, i.e., permeability of the matrix decreases due to decreased pore size. Further, many tissues (for example cartilage and bladder) have a high aspect ratio (large surface area relative to the thickness of the matrix).

The perfusion systems described above hold scaffold of desirable thickness for implantation (~ 2 mm thick) but the surface area is very small; because of which the flow is across the thickness rather than across the cross section of the scaffold. However,

tissues such as skin and bladder have larger surface area compared to the thickness of the reactor. Thus, the surface areas to the thickness ratio are high for these tissues and hence, are called as high aspect ratio tissues. Ultimately a parallel plate reactor with high aspect ratio is to be used in order to grow these large tissues. To overcome the disadvantages mentioned earlier in the traditional reactors for growing tissues like skin, and bladder that have high aspect ratio, a bioreactor that can grow tissues as large as 10 cm in diameter and 2 mm thick was designed. One of the ways to understand the fluid flow in a reactor system is by performing residence time distribution (RTD) studies.

***Residence time distribution:*** The amount of time spent by different molecules in the reactor is called as residence time (Fogler 2006a; Fogler 2006b). The non-ideal distribution of the fluid is characterized by using the residence time distribution. Channeling and dead zones within the reactor would lead to non ideal flow patterns. The non ideal flow patterns would restrict the uniform distribution of the nutrients and the shear stresses throughout the reactor. This may lead to the non uniform growth of tissue. Thus, understanding of the residence time distribution is needed in order to optimize the reactor shape, inlet and outlet. The residence time distribution characteristics of the bioreactor are studied by giving a sudden step input of a tracer that has properties similar to water. Step input is a sudden change given to a system under steady state. The component which is suddenly introduced affects the output of the system and requires some time to reach a steady output. The RTD studies were overlooked in reactors designed for tissue engineering scaffolds because of two main reasons:

- (a) small scale reactor design in which RTD was not significant

(b) The cell growth was along the thickness rather than along the length of the scaffold

**Concentration profile:** The amount of nutrients (oxygen and glucose) consumed by a particular cell type and the residence time distribution of the nutrient are interconnected. The fluid flow analysis along with the concentration distribution of the nutrients is analyzed in our study using computational softwares like CFX 11 and Comsol Multiphysics 3.4.

Initially the RTD studies were done without the porous structure and then fluid flow was analyzed with the porous structure to understand the effect of 3D porous structure on the fluid flow. Once, the fluid dynamics of the system was understood the convection diffusion term was incorporated into the simulations to understand the nutrient consumption patterns of different cell types. Apart from analyzing the system using simulation software the results were validated by running some RTD experiments. The experiments proved that the presence of porous structure would increase the channeling within the system thus not allowing the nutrients to get completely consumed.

In the present study, the concepts of RTD and law of conservation of mass were successfully used to understand the flow system and design a bioreactor that serves the purpose of growing tissues of high aspect ratio. As said earlier, shear stresses do affect the cell proliferation and growth. Hence, the shear stress within the porous structure was analyzed and its affect on the tissue growth was minimized by moving the high stress regions away from the porous structure.

## **CHAPTER III**

# **FLOW DYNAMICS IN CIRCULAR BIOREACTORS CONTAINING TISSUE ENGINEERING SCAFFOLDS**

### **3.1. INTRODUCTION**

Flow within bioreactors containing large porous structures with high aspect ratios has not been studied. In these scale-up systems, non-ideal fluid distribution conditions could arise from two possible factors: channeling, and dead zones. When channeling is present, some of the fluid leaves the reactor immediately without dispersing within the reactor. Dead zones reduce the effective volume of the reactor and prolong the residence time of some of the fluid elements. Non-uniform flow patterns lead to i) poor distribution of nutrients and ii) non-uniform shear stress distribution. These factors affect cellular colonization and the assembly of extracellular matrix elements which affect the quality of regenerated tissues. Hence, one has to understand the fluid distribution and the effect of shape of the reactor.

The non-ideal fluid distribution is characterized using the residence time distribution (RTD). The RTD measures the amount of time different molecules present in the fluid spend within the reactor (Fogler 2006b; Lawrence et al. 2004). In other words, RTD is a measure of dispersal of a molecule in a flowing medium owing to the combined action of a velocity profile and molecular diffusion. Understanding these

characteristics is important in designing the reactor shape and optimizing the location of the inlets and outlets.

From the fundamentals of reactor design, it is known that reactor shapes with sharp corners are potential dead zones and an approach to minimize dead zones is avoiding shapes with sharp corners. Hence, this study utilized a circular parallel plate reactor that allows large tissue scaffolds (~10 cm diameter). The circular reactor was studied to understand the effect of inlet and outlet location on fluid flow distribution with and without the porous structure. The reactor with three different inlet and outlet conditions was simulated using CFD packages CFX 11 (ANSYS Inc, Canonsburg, PA.) and/or Comsol Multiphysics 3.4 (COMSOL, Inc., Burlington, MA) to understand the effect of variation in the inlet and outlet positions and experiments were performed to validate the simulation results. These results show significant increase in pressure drop when the porous characteristics are modified.

## **3.2. MATERIALS & METHODS**

### **3.2.1. Sources of Materials**

Chitosan with >310 kDa MW and 85% degree of deacetylation, and glacial acetic acid were obtained from Sigma Aldrich Chemical Co (St. Louis, MO). Ethanol (200 proof) was obtained from Aaper Alcohol and Chemical Company (Shelbyville, KY). All other reagents were purchased from Fisher Scientific (Waltham, MA).

### **3.2.2. Obtaining RTD function using CFD**

Circular reactor of 10 cm diameter and 0.2 cm high, with a 0.6 cm inlet and outlet

diameter were used. The three inlet and outlet configurations (**Figure 3.1**) were chosen to understand the effect of inlet and outlet locations and design on flow patterns.

*Case 1:* with inlet at the center and outlet at the periphery on the opposite side.

*Case 2:* with inlet and outlet at the periphery and outlet on the periphery, but on the opposite sides.

*Case 3:* was similar to case 2 except both the inlet and outlet were on the same side.

These reactor geometries were created using a CAD package (Solidworks™ or ANSYS Workbench 11). The CFX mesh was then created using ANSYS CAD2Mesh software. A critical challenge was overcoming problems associated with the aspect ratio i.e., very large surface area relative to the thickness of the channel. To ensure at least 10 nodes over the thickness of the reactor, the maximum element size of 0.2 mm was chosen. A detail description of designing the reactors in CFX is given in **Appendix A**

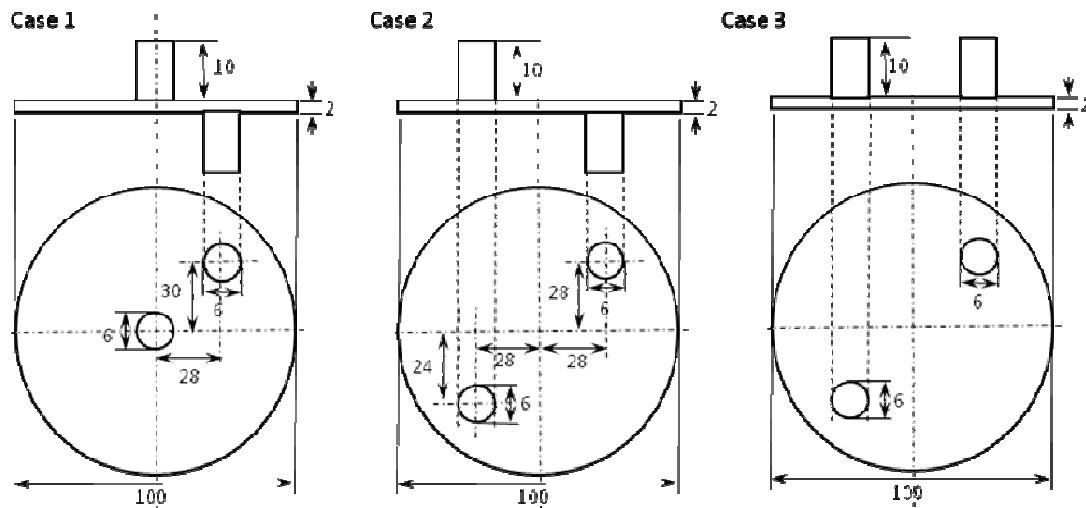


**Figure 3.1.** Schematic of reactor designs utilized in this study showing major dimensions in millimeters.

Preliminary simulations used a water mass flowrate that corresponded to the

average wall shear stress present in human blood vessels, 2.6 g/s (156 mL/min) (Huang et al. 2005a). Flow rates of 0.33 g/s (20 mL/min) and 0.0825 g/s (5 mL/min) were used for later simulations and experimental validation because higher flowrates compressed the porous structure. The simulation was run at steady state in order to visualize flow distributions and to generate the initial velocity profile for transient simulations. The outlet was set at atmospheric pressure and the walls were smooth with no slip condition.

Residence time distributions (RTDs) were obtained by introducing a tracer into the reactor feed starting at time equal to zero seconds. The tracer for the simulations was created as a duplicate fluid based on water and then renamed as tracer. This created a tracer with the same physical properties as that of water. The tracer was introduced as a step change in the concentration (represented as  $C_0$ ). The values for steady state flow of water were used as initial conditions. Then, the inlet fluid was switched from 100% water to 100% tracer at time equals zero seconds.

The simulations were performed using 5s time-steps until the concentration reached 0.99 of the initial concentration (25 steps, 120 s). Transient results were written for every 5 s and  $C_{mix}(t)$  was calculated using:

$$C_{mix}(t) = \frac{\sum C_{avg} V_{avg} r \Delta r \Delta \theta}{\sum V_{avg} r \Delta r \Delta \theta} \quad (3.1)$$

where  $C_{avg}$  is the average tracer concentration across the two finite elements and  $V_{avg}$  is the average velocity in the  $z$ -direction between those elements and  $r, \theta$  were obtained using cartesian coordinates relations  $r = \sqrt{x^2 + z^2}$  and  $\theta = \tan^{-1}(x/z)$ .  $C_{mix}(t)$  is also measured from the experiments at a given time. Next the RTD function,  $E(t)$ , was

calculated for a positive step change in the tracer concentration using the equation (Fogler 2006b)

$$E(t) = \frac{d}{dt} \left[ \frac{C_{mix}(t)}{C_0} \right]_{Step} \quad (3.2)$$

Additionally, the RTD function was converted to dimensionless time ( $\Theta$ ) in order to directly compare multiple geometries and flow rates. The dimensionless form of the equation ( $E(\Theta)$ ) was calculated using the equation

$$\Theta = \frac{t}{\tau} \quad (3.3)$$

where  $\tau$  is the space time of the reactor i.e., the ratio of the volume of the reactor to volumetric flow rate. The data obtained from simulations was used to find out the theoretical residence time distribution. The sample calculations of determining the RTD from the data obtained from the simulations is shown in **Appendix A**.

### 3.2.3. Obtaining RTD function using experimental setup

The RTD function was determined experimentally by introducing a red food dye as a step change in the inlet concentration. A circular reactor similar to Case 3 (diameter of 10 cm, a height of 2 mm, and a 0.6 cm inlet and outlet) was constructed in-house from polycarbonate as shown in **Figures 3.2A and 3.2B**.

The reactors were attached to a flow system (**Figure 3.2C**) consisting of two fluid reservoirs, a variable speed Masterflex L/S peristaltic pump (Cole-Parmer, Vernon Hills, IL), an in-line physiological pressure transducer (Capto SP844, Capto, Skoppum, Norway), the bioreactor, and two waste reservoirs. The pressure transducer was connected to a computer via Powerlab/4SP System (ADI Instruments, Inc., Colorado

Springs, CO) and data were acquired through Chart™ 5 for Windows. The tubing system for the reactor was designed in order to produce a step change in the reactor's inlet concentration. Two separate tubes were run through a peristaltic pump, one from a water reservoir and another from a reservoir filled with dye tracer solution. These tubes each led to a three way stopcock (V1 and V3) that would send the fluid either towards the reactor or into a waste reservoir. The two sides were connected to a T-joint (V2), allowing dye solution or water to enter the reactor.

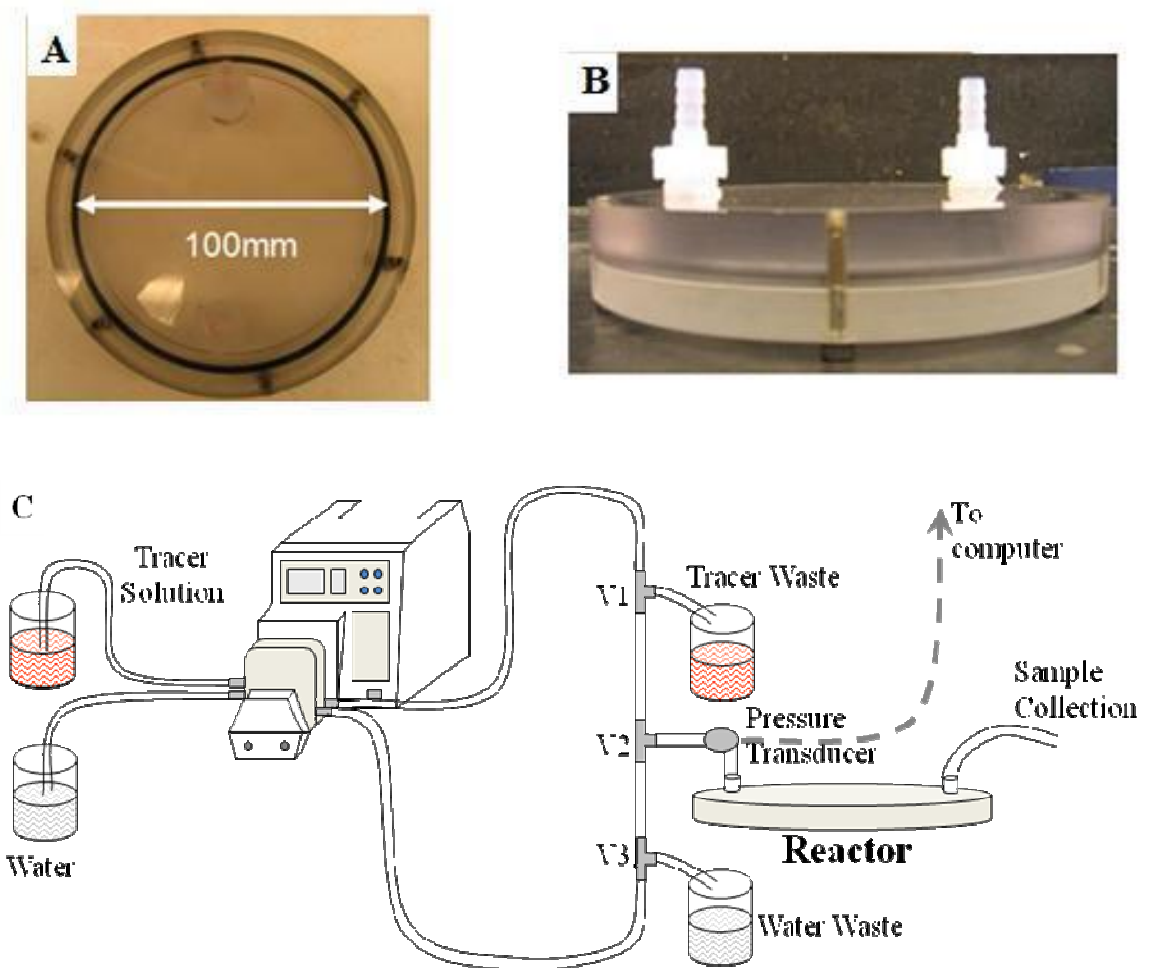


**Figure 3.2.** Reactor set-up used in experimentation (a) Top view of the circular reactor. (b) Side view of the circular reactor. (c) Flow-loop used for RTD analyses.

Initially the flow loop was primed with the valve positions (V1 to dye waste and V3 to reactor) set so as the water traveled through the reactor while the dye solution was sent to a waste container. Water was run through the system until steady state was obtained. At time zero, V1 and V3 were changed simultaneously (V1 to reactor and V3 to water waste) so the dye solution traveled through the reactor and water was sent to the waste container. Fractions were collected in a 24 well plate at the reactor outlet over regular intervals. Next 100  $\mu\text{L}$  of each fraction was transferred to a 96 well plate and the absorbance was measured at 490 nm; initial spectral scan over visible spectra showed that the maximum absorbance was at 490 nm wavelength. The relative concentration ( $C(t)/C_0$ ) was calculated from the relative absorbance ( $A/A_0$ )

$$\frac{C(t)}{C_0} = \frac{A(t)}{A_0} \quad (3.4)$$

where  $A_0$  is the initial concentration of the dye solution. The RTD function ( $E(t)$ ) was calculated using Eq.(4) as before. Since 20 mL/min flowrate compressed the porous scaffold structure, 5 mL/min was used. Samples (5 drops) were collected every 5 s for 20 mL/min flow rate and at every 20 s for the 5 mL/s flow rate.

#### 3.2.4. Preparation of porous structure

Porous structures (**Figure 3.3**) of dimensions appropriate for the reactor were generated by freezing 0.5% (wt/v) chitosan solution prepared in 0.1 M acetic acid at -80°C, then lyophilized overnight (Virtis, Gardiner, NY). The porosity and pore size distribution of these matrices in hydrated condition has been extensively characterized in our laboratory (Huang et al. 2005a; Huang et al. 2006; Tillman et al. 2006a). Scaffolds were stabilized in 100% ethanol and incubated in red-dye prior to use in experiments.

The pore size distribution and porous structure characteristics of the wet scaffolds were analyzed using light microscopy. Prior to viewing under light microscopy, chitosan structures were sectioned to view cross sectional architecture. Pore size and number of pores was determined from digital micrographs using Sigma Scan Pro software (Systat Software, Inc., Point Richmond, CA).

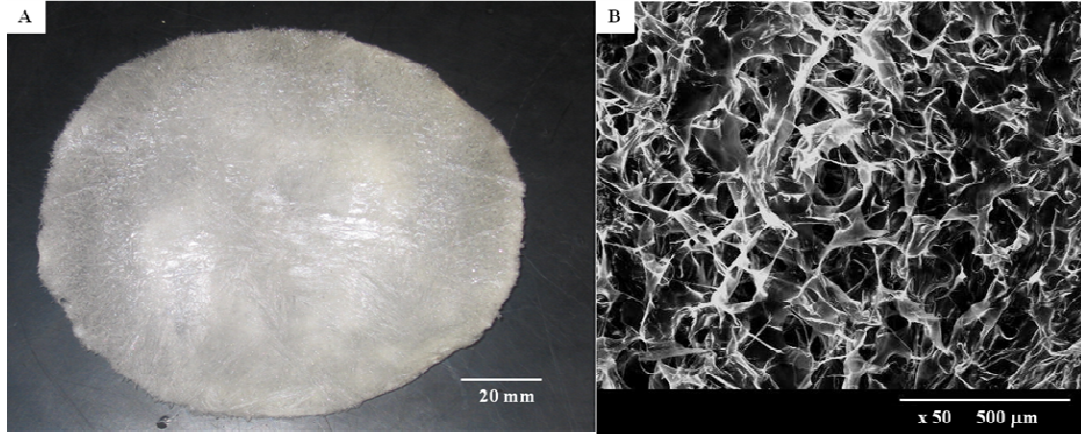


**Figure 3.3:** Chitosan porous structure (A) 10 cm in diameter and 2 mm thick (B) Scanning electron microscopy (SEM) picture of chitosan.

### 3.2.5. Simulation including the porous structure

Next, a porous medium was created within the reactor space to better understand the effect of porous structure on fluid flow, simulations were performed using COMSOL Multiphysics 3.4 (COMSOL inc, Burlington, MA). Case 3 geometry was created in COMSOL using configuration identical to described above. Fluid flow through the porous structures was modeled using the Brinkman equation

$$\mu \nabla^2 u_s - \frac{\mu}{\kappa} u_s = \nabla p \quad (3.5)$$

$$\nabla \bullet u_s = 0 \quad (3.6)$$

where  $\kappa$  is the permeability of the porous medium,  $u_s$  denotes the fluid superficial

velocity vector,  $p$  is the fluid pressure, and  $\mu$  the effective viscosity in the porous medium (Truskey et al. 2004). Nonporous sections of the reactor were modeled as incompressible Navier-Stokes regions. The permeability ( $\kappa$ ) of the porous medium is a geometric characteristic of the porous structure at several length scales (Truskey et al. 2004). The permeability was calculated using  $85\mu\text{m}$  and  $120$  pores/ $\text{mm}^2$  and the equation

$$\kappa = \frac{\pi}{128} n_A d^4 \quad (3.7)$$

where  $n_A$  is the number of pores per unit area and  $d$  is the pore diameter assuming the pores to be circular in shape. To understand the effect of pore size and number of pores,  $\kappa$  values were calculated for (**Table 3.1 and Table 3.2**) different pore sizes and pore numbers. These values were used in the simulation. Shear stresses within the reactor were calculated using the shear stress tensor equation

$$\tau = \eta \left( \nabla u + (\nabla u)^T \right) \quad (3.8)$$

where  $\eta$  is the dynamic viscosity (Pa·s) and  $u$  is the velocity in the open channel (m/s). The shear stress tensor is an integral part of the Navier-Stokes equations describing flow in a free channel at steady state, given by

$$\rho(u \bullet \nabla)u = -\nabla \bullet \left[ -\tau + p\delta_{ij} \right] \quad (3.9)$$

$$\nabla \bullet u = 0 \quad (3.10)$$

where  $\rho$  is the fluid's density ( $\text{kg}/\text{m}^3$ ),  $p$  is the pressure (Pa) and  $\delta_{ij}$  is the Kronecker delta function. Both the permeability ( $k$ ,  $\text{m}^2$ ) and void fraction ( $\epsilon_p$ , dimensionless) were incorporated into Eq.(9) in order to account for the porous characteristics of the matrix, yielding another form of the Brinkman Equation

$$\frac{\eta}{\kappa} u = -\nabla \cdot \left[ \frac{-\tau}{\varepsilon_p} + p \delta_{ij} \right] \quad (3.11)$$

The simulation was run at 5 mL/min (similar to experiments), with atmospheric pressure as the outlet condition. From the steady state output results, the pressure drop and the maximum shear stress were determined across the porous subdomain. Further, the shear stress was visualized as the viscous force per area in the z direction, as calculated by

$$\tau \cdot n \quad (3.12)$$

### 3.3. RESULTS

#### 3.3.1. Steady state profile in reactors without porous structure:

The streamline patterns for water flowing through the reactor without porous structures were analyzed in all the reactors at steady state. For individual reactor cases, no significant difference in the streamline patterns was observed between 156 mL/min and 20 mL/min flow rates. In case 1 (**Figure 3.4A**), streamlines were not observed in the entire reactor, particularly on the opposite end of the outlet. A reduced flow velocity and distribution at the opposite end of the outlet, indicating that there is dead volume and channelling. The fluid travelled around the edges of the reactor and then reversed direction to reach the exit. Flow patterns in case 2 and case 3 (**Figure 3.4A**) showed no significant difference and uniform streamlines, indicating minimal dead-volumes. This shows that changing that the outlet side may not be a factor in thin reactors.

#### 3.3.2. Transient profile in reactors without porous structure:

The contour plots for the tracer flowing through the reactor without the porous

structure were analyzed in all the three reactors. The contours indicate that Case1(**Figure 3.4B**), is least preferred among all the three, as by the end of 20<sup>th</sup> second there were some dead space at the edges of the reactor indicating minimal nutrient flow in those regions. In Case 2 and Case 3 (**Figure 3.4B**), the tracer was distributed uniformly throughout the reactor indicating that there are no dead spaces. Since, it was easier to set up Case 3 than Case 2 for ease purpose we choose Case 3 for further experimentation and validations.

### **3.3.3. Residence time distributions without porous structure**

Transient residence time distributions for the tracer were analyzed at the reactor outlet to better understand the flow distribution of nutrients. First, the changes in the tracer concentration across the outlet diameter were examined so that a method to determine  $C_{mix}(t)$  from the simulation results could be developed.

All the Cases showed non-linear change in tracer concentration except few initial and final time steps(**Figure 3.6**). Further, the concentrations were not uniform or symmetric. Among all the three, the degree of non uniformity is more in Case1 than in the other two Cases. Since the concentration profile in the circular reactors were not linear, expressions for  $C_{mix}(t)$  were developed using multi-parameter regression approach at each time step. Results obtained using these equations showed large errors with the RTD calculations and were not utilized further. Therefore, in circular reactors  $C_{mix}(t)$  was approximated using Eq.(1).

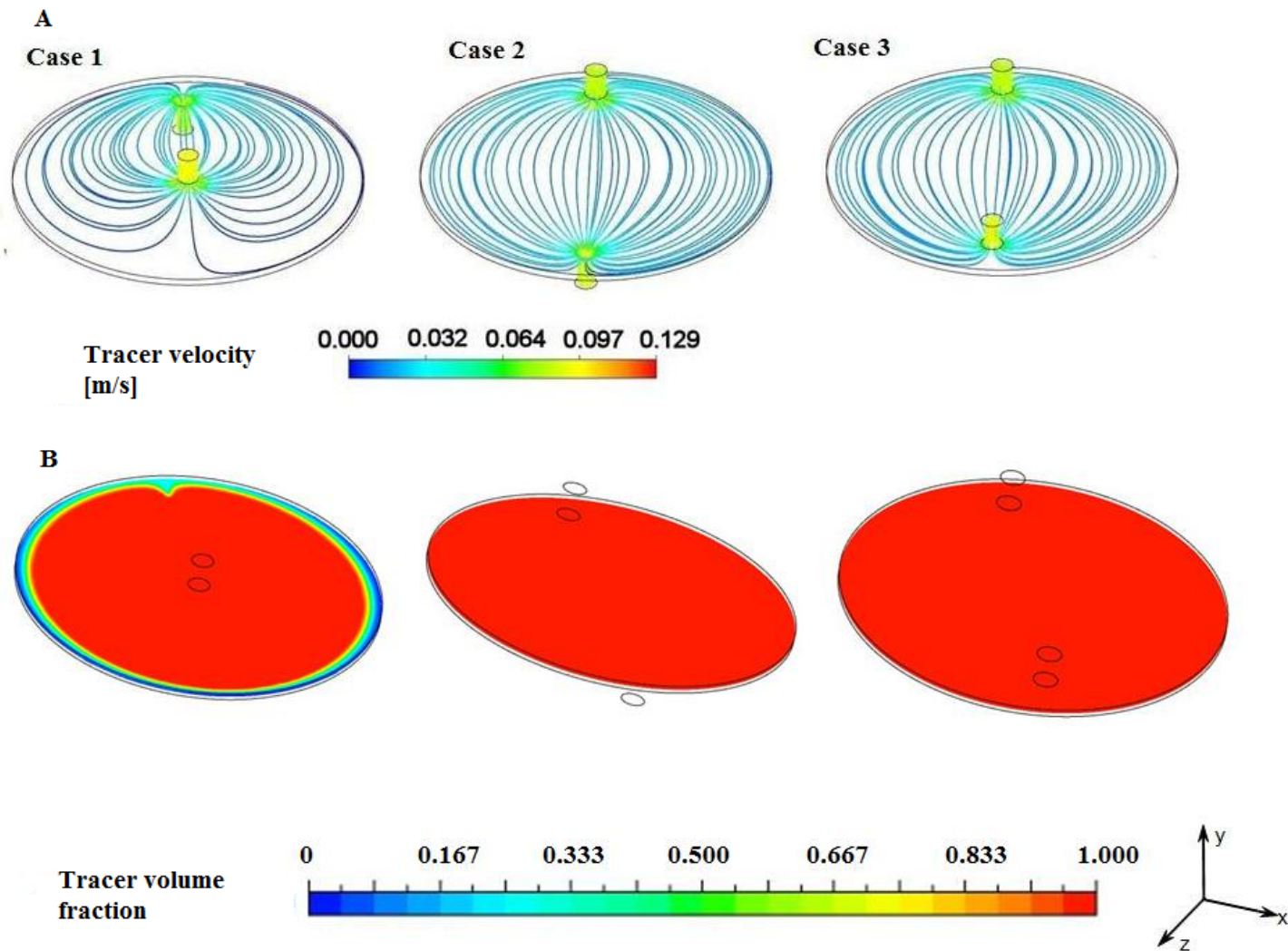


**Figure 3.4.** (A) Steady state stream line profiles in different reactors simulated with a flow rate of 20 mL/min. (B) Contour plots of tracer concentration in different reactors at 20 mL/min flow rate.

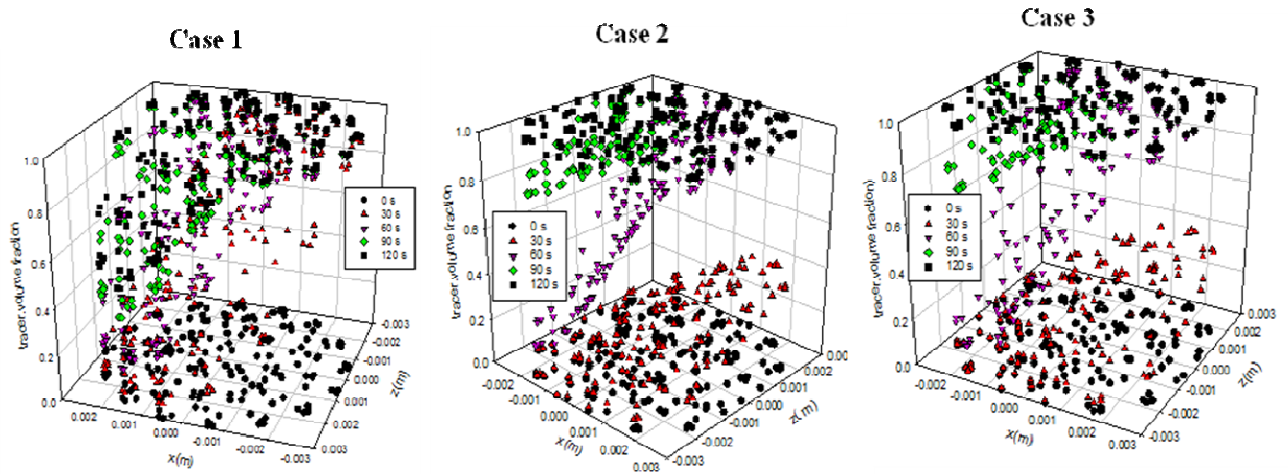


**Figure 3.5.** Concentration profiles at the reactor outlet for different times at 20 mL/min flow rate.

The relative concentration ( $C_{mix}/C_0$ ) was plotted against dimensionless time (**Figure 3.6C**). In case 1 the tracer exited the reactor much sooner than in other geometries. This premature exit of the tracer could be attributed to the dead volume or channeling. Next,  $E(t)$  was calculated for different time steps and plotted as a function of dimensionless time (**Figure 3.6D**). For case 1 the peak was higher and shifted left compared to case 2 and case 3 indicating an increase in dead volume and channeling.

The bump in the  $E(t)$  curve in case 3 ( $\Theta \approx 1.3$ ) is further evidence for channeling. The simulation results for case 3, were validated by experiment. The simulations and experiments had similar concentration and RTD profiles when plotted, showing that methodology is a valid approach to analyze flow properties in the reactor systems. **Figure 3.6A, 3.6B** shows similar variation in the relative concentration with respect to dimensionless time. The peaks in case of 156 mL/min are much higher than in case of 20 mL/min indicating that the channeling is much higher at higher flow rates.

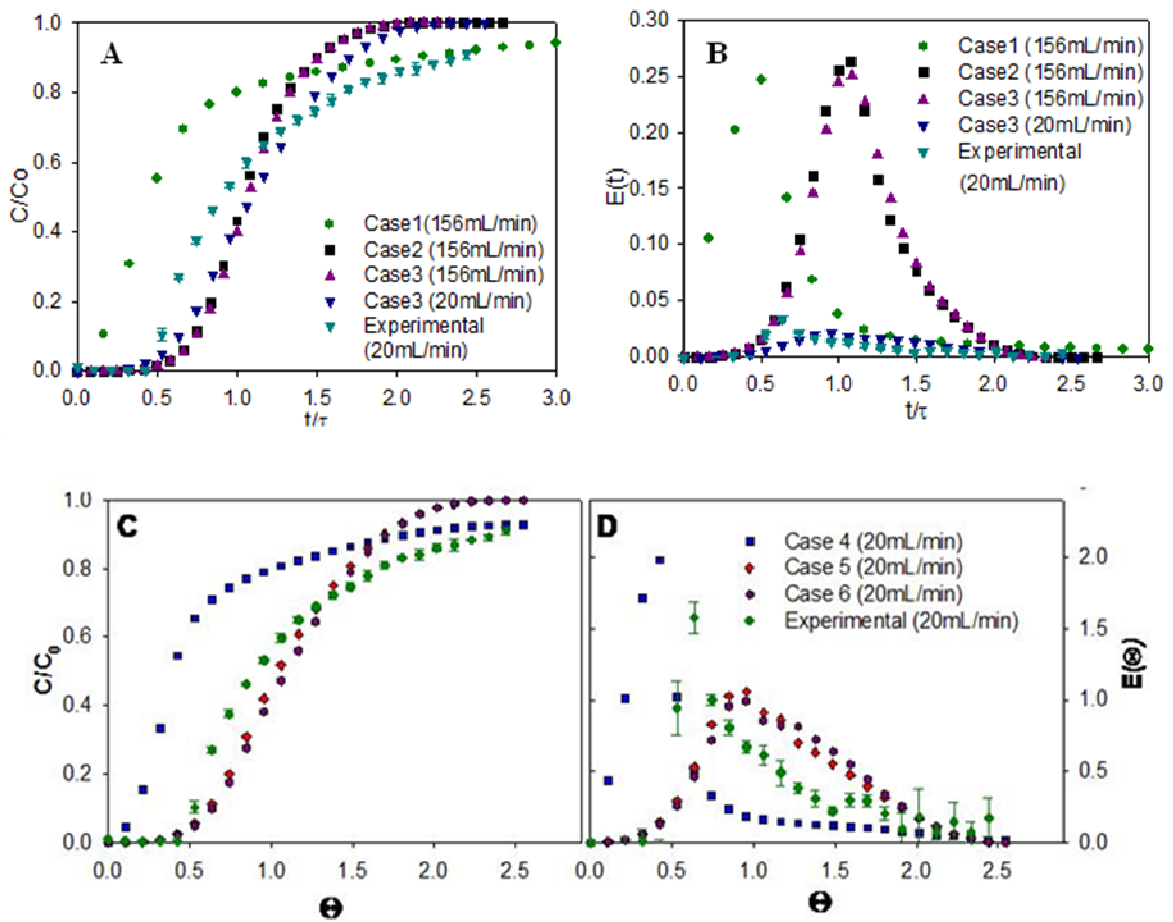


**Figure 3.6.** The residence time distribution of the tracer at 156 mL/min and 20 mL/min (A,C) Concentration of the tracer at the outlet of circular reactor. (B,D) E-curve for circular reactor.

### 3.3.4. Effect of porous structure on flow distribution

This study utilized chitosan porous structures prepared by freeze drying at  $-80^{\circ}\text{C}$ . Chitosan was selected because i) it is optically transparent, enabling visual monitoring of the flow distribution, ii) the matrix will not degrade in the absence of enzymes, iii) its mechanical properties are well described, and iv) pore characteristics of the scaffold have been analyzed extensively (Huang et al. 2005a; Huang et al. 2005b; Huang et al. 2006; Tillman et al. 2006a). Scaffolds formed by freezing at  $-80^{\circ}\text{C}$  showed an average pore

size of  $85 \mu\text{m} (\pm 20 \mu\text{m})$  and  $120 \text{ pores/mm}^2$ , and a porosity of 85%. Porosity values were used to calculate the available reactor volume and space time.

When RTD was examined for reactors containing the porous structure, results indicated (**Figure 3.7**) that the tracer exited the reactor sooner relative to conditions without the porous structure. This could be attributed to the increased resistance to flow caused by the presence of the porous structure which could favor channeling. When fluid entered the system, the hydrodynamic forces deformed the polymer scaffold, creating a shorter path to the outlet of the reactor. This deformation was especially prevalent in the circular reactors where the inlets are located directly above the porous matrix. While performing experiments, it was observed that the scaffolds were compressed at the inlet and the flow traveled over the top of the matrix and along the walls without significantly infiltrating into the porous structure.

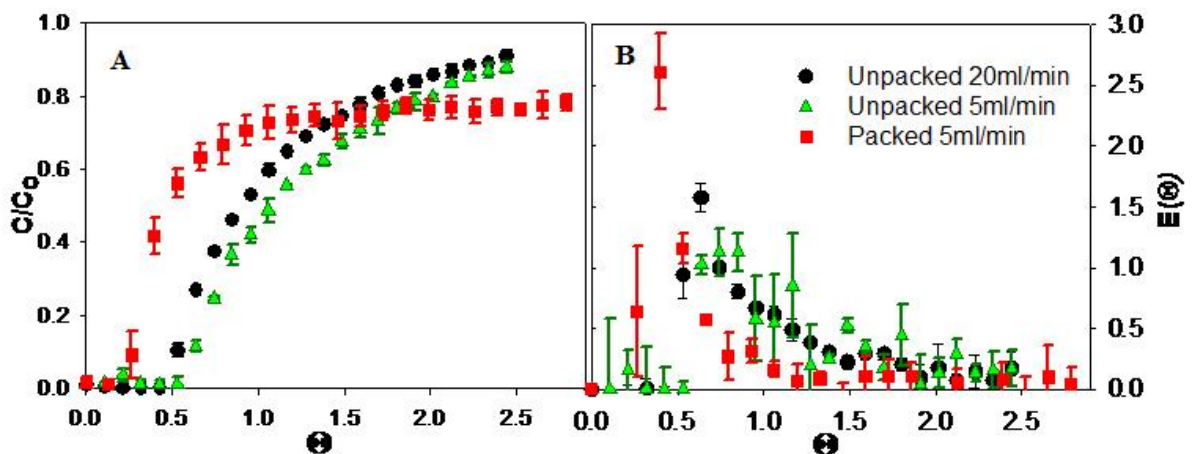


**Figure 3.7.** Effect of flow rate and porous structure on the residence time of the tracer. a) Concentration of the tracer at the outlet of circular reactor. b) E-curve for circular reactor.

### **3.3.5. Effect of changing pore sizes of the porous structure on pressure drop and shear stress**

Next, the pressure drop across the reactors and the shear stresses developed within the porous structures were assessed. When fabricating scaffold the number of pores and the pores per area do not change independently. For example, a matrix with smaller pores should have more pores in any given area than a scaffold with larger pores. Therefore, simulations were performed using various pore sizes and pores per area to better understand the effects of the porous architecture. Values for pore size and pores per area were centered on an experimentally determined value (85  $\mu\text{m}$  diameter pores and 120 pores/ $\text{mm}^2$ ) (**Table 3.1**). These results showed significant changes in the pressure drop across the porous structure of the reactor (**Figure 3.8A**). The pressure drop increased when the pore size was reduced, and increased when the number of pores per unit area (pores/ $\text{mm}^2$ ) was increased. Additionally, the pressure drop was inversely proportional to  $1/\kappa$  as predicted by the Brinkman equation (Eq.(3.11))

**Table 3.1. Effect of pore size and pore number on pressure drop and shear stress. (5 mL/min)**

Pore Size ( $\mu\text{m}$ )	Pores/ $\text{mm}^2$	k ( $\mu\text{m}^2$ )	Circular Reactor		
			Pressure Drop (kPa)	Maximum Shear Stress	
				in x ( $\text{dyne/cm}^2$ )	in y ( $\text{dyne/cm}^2$ )
10	13813	3.390	12.526	0.26	0.271
17.5	4510	10.382	4.091	0.258	0.271
25	2210	21.188	2.005	0.256	0.27
37.5	982	47.662	0.891	0.251	0.269
50	553	84.829	0.501	0.245	0.267
85	191	244.708	0.174	0.226	0.259
120	96	488.580	0.087	0.208	0.246
150	61	757.939	0.056	0.195	0.232
200	35	1374.447	0.031	0.177	0.207

The experimentally measured pressure drop (**Figure 3.8A**) within the reactors was slightly higher than pressure drop predicted by the simulation. The experimental pressure drop varied from 7-9 mmHg (0.930 – 1.20 kPa) which is higher than the simulated value (0.570 kPa). This slight increase from simulation results could be attributed to multiple reasons. (a) A slightly thicker porous structure than the reactor height was used in order to anchor the porous structure to the reactor, leading to compression of the structure/pores and increased pressure drop. (b) The scaffold may also have been compressed by fluid flow, leading to increased pressure drop.

The shear stress increased in a linear fashion as the pore size decreased, but that the shear stress increased exponentially as the pore density (pores/ $\text{mm}^2$ ) increased. Flow in the circular reactor follows a curved path. Therefore, shear stress for the circular reactor varied in two directions (both  $x$  and  $y$ ). The maximum shear stress values for the circular reactor were determined in both the directions. Shear stress was almost uniform

throughout the reactor with maximums near the inlet and the outlet in both  $x$  and  $y$  directions (**Figure 3.9**) but not necessarily at the same point. The maximum shear stress observed in both  $x$  and  $y$  directions are around 0.237 and 0.271 dynes/cm<sup>2</sup> respectively.

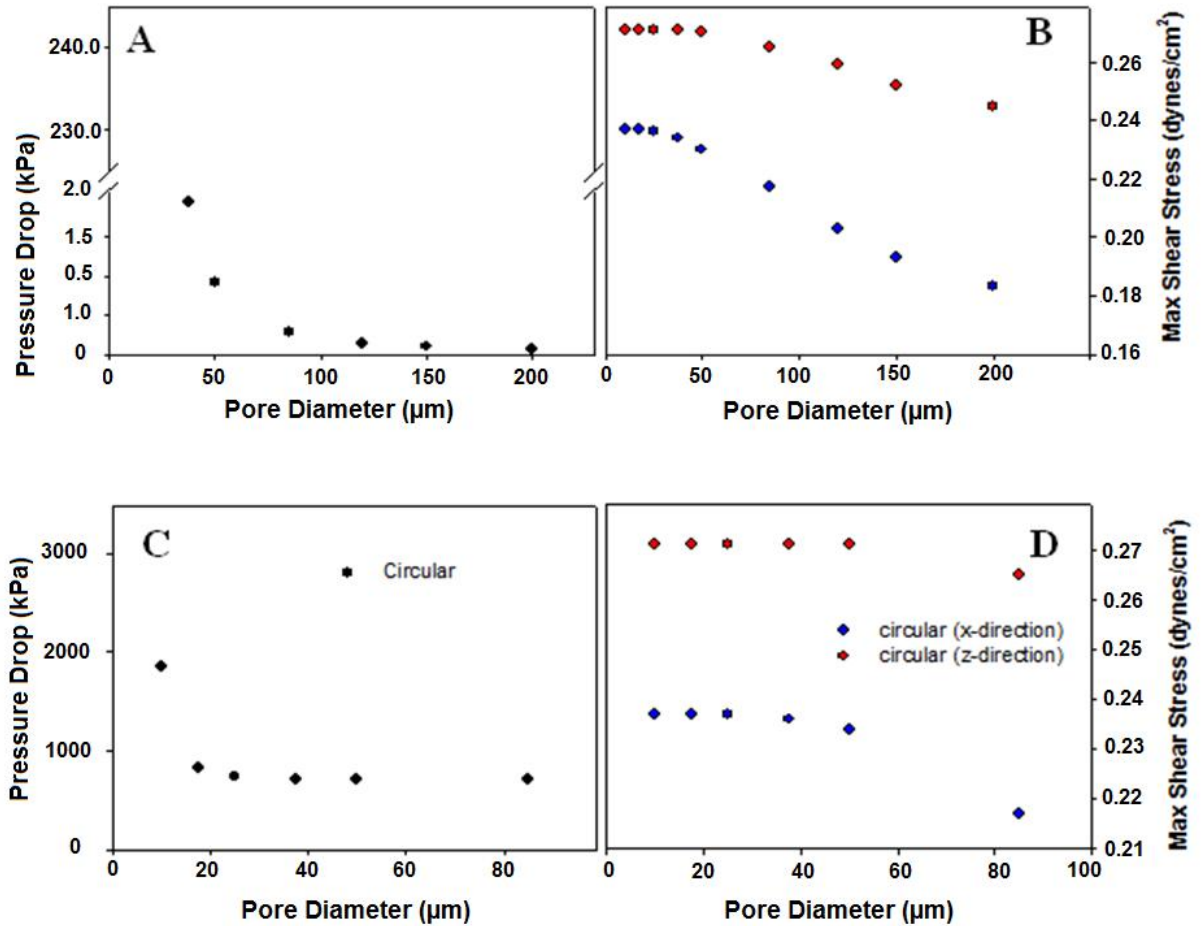


**Figure 3.8.** Effect of pore size and pore number on the pressure drop and maximum shear stress in the reactor. a) Effect of changing pore size with pore number on pressure drop. Gray box correspond to the experimental result. b) Effect of changing pore size with pore number on maximum shear stress. c) Effect of changing pore size with 120 pores/mm<sup>2</sup> on pressure drop.

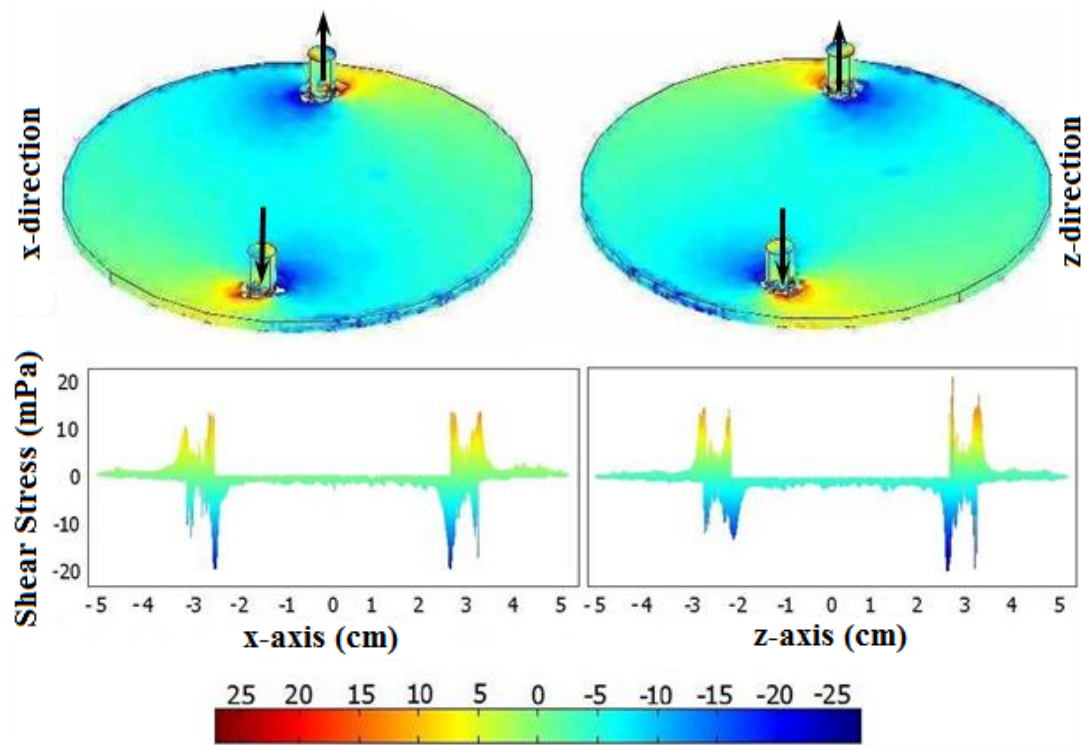


**Figure 3.9.** Shear stress distribution within the porous structure for the case with 85  $\mu\text{m}$  pore size and 120 pores/ $\text{mm}^2$ . Arrows indicate the flow direction. Below the reactor are the histogram profiles for each condition.

### 3.3.6. Effect of changing porosity of the porous structure on pressure drop and shear stress

During the course of tissue remodeling, cells will proliferate and *de novo* synthesize extracellular matrix elements which are deposited in the porous structures. These processes reduce the pore space available for fluid flow. Hence the pore size decreases but the number of pores per area does not.

To understand the implications of these dynamic changes, simulations were carried out with six decreasing pore sizes (**Table 3.2**) with constant the number of pores per unit area that was determined experimentally (120 pores/mm<sup>2</sup>). These results showed (**Figure 3.8A**) significant increase in the pressure drop across the bed with decreased pore size. The shear stresses increased in a nonlinear manner as the pore size decreased.

Table 3.2. Effect of reduced pore size with constant pore number on pressure drop and shear stress.

Pore Size ( $\mu\text{m}$ )	Pores/mm <sup>2</sup>	k ( $\mu\text{m}^2$ )	Circular Reactor		
			Pressure Drop (kPa)	Maximum shear stress	
				x-direction (dyne/cm <sup>2</sup> )	y-direction (dyne/cm <sup>2</sup> )
85	191	244.708	0.174	0.226	0.259
50	191	29.299	1.449	0.255	0.27
37.5	191	9.270	4.581	0.259	0.271
25	191	1.831	23.189	0.260	0.271
17.5	191	0.439	96.574	0.260	0.271
10	191	0.0469	905.781	0.261	0.271

### 3.4. DISCUSSION

In this study, simulations and experimental validation were performed with and without porous structures to understand the fluid flow distribution within the bioreactor. The reactor systems used have distinct advantages for regenerating large clinically transplantable tissues such as cartilage, bladder and skin; scaffolds can have very large surface area to volume ratios with very small thickness. Another popular bioreactor configuration involves growing cell seeded constructs in microgravity (Marolt et al. 2006). However, for growing large aspect ratio tissues, microgravity reactor would deform the structure due to bending and rolling while tumbling through the growth medium, creating a random stress pattern within the developing material. Hence, microgravity reactors may not be suitable for regenerating thin cross-sectional tissues. The parallel plate reactors provide stability and support for the porous structure and developing tissue.

Unlike in the traditional rectangular reactor, the circular curvature induced secondary circulations in the flow field. The RTD analyses showed increased non-ideal fluid distribution pattern in the circular reactor. Presence of porous structure further increased channeling effects in the circular reactors. The RTD analysis was based on the average concentration profile, which is valid for smaller outlet size. However, one has to consider the non-linear concentration profile while averaging across larger outlets. Further, the experimental results showed compression of the porous structure at 20 mL/min flowrates. The compression can be attributed to the mechanical properties of the chitosan porous structure (elastic modulus is 2-6 kPa). To minimize the compressive damage on the porous structure, flow rate was reduced to 5 mL/min. However, in the

simulation results, these compressive changes were not considered and the porous medium was treated as a rigid matrix. Hence, further studies in which the elastic properties of the porous structure are coupled to the fluid force are necessary to better understand the fluid distribution.

Understanding pressure drop changes is important to determine the pressure to be maintained during tissue regeneration (Sodian et al. 2000). To mimic tissue regeneration process, the number of pores was kept constant while decreasing the pore size. The exponential increase in pressure drop as pore sizes shrink indicates that liquid flow through a porous scaffold will decrease and possibly stop unless flow system is adjusted to provide large pressure gradients. The nonlinear properties of both shear stress distributions and pressure drop suggest that there is room for optimization of the porous structure. Others have reported the effect of changing porous structure due to cell growth on the growth media distribution in cylindrical scaffolds (Chung et al. 2007). These studies used porosity based permeability values, which could change by either decreased number of pores or decreased the pore size. Hence, it may not reflect the true regeneration characteristics.

While the scaffold is subjected to the bulk forces supplied by the tissue and fluid flow, the cells experience the micromechanical properties of the individual fibers and local shear stresses within the porous structure. Flow within the reactor determines the orientation of cells within the material. Shear stresses generated by the fluid motion influence alignment of endothelial cells (Huang et al. 2005a) and chondrocytes (Gray et al. 1988) grown in the parallel plate reactor. Alignment of cells and the de novo synthesized matrix elements determine the ultimate quality of the regenerated tissue. We

evaluated the shear stresses within the porous structure through simulations. Shear stress in the porous structures are less compared to the estimated wall shear stresses (Gutierrez and Crumpler 2008). The shear stress in the porous structure is (-0.01 to 0.01 dynes/cm<sup>2</sup>) in the circular reactor. The shear stresses were higher in, the regions that were near the inlet and the outlet where the porous structure gets compressed because of the flow. A microgravity reactor rotating at 10 rpm has an average wall shear stress of 0.2 dyne/cm<sup>2</sup> and a maximum shear stress of 0.3 dyne/cm<sup>2</sup> (Chen and Hu 2006), comparable to parallel plate bioreactors. However, the tumbling free fall motion of the scaffolds produces a non-uniform stress distribution. Another method uses mechanical action to stretch or compress the scaffold material (Altman et al. 2002; Kim et al. 1999). One configuration utilizes screw driven actuators to impart bidirectional stresses to the material (Grashow et al. 2006). Further studies are necessary to determine the optimal method or methods for controlling the mechanical forces acting on material within bioreactors (Arrigoni et al. 2008). Cellular constructs grown *in vitro* shrink, possibly as a result of cellular attachment and contraction or as a result of hydrodynamic forces compressing the scaffold.

Non-ideal fluid flow patterns lead to non-uniform distribution of nutrients present in the fluid. The RTD analysis is independent of the metabolic reactions and hence nutrient consumption is not integrated into the CFD modeling. To understand the implications of non-ideal fluid distribution on tissue regeneration, nutrient transfer characteristics have to be analyzed. Nutrient transport and consumption can be investigated through the use of the reactions package. Flow rate needs to be optimized based on the i) nutrient distribution, ii) effect on assembly of matrix elements, and iii)

cellular response to local shear stress. Further experiments have to be performed in this regard.

#### **ACKNOWLEDGEMENT**

The author would like to thank Dr. Benjamin J. Lawrence for helping in carrying out the RTD simulations in CFX and Pooja Iyer for helping out in taking the SEM pictures of the chitosan structure.

# **CHAPTER IV**

## **OPTIMIZATION OF BIOREACTOR FOR TISSUE ENGINEERING: NUTRIENT CONSUMPTIONS**

### **4.1. INTRODUCTION**

Regeneration of tissues outside the body utilizes a system where cells are populated in a porous biodegradable scaffolds in an optimum environment similar to the human body. Bioreactors of different shapes and flow systems have been utilized as a way to maintain optimum environmental conditions including sufficient amount of nutrients (Cummings and Waters 2007; Martin et al. 2004; Martin and Vermette 2005). To ensure complete nutrient distribution, flow-through configuration has been utilized as an approach to grow tissues (Botchwey et al. 2003; Goldstein et al. 2001; Jeong et al. 2005; Phillips et al. 2006; Sikavitsas et al. 2003; Sikavitsas et al. 2005). Apart from improving the distribution of the nutrients and replenishing the medium, the flow-through configuration stimulates mechanical stresses induced due to the nutrient flow which improves the proliferation, attachment and activity of some of the cell types.

Flow rate through the scaffold microarchitecture directly dictates the sufficiency of nutrients necessary for cellular activity and local shear stresses experienced by the cells. Very low flow rate could lead to nutrient deficiency and limited cell survivability. However, high flow rate leads to high shear stresses and cells respond to the level of hydrodynamic stress by remodeling their surrounding extracellular matrix and changing

the tissue composition (Chatzizisis et al. 2007; Cooper et al. 2007). Further, high flow rates could deteriorate the quality of the regenerated tissues via washout of the *de novo* synthesized matrix elements prior to complete assembly. Flow conditions also affect scaffold degradation rates which in turn affect the structural and mechanical properties (Agrawal et al. 2000). Cellular constructs grown *in vitro* shrink, possibly as a result of contraction or as a result of hydrodynamic forces compressing the scaffold (Lo et al. 2000). Optimizing the flow rate of the nutrients is very important while designing a bioreactor for tissue regeneration.

Nutrient consumption and shear stress distribution in flow-through perfusion reactors have been widely investigated using computational fluid dynamic methodologies (Chung et al. 2008; Chung et al. 2007; Porter et al. 2005b; Raimondi et al. 2006). The majority of these studies assess the flow patterns and shear stresses around small porous constructs. However, the fundamental concepts in developing these reactors for regenerating large tissues (for example skin, bladder, and cartilage) are not well defined. Many tissues have a high aspect ratio (large surface area relative to the thickness of the matrix) and contain multiple cell types. Effect of flow-through configuration within these systems has not been studied.

Previously, we reported the effect of the bioreactor shape and position of inlets and outlets on flow distribution and shear stress in high aspect ratio reactors containing porous structures (Lawrence BJ 2008). The non-ideal fluid distribution was characterized using the residence time distribution (RTD) analysis, which measures the amount of time different molecules present in the fluid spend within the reactor (Fogler 2006b; Lawrence et al. 2004), allowing for consumption by the cellular components. The RTD analysis is

independent of the metabolic reactions, although the total consumption of nutrients is determined by the residence time. Hence, simulations have to be performed with consumption to understand the nutrient distribution.

The objective of this study was to evaluate the nutrient distribution with consumption in high aspect ratio flow-through bioreactors containing porous structures. Since the previous circular reactors showed high shear stress regions at the inlet and outlet, six new reconfigured reactors with different extension shapes were analyzed for shear stress distribution. Simulations were performed using CFD packages CFX 11 (ANSYS Inc, Canonsburg, PA.) for flow distribution without porous structure and Comsol Multiphysics 3.4 (COMSOL, Inc., Burlington, MA) for flow distribution with nutrient consumption in the porous structure. One design was chosen depending on the pressure drop and shear stress distribution. Metabolic consumption for both oxygen and glucose was included using Michaelis-Menten type rate law for oxygen (and glucose consumption in some cell types). Nutrient transport and consumption was investigated in three different cell types based on the reaction rates reported in the literature (Alpert et al. 2002b; Fogler 2006b; Motterlini et al. 1998b; Sengers et al. 2005b)

- a. smooth muscle cells – present in various tissues, very responsive to stress levels
- b. hepatocytes – metabolically very active, and very sensitive to nutrient levels
- c. chondrocytes – anatomically located in a less metabolic demand area and it is less proliferative.

The shear stress and pressure drop analysis was also done and compared with the previous design. To understand the effects of changing porous characteristics during tissue regeneration attributed to *de novo* synthesis of matrix elements and cell

colonization, simulations were also performed. These results show significant flow rate dependency on cell type used.

## **4.2. MATERIALS & METHODS**

### **4.2.1. Reactor Designs**

*Design 1* was similar to Case 3 in the previous Chapter with inlet and outlet located directly on top of the porous structure. Six different reactor designs with different inlets and exits shapes were evaluated (**Figure 4.1**):

*Design 2* had a 0.6 cm wide channel extension at the entrance and the exit. The center of the inlet and the outlet were at a distance of 1.3 cm away from the porous region.

In *Design 3*, the rectangular extensions were increased to a length of 1.8 cm and a breadth of 1cm. Further, a 2 mm region to the back of the inlet or outlet was also placed to allow the fluid to flow to the back of those regions with the idea of dispersing the stresses.

In *Design 4*, the rectangular extensions were further increased to a length of 5 cm and a breadth of 3 cm. The inlet and outlet were around 2.7 cm away from the porous region.

*Design 5* had triangular extensions with an angle of 45 and a hypotenuse of 4 cm length. The inlet and outlet were at a distance of 8mm from the porous region.

*Design 6* had semicircular extensions of radius 2.5 cm for the inlet and the outlet. The center of the inlet and the outlet were at a distance of 1.3 cm away from the porous region.

*Design 7* had curved extensions. The fluid at the inlet was forced to flow through a constricted area which expanded smoothly into the large area where the scaffold was placed. The outlet was the mirror replica of the inlet.

These reactor geometries were created using a CAD package (Solidworks<sup>TM</sup> or ANSYS Workbench 11). The CFX mesh was then created using ANSYS CAD2Mesh software. A critical challenge was overcoming problems associated with the aspect ratio i.e., very large surface area relative to the thickness of the channel. Maximum element size of 0.1 mm was chosen and a fine triangular mesh was created such that there were at least 10 nodes across the thickness of the reactor. The simulations were performed under steady state conditions. The outlet was set at atmospheric pressure and the walls were smooth with no slip condition. All the simulations in ANSYS were carried out at a flow rate of 1 mL/min.

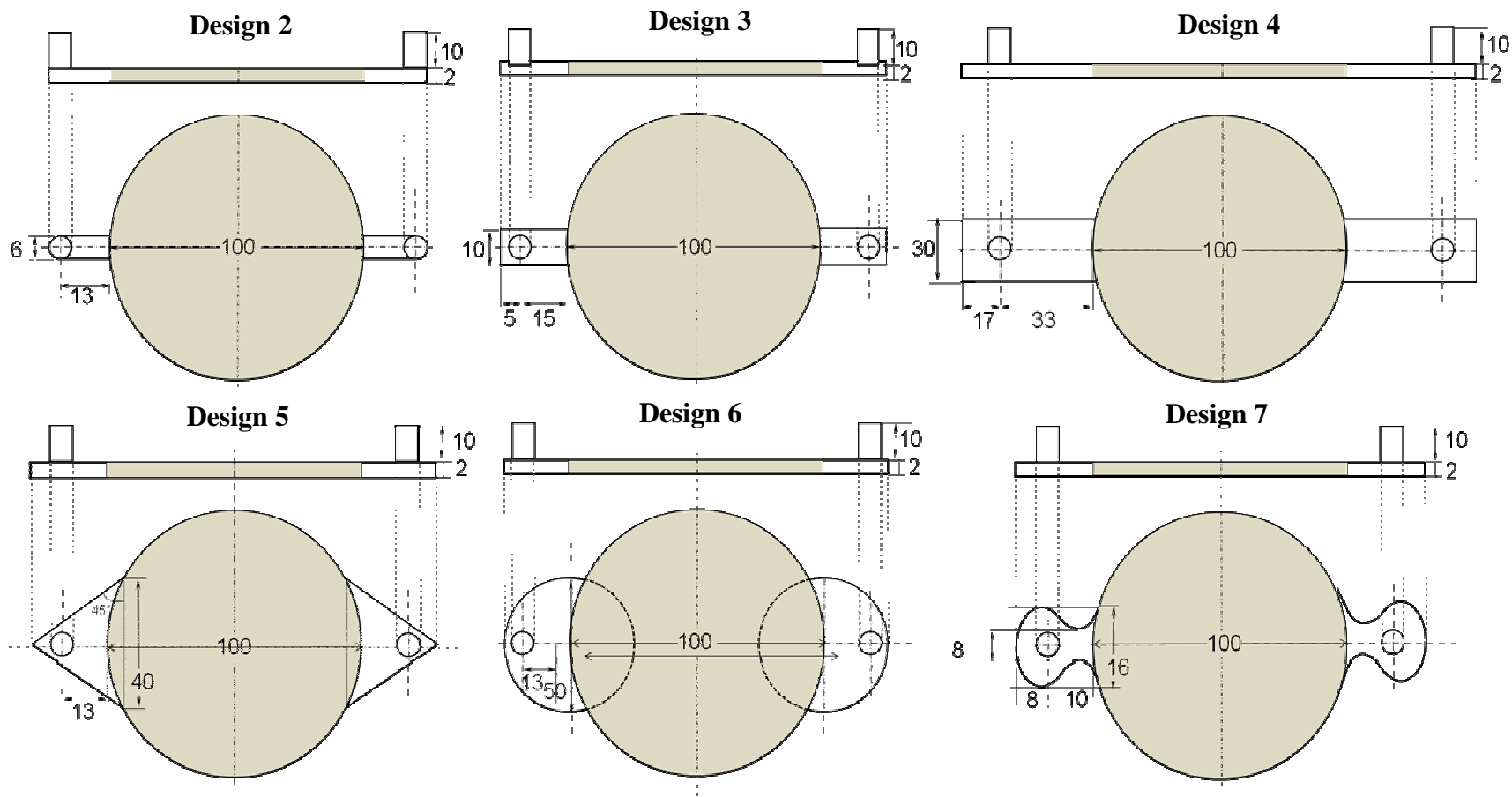


**Figure 4.1.** Schematic of the six reactor designs.

#### **4.2.2. Simulating fluid flow in the porous structure**

Based on the pressure drop and shear stress distribution analysis, Design 6 was selected for further analysis using porous structure. The steady state analysis of the fluid flow was performed using the COMSOL 3.4 Multiphysics (COMSOL, Inc., Burlington, MA). Three dimensional (3D) reactor models were created by using work plane settings option in the Draw tab; this allows drawing a 2D reactor model which can be extruded to create a 3D reactor model in the 3D Model View. Next, the subdomain and boundary conditions were set in the Physics tab. As the surface area is very large compared to the thickness of the reactor, a rectangular mesh was created to ensure that there were minimum 4 nodes across the 2 mm thickness of the reactor by doing a swept mesh; rectangular mesh is more uniform than the regular triangular mesh and computationally less demanding. Initially the flow rate was set at 5 mL/min, which is the maximum possible flow rate that can be used without affecting the chitosan porous structure. Further, the flow rate was reduced by ten folds from 1 mL/min to 0.001 mL/min until the nutrients were consumed fully. First, the simulations were performed to determine the velocity profiles by solving (a) the Incompressible Navier –Stokes equation on the non-porous regions and (b) the Brinkman equation on the porous regions, as described in the previous chapter. While solving the incompressible Navier-Stokes equations, the flow rate was given as 5 mL/min and the outlet boundary condition was set as zero pressure.

#### **4.2.3. Simulating reaction in the porous region of the reactor**

Using the steady state velocity profiles, the steady state concentration profiles of oxygen and glucose were obtained by solving the equation of continuity using the

chemical reaction engineering module in COMSOL 3.4 Multiphysics. Nutrient consumption was included in the simulation via the rate law. The convective diffusion equation was used to obtain the concentration at varying position along the cross section of the reaction:

$$\nabla \bullet (-D\nabla c) + u \bullet \nabla c = r_A \quad (4.1)$$

where  $c_A$  is the concentration of the species (mol/m<sup>3</sup>),  $r_A$  is the rate of reaction of the species under consideration (mol/m<sup>3</sup>.s),  $D$  is the diffusivity of the species (m<sup>2</sup>/s), and  $u$  is velocity vector (m/s). Physical properties of water were used as it constitutes bulk of the growth medium. The flow properties (i.e., viscosity and density) of the nutrient stream depend on the properties of the bulk fluid. Since the cells are present only in the porous scaffolds, the consumption of nutrients was defined only in the porous region, the reaction term was zero in the non-porous regions.

A Michaelis-Menten rate law was used for both oxygen and glucose consumption based on the reaction rates reported in the literature (Alpert et al. 2002b; Fogler 2006b; Motterlini et al. 1998b; Sengers et al. 2005b). The rate law is given by the expression

$$-r_A = \frac{v_m c_A}{k_m + c_A} \quad (4.2)$$

where  $r_A$  is the reaction rate,  $v_m$  is the maximum reaction rate, and  $k_m$  is the Michaelis constant. For oxygen  $c_A$  was replaced by  $c_1$  the concentration of oxygen. In the case of glucose,  $c_A$  is replaced by  $c_2$  the concentration of glucose. Both the rate laws were defined in the COMSOL, enabling the simultaneous visualization of both the oxygen and glucose profiles within the porous structure.

#### 4.2.4. Determination of Michaelis-Menten parameters from Literature

Based on the reaction rates reported in the literature for cells cultured on tissue culture surface plastic (Alpert et al. 2002b; Fogler 2006b; Motterlini et al. 1998b; Sengers et al. 2005b), the  $k_m$  and  $v_m$  values were obtained for three cell types. The kinetic parameters for oxygen and glucose consumption in chondrocytes reported by Sengers *et al* was used (Sengers et al. 2005a). For smooth muscle cells, the oxygen kinetic parameters were calculated from the partial pressure vs time plot reported by Motterlini *et al* (Motterlini et al. 1998b). Partial pressure of oxygen with respect to time was converted to concentration using Henrys law constant at 37°C and 1 atm. Then, Hanes-Woolf plot was developed to determine  $k_m$  and  $v_m$  values. The kinetic parameters reported by Alpert *et al* data was used (Alpert et al. 2002a) for glucose consumption in smooth muscle cells. For hepatocytes the kinetic parameters of oxygen were calculated from the partial pressure vs time reported by Balis et al. (Balis et al. 1999). **Table 4.1** shows the kinetic parameters calculated for the three cell types at  $1.20 \times 10^{12}$  cells/m<sup>3</sup>.

**Table 4.1. Kinetic parameters for different cell types.**

Cell type	Oxygen		Glucose		Inlet concentrations	
	Km (mol/m <sup>3</sup> )	V <sub>m</sub> (μmol/m <sup>3</sup> .s)	Km (mol/m <sup>3</sup> )	Vm (μmol/m <sup>3</sup> .s)	Oxygen (mol/m <sup>3</sup> )	Glucose (mol/m <sup>3</sup> )
Chondrocytes	$6.0 \times 10^{-3}$	2.47	0.35	45.1	0.205	5.1
SMCs	0.205	31.6	0.93	48.6	0.199	5.5
Hepatocytes	0.0263	41.1	-	-	0.214	-

The concentration of oxygen and glucose at the inlet is given as:

$$c_i = c_{i0,inlet} \quad (4.3)$$

The initial concentration of oxygen in the growth medium was determined using

the Henry's law constant at 37°C for each cell type. Initial concentrations of glucose were based on the growth media formulations used for each cell type. Mass transport at the outlet was assumed to be dominated by convection with negligible contribution from diffusion i.e.,

$$n \cdot c_i u = R_A \quad (4.4)$$

At all other boundaries, insulating conditions were specified as

$$n \cdot (-D_i \nabla c_i + c_i u) = 0 \quad (4.5)$$

### 4.3. RESULTS

#### 4.3.1. Effect of Inlet and Outlet shape on pressure drop and shear stress

Assessment of shear stresses developed within the porous structures in Design 1 showed an increase in shear stress at the inlet and the outlet locations. In addition, while performing experiments in circular reactors, it was observed that the porous structures were compressed at the inlet and the flow traveled over the top of the porous structures and along the walls with some infiltration into the porous structure

Based on these observations, the circular reactor was reconfigured by placing the inlets and outlets away from the porous structures. When the pressure distribution across the porous region where the cells are grown was analyzed (**Figure 4.2**), Design 7 showed significant pressure drop across the reactor, probably due to the sudden expansion at the inlet and sudden reduction at the outlet. Design 3 operated at a higher pressure relative to other designs within the porous region. In Designs 2, 4, 5 and 6 the pressure distribution throughout the porous structure was uniform with high and low pressures near the entrance and exit respectively. Thus, from the pressure distribution analysis, Designs 2,

4, 5, and 6 were considered as potential designs useful in tissue regeneration.

Next, the shear stress distribution was analyzed in all the six designs. These results showed (**Figure 4.3**) that the shear stress was high near the entrance and the exit in designs 2, 3 and 7. In design 2, the shear stress was higher than in any other designs and it was higher near the entrance. As shown in **Figure 4.3**, only Design 6 had uniform shear stress in the region where porous structure was present (indicated by the dotted circle). All other designs had some region within the reactor area where shear stress varied. Based on these observations, Design 6 was considered for further analysis along with Design 1.

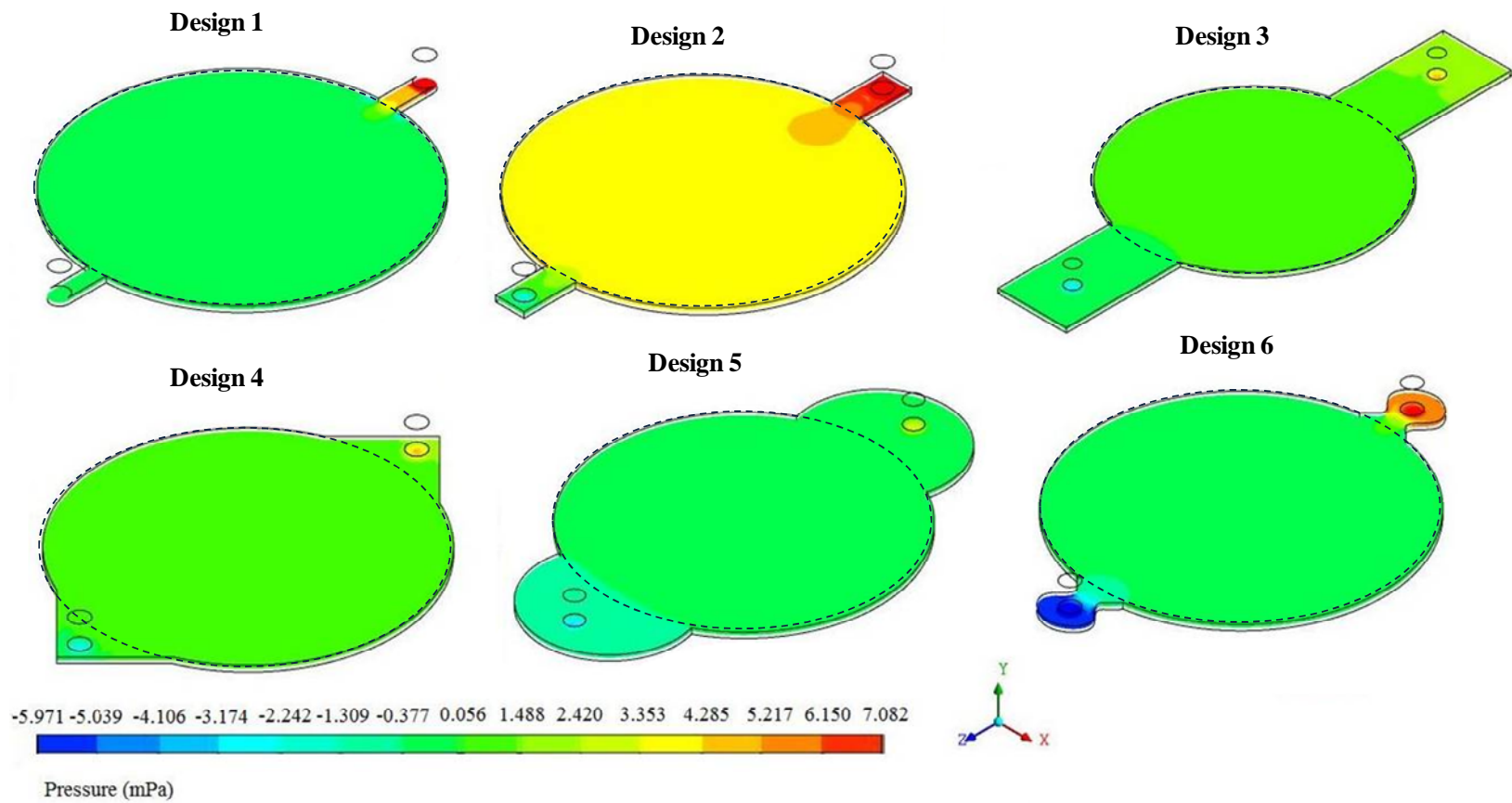


**Figure 4.2: Pressure Distribution across the cross section in all the six designs**

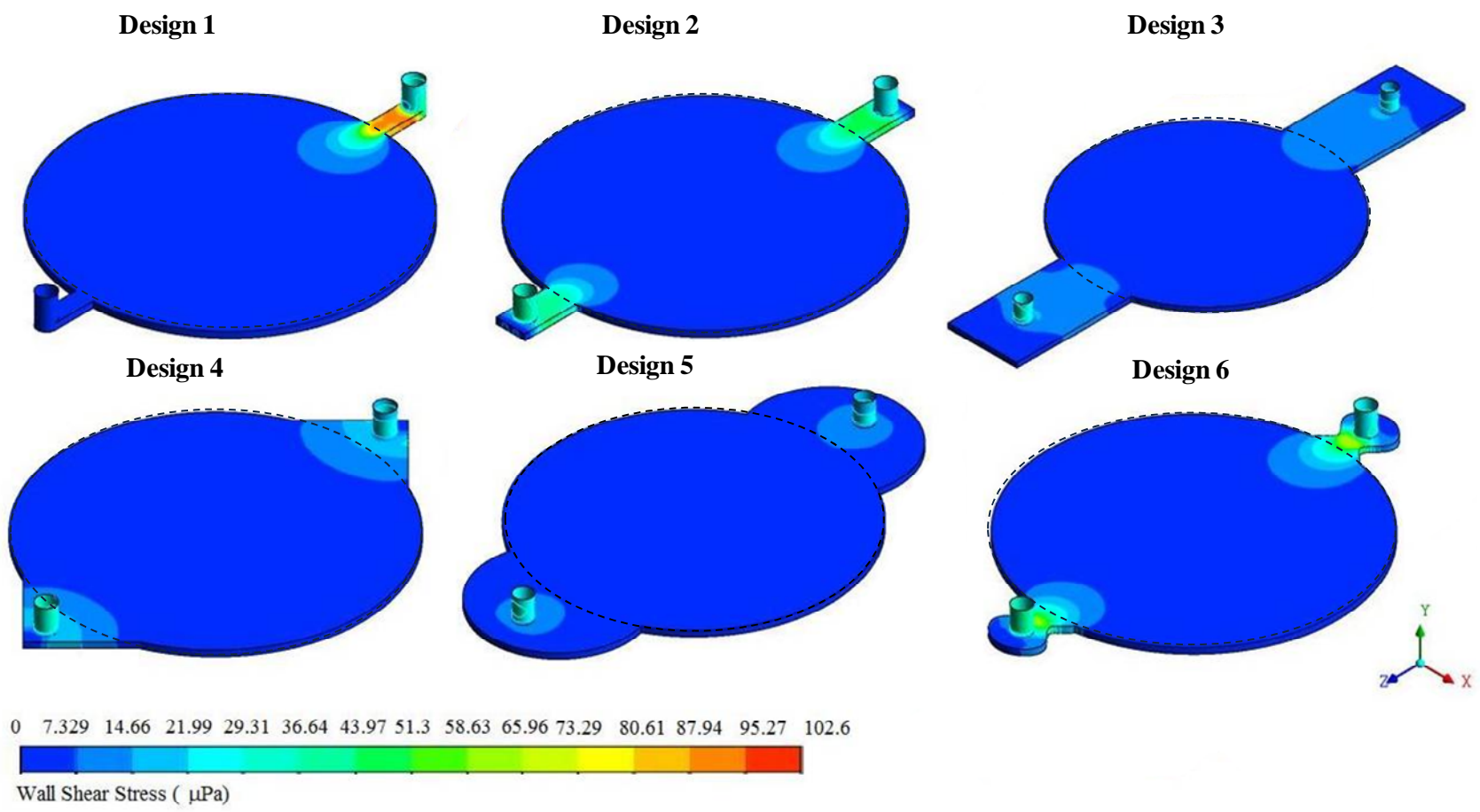


Figure 4.3: Shear Stress Distribution across the cross section in all the six designs

#### **4.3.2. Effect of flow rate on pressure drop and shear stress**

Next, the pressure drop across different reactors and the shear stresses developed within the porous structures were assessed for different flow rates. **Table 4.2** shows the variation in the pressure drop and the shear stresses for chondrocytes and smooth muscle cells are same in Design 1 and they are only function of the flow rate. These were based on Brinkman equation, without the effect of the consumption of the nutrients. Hence, the pressure drop and shear stress were function of the flow rate and not of the cell types and their rate constants. Nevertheless, increase in flow rate increased pressure drop and shear stress in both the designs. However, Design 6 showed marginal decrease in pressure drop in all the flow rates. Importantly, the shear stress levels in Design 6 were lower by an order of magnitude relative to Design 1 for similar flow rates. Further shear stress levels were uniform in the region where porous structure was present in Design 6, unlike Design 1 where significantly high level of shear stresses were observed at the inlet and the outlet.

**Table 4.2. Pressure drop and shear stress within the reaction simulations at a variety of different flowrates. 85  $\mu\text{m}$  Pore Size, 120 Pores/ $\text{mm}^2$ , 154 K( $\mu\text{m}^2$ )**

	Design 1						Design 6		
	Chondrocytes			Smooth Muscle Cells					
Flow rate (mL/min)	$\Delta\text{P}$ (Pa)	Max.Shear Stress (dynes/ $\text{cm}^2$ )		$\Delta\text{P}$ (Pa)	Max.Shear Stress (dynes/ $\text{cm}^2$ )		$\Delta\text{P}$ (Pa)	Max.Shear Stress (dynes/ $\text{cm}^2$ )	
		x-direction	y-direction		x-direction	y-direction		x-direction	y-direction
5	276.105	0.0153	0.0174	276.105	0.0153	0.0174	212.612	$3.785 \times 10^{-3}$	$7.513 \times 10^{-4}$
1	55.248	$3.055 \times 10^{-3}$	$3.481 \times 10^{-3}$	55.248	$3.055 \times 10^{-3}$	$3.481 \times 10^{-3}$	42.542	$7.573 \times 10^{-4}$	$1.431 \times 10^{-5}$
0.1	5.525	$3.055 \times 10^{-4}$	$3.481 \times 10^{-4}$	5.525	$3.055 \times 10^{-4}$	$3.481 \times 10^{-4}$	4.254	$7.573 \times 10^{-5}$	$1.431 \times 10^{-6}$
0.01	0.552	$3.055 \times 10^{-5}$	$3.481 \times 10^{-5}$	0.552	$3.055 \times 10^{-5}$	$3.481 \times 10^{-5}$	0.425	$7.573 \times 10^{-6}$	$1.431 \times 10^{-7}$
0.001	0.055	$3.055 \times 10^{-6}$	$3.481 \times 10^{-6}$	0.055	$3.055 \times 10^{-6}$	$3.481 \times 10^{-6}$	0.042	$7.573 \times 10^{-7}$	$1.431 \times 10^{-8}$

### **4.3.3. Effect of permeability on Pressure drop and shear stresses:**

During the course of tissue remodeling, cells proliferate and synthesize matrix elements which are deposited in the porous structures. These processes reduce the pore space available for fluid flow. Hence the pore size decreases but the number of pores per area does not. To understand the implications of these dynamic changes, simulations were carried out with six decreasing pore sizes (from 85  $\mu\text{m}$  to 10  $\mu\text{m}$ ) at constant number of pores per unit area determined experimentally (120 pores/ $\text{mm}^2$ ). These results (**Table 4.3**) showed significant increase in pressure drop across the reactor with decreased pore size. Comparison of results from Design 1 with Design 6 showed that pressure drop in Design 1 was consistently higher than Design 6.

The shear stresses increased in a non-linear manner as the pore sizes decreased. However, the change was not as significant as the pressure drop. Based on Eq.(3.11), shear stress is a function of void fraction, unlike pressure drop. Since, void fraction was kept constant at 85% in these simulations, reduced sensitivity of shear stress to altered pore structure could be void fraction in shear stress. To understand the role of void fraction, simulations were performed by varying the void fraction. These results showed a marginal increase in shear stress with nearly 50% reduction in void fraction.

**Table 4.3 Pressure Drop and Shear Stress within the reaction simulations for decreasing pore size in the reactors at 0.1 mL/min.**

Pore Size ( $\mu\text{m}$ )	Pores/ $\text{mm}^2$	k ( $\mu\text{m}^2$ )	$\epsilon$	Design 1				Design 6			
				Pressure Drop (Pa)	Maximum Shear Stress ( $\mu\text{Pa}$ )		Outlet Oxygen Concentration ( $\text{mol}/\text{m}^3$ )	Pressure Drop (Pa)	Maximum Shear Stress ( $\mu\text{Pa}$ )		Outlet Oxygen Concentration ( $\text{mol}/\text{m}^3$ )
					x-direction	y-direction			x-direction	y-direction	
85	120	154	0.85	5.525	305.5	348.1	0.084	4.254	75.73	14.31	0.07
50	120	18.4	0.85	46.077	308.1	351.6	0.084	35.472	76.23	15.24	0.07
37.5	120	5.82	0.85	145.606	308.3	352.0	0.084	112.114	76.29	16.80	0.07
25	120	1.15	0.85	737.236	373.6	336.8	0.084	567.322	76.32	17.57	0.07
17.5	120	0.276	0.85	3070.54	373.7	336.8	0.084	2363.79	76.33	17.73	0.07
10	120	0.029	0.85	28796.7	373.7	336.8	0.084	22150	76.33	17.78	0.07
85	120	154	0.42	5.534	302.8	344.2					
50	120	18.4	0.086	46.154	305.2	347.5					
37.5	120	5.82	0.036	145.802	305.9	348.6					

#### 4.3.4. Steady state concentration profile of nutrients

To understand the nutrient distribution with consumption, simulations were performed with defined rate laws using both oxygen and glucose rate law data for three cell types namely smooth muscle cells, chondrocytes and hepatocytes. The simulations were performed at the same cell density ( $1.2 \times 10^{12}$  cells/m<sup>3</sup>). These results showed that oxygen being the limiting reactant was consumed much faster than glucose for all cell types in all the reactors [Figure 4.4 and Figure 4.5]. The simulations also show that the oxygen consumption is higher in hepatocytes than in other two cell types. This can be attributed to the fact that hepatocytes are highly metabolic in nature compared to the other two cell types.

Next, we asked the question: what is threshold flow rate at which the outlet oxygen concentration (and glucose) reaches zero. The simulation of concentration profile was started with an experimental flow rate obtained from the RTD studies (Lawrence BJ 2008) as 5 mL/min. This flow rate was reduced by ten folds until a minimum flow rate was reached where the nutrients are completely consumed by the cells. Simulations were performed using flow rates ranging from 0.001 mL/min (very close to static culture) to 5 mL/min. From simulations, for Design 6 the theoretical oxygen limitation was (Figure 4.4) from 0.1 to 0.01 mL/min in case of chondrocytes, 1 to 0.1 mL/min in case of smooth muscle cells and 5 to 1 mL/min in case of hepatocytes.

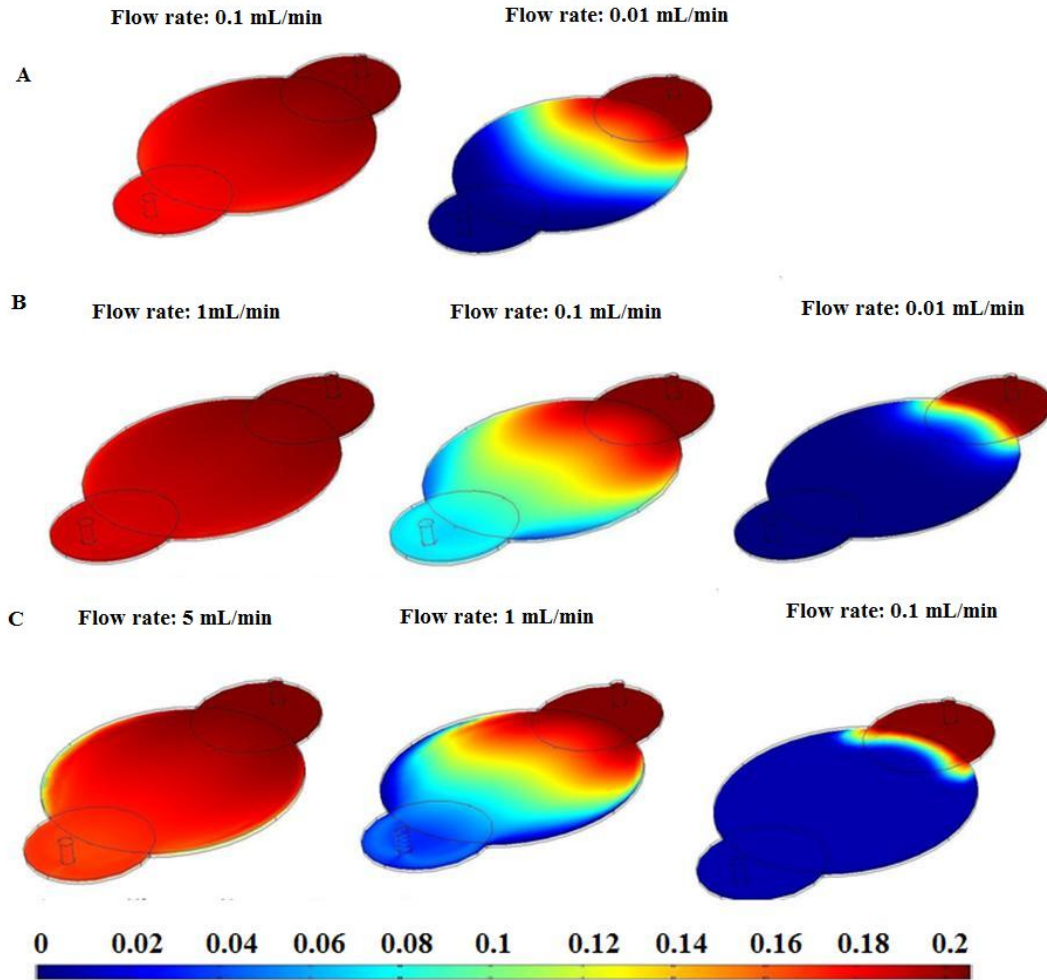


**Figure 4.4.** Oxygen concentration profile across Design 6 at different flow rates (A) Chondrocytes (B) Smooth Muscle Cells (C) Hepatocytes.

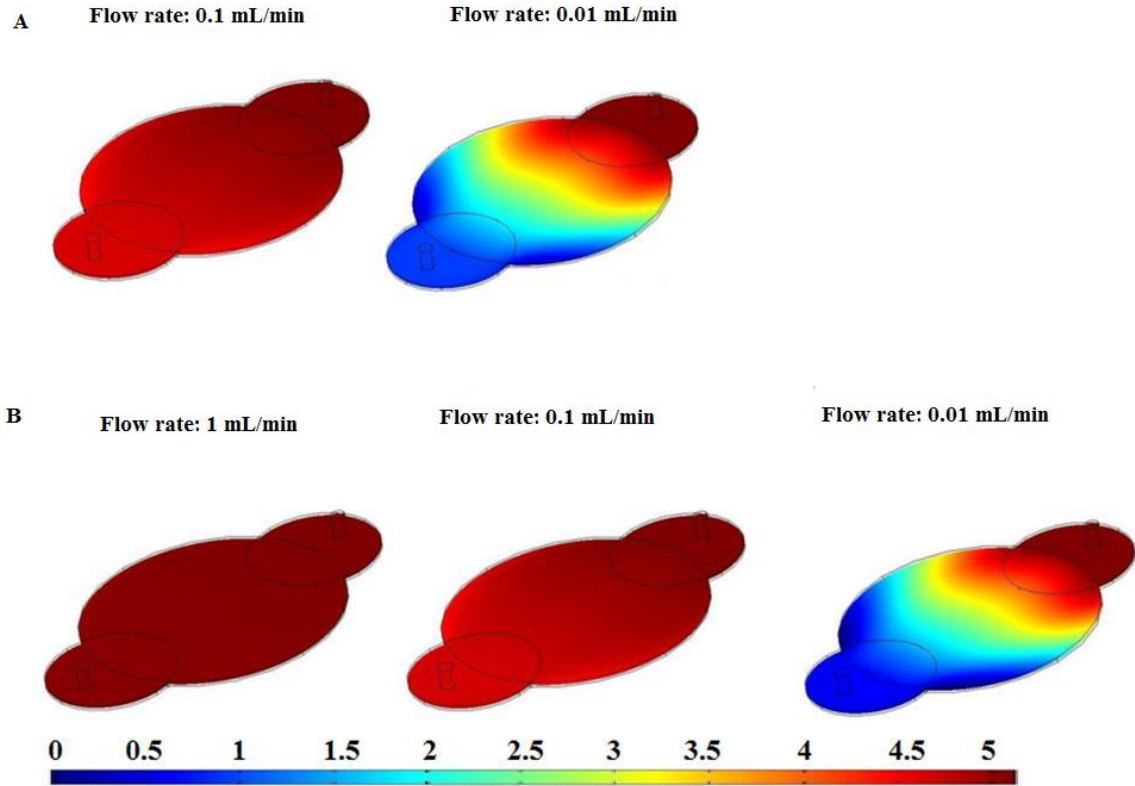


**Figure 4.5.** Glucose concentration profile across Design 6 at different flow rates (A) Chondrocytes (B) Smooth Muscle Cells

#### 4.3.5. Influence of residence time distribution on oxygen consumption for SMCs

The residence time distribution analysis is independent of the metabolic reactions, although the total consumption of nutrients is determined by the residence time. The contact time between cells and the nutrients depends on the residence time of the oxygen in the reactor and the residence time in turn depends on the volume of fluid distribution at constant flow rate. To understand the improvements in fluid distribution in Design 1 and Design 6, concentration of oxygen at the outlet,  $C_{mix}$ , was calculated using

$$C_{mix} = \frac{\sum C_{avg} V_{avg} r \Delta r \Delta \theta}{\sum V_{avg} r \Delta r \Delta \theta}$$

where  $C_{\text{avg}}$  is the average oxygen concentration across the two finite elements and  $V_{\text{avg}}$  is the average velocity in the  $z$ -direction between those elements and  $r, \theta$  were obtained using Cartesian coordinates relations  $r = \sqrt{x^2 + z^2}$  and  $\theta = \tan^{-1}(x/z)$ . Averaging was necessary as the concentration of the nutrients at the exit in Design 1 was not uniform due to the occurrence of reaction in the porous region. These results indicated that the consumption of oxygen was high in Design 6 relative to Design 1; the outlet oxygen concentration was 0.070 mol/min in Design 6 and 0.084 mol/min in Design 1.

Increased consumption could be attributed to improved fluid distribution i.e., with reduced channeling and dead volume. For example, presence of regions with decreased flow rate would reduce the replenishment of nutrients, creating a local minimum in the nutrient concentration. To assess whether the outlet oxygen concentration corresponds to the minimum concentration in the reactor i.e., the ideal fluid flow characteristics, stream line plots of oxygen concentration were generated. These results indicated that both Design 1 and Design 6 had a minimum point (**Figure 4.6**) near the exit of the reactor. There is a significant difference between the two designs in the minimum oxygen concentration and the outlet oxygen concentration: in Design 1, the minimum oxygen concentration was 0.016 mol/min although the outlet concentration was 0.084 mol/min which implies that the medium has enough oxygen but not being utilized completely; in Design 6, the minimum oxygen concentration was 0.046 mol/min which was very close to the outlet oxygen concentration of 0.070 mol/min, implying better utilization of oxygen. Thus the low flow regions were reduced in Design 6, if not completely eliminated. This suggests a significant improvement in fluid flow although one needs to completely eliminate the low flow regions for generating a healthy tissue.

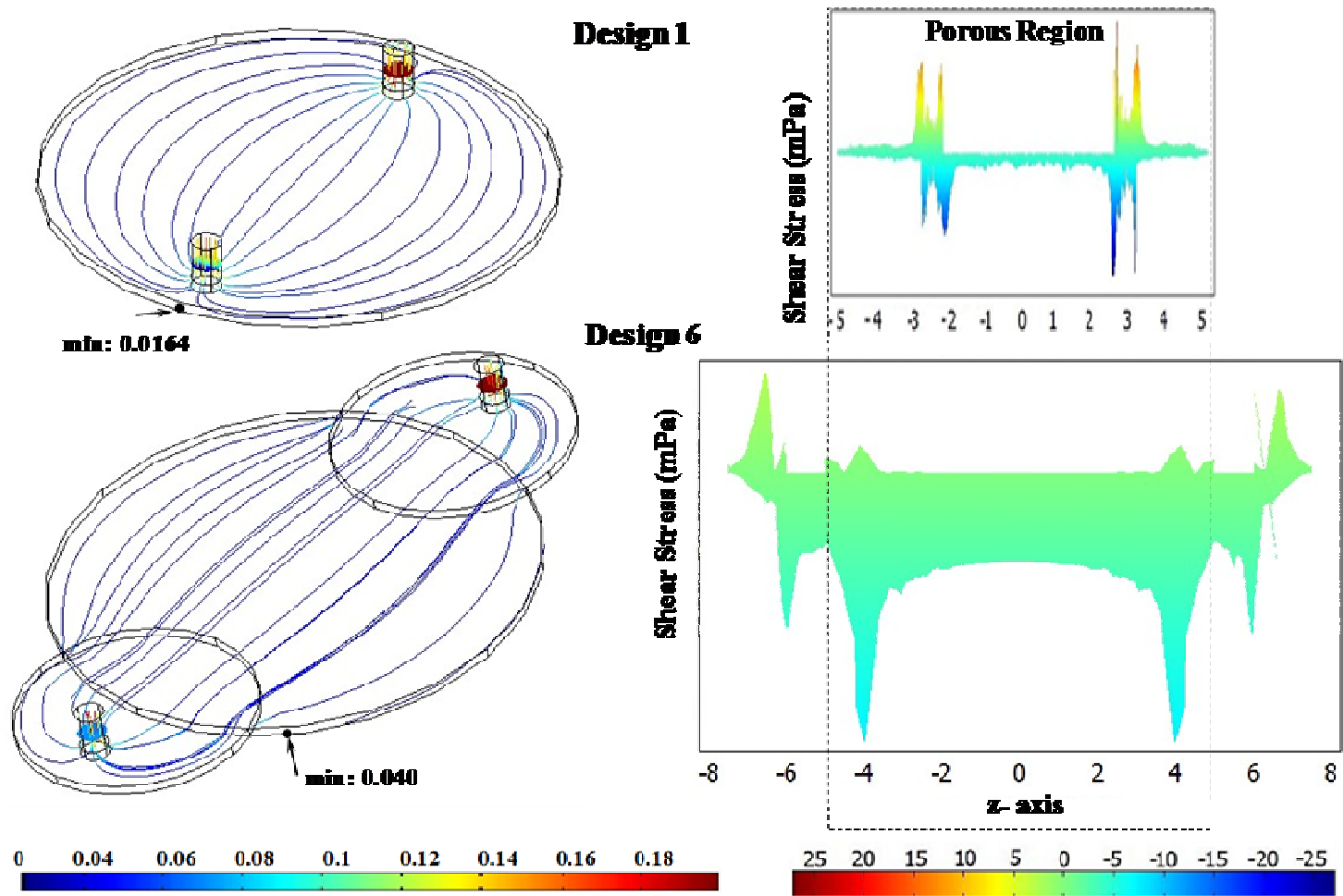


**Figure 4.6.** Comparison of (A) Oxygen outlet concentration (B) shear stress distribution in Design 1 and Design 6

From **Figure 4.6** it is clear that the concentration of the nutrients at the exit in Design 1 is not uniform as the reaction is taking place at that region and hence a difference was observed in the consumption pattern near that region due to the fluid flow. In case of Design 5 the exit concentration seems to be much uniform as there is no consumption taking place near this region. By modifying Design 1 to Design 6 (i) the high stress areas within the porous structure were eliminated and (ii) the low flow regions were reduced. Though the minimum in Design 6 is at the boundary near the porous structure it was observed that the concentration of oxygen is much higher in this case than in Design 1 which implies that the low flow regions have been reduced if not completely eliminated in Design 6. The difference between the minimum concentration in these low flow regions and the outlet concentration showed that there is a huge difference between these two. In case of Design 1 the minimum oxygen concentration is 0.016 mol/min where as the outlet concentration is 0.084 mol/min which implies, the medium is having enough oxygen for the cells to grow but this is not being utilized completely. Whereas in Design 6 the outlet oxygen concentration (0.070 mol/min) and the minimum concentration (0.046 mol/min) are comparable which implies that oxygen is being consumed to the maximum extent. These low flow regions are dependent on the residence time distribution within the reactor. Hence, one needs to have a thorough understanding of this to completely eliminate the low flow regions and thus generate a healthy tissue.

#### **4.3.6 Effect of varying cell density on oxygen consumption**

During tissue regeneration, cells grow and populate the porous structure. This increase in cell number could affect the fluid flow requirement. To understand the effect of increasing cell number on nutrient consumption, simulations were performed by assuming one and two doublings of initial cell seeding density. These results (**Figure 4.7**) showed that concentration of oxygen drastically decreased with increasing cell density of smooth muscle cells at the same flow rate. Regions with insufficient oxygen concentrations were observed in both reactor designs with two doublings in addition to the outlet concentration reaching zero, suggesting a need to increase the fluid flow rate. Thus dynamic changes in the cell population also affect the nutrient requirements. However, changes in cell number (**Table 4.4**) at constant permeability did not alter the pressure drop and shear stress at a constant flow rate. This could be explained by the fact that shear stresses and pressure drop were determined by the Navier-Stokes equation and Brinkman equation, independent of the reaction. Hence, change in cell number did not change shear stress and pressure drop.

**Table 4.4 Effect of Cell density on Pressure Drop, Shear Stress and Outlet oxygen concentration at 85  $\mu\text{m}$  and 25  $\mu\text{m}$  pore size, 120 pores/ $\text{mm}^2$**

			Design 1		Design 6	
Cell Multiplier	Pore Size ( $\mu\text{m}$ )	$\kappa$ ( $\mu\text{m}^2$ )	Minimum Oxygen Concentration ( $\text{mol}/\text{m}^3$ )	Outlet Oxygen Concentration ( $\text{mol}/\text{m}^3$ )	Minimum Oxygen Concentration ( $\text{mol}/\text{m}^3$ )	Outlet Oxygen Concentration ( $\text{mol}/\text{m}^3$ )
1 $\times$	85	154	0.0164	0.084	0.040	0.070
2 $\times$	85	154	$9.679 \times 10^{-4}$	0.036	0.005	0.017
4 $\times$	85	154	<0	0.006	$7.605 \times 10^{-5}$	0.001
1 $\times$	25	1.15	0.017	0.084	0.040	0.070
2 $\times$	25	1.15	$9.677 \times 10^{-4}$	0.036	0.005	0.017
4 $\times$	25	1.15	<0	0.006	$7.794 \times 10^{-5}$	0.001

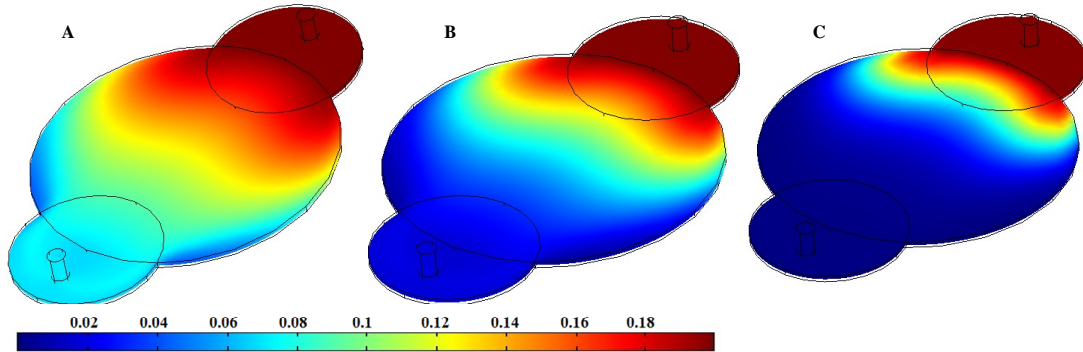


**Figure 4.7.** Effect of Cell density on oxygen consumption (A)  $\rho = 1.2 \times 10^{12}$  cells/ $\text{m}^3$  (B)  $\rho = 2.4 \times 10^{12}$  cells/ $\text{m}^3$  (C)  $\rho = 4.8 \times 10^{12}$  cells/ $\text{m}^3$

#### 4.4. DISCUSSION

This study focused on understanding the fluid distribution with consumption in a flow-through bioreactor system useful in generating large pieces of high quality tissues. In a recent report from our laboratory, the effect of inlet and outlet locations on fluid

distribution was demonstrated (Lawrence et al. 2008). These results showed that presence of inlet and outlet of the reactor directly on top of the porous structure compressed the porous structure. Further, simulation results confirmed a significant increase in shear stresses at the inlet and the outlet of the reactor while performing experiments and in simulation results. Since cells respond to hydrodynamic stress by remodeling their surrounding ECM and change the tissue structure and composition to meet the functional demands (Gooch et al. 2001; Huang et al. 2005a; Waters et al. 2006), it is important to have uniform shear stress distribution in the entire porous structure. To address the uneven shear stress distribution, the reactor was reconfigured by altering the inlet and outlet of the reactor was investigating. Extensions were incorporated to the design by moving the inlet and outlet away from the porous structure region. Design 6 with circular inlet and outlet shape produced uniform shear stress in the porous region.

The pressure drop in the new design was less relative to the previous design (Design 1). Previously, experimentally measured pressure drop has been reported for Design 1. However, the experimental pressure drop varied from 7-9 mmHg (0.930 – 1.20 kPa) which is higher than the simulated value (0.570 kPa) at 5 mL/min flowrate. Nevertheless, these results validated the utility of the computational fluid dynamic simulation. Hence, the effect of nutrient consumption for three different cell types was effectively integrated into the simulations in the next step.

A number of different cell types have been studied under flow conditions in bioreactors to regenerate various tissues including bladder, cartilage, blood vessels, skin, and bone (Botchwey et al. 2003; Hoerstrup et al. 2000; Shito et al. 2001). These structures are located at various anatomical locations with variations in the blood flow

rate. However, there is no comparison of physiological function to metabolic demand which determines the necessary minimum flow rates for each cell type. As such, three different cell types were analyzed via simulation using the rate constants data from literature. These results showed different minimum flow requirements before reaching the nutrient limiting conditions. Chondrocytes are the cells primarily responsible for maintaining cartilage, an avascular tissue whose function is to provide cushioning and lubrication at joints. Smooth muscle cells expand and contract to ensure involuntary movement within the body. Hepatocytes form the metabolic hub of the body and there is significant blood circulation. Chondrocytes are far from the blood supply while smooth muscle cells are near the blood stream. The simulation data confirmed that chondrocytes consumed oxygen and glucose slower than smooth muscle cells, and that the minimum flow rate required for smooth muscle cells is an order of magnitude higher than for chondrocytes. Hepatocytes being highly metabolic consumed oxygen and glucose faster than chondrocytes and smooth muscle cells.

The reconfigured reactor showed improvement in nutrient distribution with consumption. Local minimum was nearer to the outlet concentration. However, these simulations are based on the bulk phase fluid flow by considering diffusivity in water and indicate only the macroscopic gradient. Hence, they do not account for the transport across the cell membrane. Evaluating the microscopic concentration gradient at the cell wall necessary for oxygen to freely diffuse across the cell wall at a specific rate of diffusion as established by Fick's first law is necessary. Importantly, rate constants were obtained from literature which is based on either two-dimensional cultures or cells cultured on gels (Alpert et al. 2002a; Balis et al. 1999; Motterlini et al. 1998a; Sengers et

al. 2005a). However, recent developments in tissue regeneration have demonstrated that cell growth kinetics in three-dimensional cultures is different than two-dimensional cultures (Cukierman et al. 2001; Stephens et al. 2007). Hence, to improve the simulation, one has to assess the glucose and oxygen consumption in three-dimensional cell cultures on substrates under investigation. Further, experimental validation in presence of cells to determine whether those minimum flow rates are sufficient to ensure nutrient distribution is necessary. In addition, one has to determine the effect of flow rate on the quality of the regenerated tissue. Evaluating the microscopic concentration gradient at the cell wall is necessary for oxygen to freely diffuse across the cell wall.

Results also showed a need for changing the flow rate or inlet pressure when tissue regeneration occurs either to ensure due to change in cell number or due to decreased permeability. Thus, one has to consider these factors during the regeneration process using flow-through reactor. Since flow rate is directly coupled to the shear stress cells would experience, one has to assess the utility of the flow-through configuration in tissue regeneration. Nevertheless, one of the limitations to the current study is that change in permeability, void fraction, and rate of oxygen consumption are treated as completely independent phenomena. However, these are interdependent factors which dynamically change during tissue regeneration. Therefore, future work should focus on providing a better understanding of the microscale phenomena that occur during tissue regeneration in order to better couple the changes in reaction rate to changes in the porous structure as cells colonize the scaffold material.

In summary, the new design decreased (i) non-uniformity in hydrodynamic stress within the porous structure and (ii) non-uniform nutrient distribution. One has to

optimize the fluid flow rate based on the type of cell to be colonized. Further, flow rate and pressure drop have to be altered during the regeneration process to ensure uniform nutrient distribution without limitation.

## CHAPTER V

### CONCLUSION AND RECOMMENDATIONS

#### 5.1 CONCLUSIONS

This study utilized a circular parallel plate reactor and evaluated the design requirements for regenerating tissues with high aspect ratio (100 mm diameter to 2 mm thick). The reactor system used has distinct advantages for regenerating large clinically transplantable tissues such as cartilage, bladder and skin; scaffolds can have very large surface area to volume ratios with very small thickness. Conclusions from these studies are summarize below according to the two specific aims

***Specific aim 1: Characterize the flow dynamics of a circular bioreactor containing porous structures.***

1. To understand the flow dynamics within the bioreactor, transient simulations were performed using CFX 11 (ANSYS Inc, Canonsburg, PA) and three different inlet and outlet locations placed directly on top of the porous structure. Analysis of the residence time distribution (RTD) showed that the inlet and outlet locations affect the fluid distribution in terms of channeling and dead volume.
2. The RTD analyses were experimentally validated using a bioreactor configuration and porous structure formed using chitosan solution and controlled rate freezing and lyophilization technique. These results confirmed the RTD results obtained from simulation results.

3. Experimental results showed that presence of inlet and outlet of the reactor directly on top of the porous structure compressed the porous structure. Analysis of fluid distribution in presence of the porous structure modeled using Brinkman equation was also performed in COMSOL software. Assessment of shear stresses developed within the porous structures showed an increase in shear stress at the inlet and the outlet locations in circular reactors.
4. The experimentally measured pressure drop varied from 7-9 mmHg (0.930 – 1.20 kPa) for circular reactors which is slightly higher than the simulated value (0.570 kPa) at 5 mL/min flowrate. This slight increase from simulation results could be attributed to: a) a slightly thicker porous structure than the reactor height in order to anchor the porous structure to the reactor, leading to compression of the structure/pores and increased pressure drop; b) compression of the scaffold due to fluid force, leading to increased pressure drop. These results validated the utility of the computational fluid dynamic simulation.
5. To mimic the tissue regeneration process, simulations were performed by decreasing the pore size at constant number of pores. These results showed significant increase in the pressure drop across the porous structure with decreased pore size (inversely proportional to  $1/\kappa$  as predicted by Brinkman equation). The exponential increase in pressure drop as pore sizes shrink indicates that liquid flow through a porous scaffold will decrease and possibly stop unless flow system is adjusted to provide large pressure gradients. The shear stresses increased in a nonlinear manner as the pore size decreased.

**Specific aim 2: Understand the consumption patterns in the bioreactor and the effect of residence time distribution on the consumption patterns**

1. To address the uneven shear stress distribution, circular reactor was reconfigured by altering the inlet and outlet of the reactor with six different designs. Extensions were incorporated to the design by moving the inlet and outlet away from the porous structure region. From the shear stress distribution and pressure drop analyses, one reactor (Design 6) with semicircular entry and exit design showed uniform shear stress distribution in the absence of porous structures.
2. To understand the nutrient distribution with consumption, simulations were performed using convective diffusion equation in COMSOL Multiphysics software. The effect of oxygen and glucose consumption was effectively integrated into the simulations using Michaelis-Menten rate law with rate constants obtained from literature. The simulation results indicated that the nutrients flow rate requirements for the cells to grow varied for different cell types; the minimum flow rate required for smooth muscle cells was an order of magnitude higher than for chondrocytes. Hepatocytes consumed oxygen and glucose faster than other two cell types.
3. Comparison of the outlet oxygen concentration with the minimum oxygen concentration also suggested improved nutrient distribution in reconfigured circular reactor. The outlet oxygen consumption was 0.084 mol/min and 0.070 mol/min in the old and new designs respectively were as the minimum oxygen concentration was 0.0164 mol/min and 0.046 mol/min.
4. During tissue regeneration, cells grow and populate the porous structure. To understand the implications of change in cell number on fluid flow rate, simulations

were performed using one and two doublings of initial cell seeding density. These results indicated presence of regions with insufficient oxygen concentration at high cell density, in addition to the outlet concentration reaching zero, suggesting a need to increase the fluid flow rate.

## 5.2 RECOMMENDATIONS

1. The simulation studies treated porous structures as rigid porous beds, without incorporating the elastic properties. However, the porous structures are elastic materials. Hence, to improve the simulations one has to incorporate changes in the porous structures due to fluid flow, using elastic properties.
2. In this study, change in permeability, void fraction, and rate of oxygen consumption are treated as completely independent phenomena. However, these are interdependent factors which dynamically change during tissue regeneration. Therefore, to better describe the changing pore size while the tissue is growing, one has to do repeated measurements of cell density and permeability using micro computer tomography at hydrated conditions. These results have to be integrated into the simulation studies.
3. The kinetic parameter  $k_m$  and  $v_m$  taken from the literature are based on either tissue culture plastic surfaces or on hydrogels which have different mechanical and physical properties compared to the porous structures. Recent developments in tissue regeneration have demonstrated that cell growth kinetics in three-dimensional cultures is different than two-dimensional cultures. Thus, to improve the predictions

of the simulation results, one has to incorporate the kinetic data obtained by culturing different cells on the three dimensional porous matrices.

4. Simulation studies showed that reconfigured bioreactor allowed uniform flow distribution (i.e., shear stress) in the entire porous structure. Further minimum flow rates to ensure nutrient distributions were also achieved in three cell types. However, experimental validation is necessary in presence of cells to determine whether those minimum flow rates are sufficient to ensure nutrient distribution. One has to measure cell viability, particularly from regions corresponding to the low oxygen concentration as determined by the simulation results.
5. Increased flow rate increases the shear stress in the microenvironment which could wash away de novo synthesized ECM components or alter cellular responses deleteriously. These changes could lead to poor quality of the regenerated tissue. Hence, one has to determine the effect of flow rate on the quality of the regenerated tissue.
6. Simulations for nutrient consumption were performed on steady state preset fluid distribution using Brinkman equation. Further, only rate kinetic data was used without stoichiometric equation which considers the phase changes in the metabolic reaction. For example, carbon dioxide produced in the reaction may not stay completely in the liquid phase. These changes would affect the density and the viscosity of the medium. To understand the implications of these changes on fluid distribution, performing simulation of flow dynamics and nutrient consumption patterns simultaneously is necessary.

## REFERENCES

- Agrawal CM, McKinney JS, Lanctot D, Athanasiou KA. 2000. Effects of fluid flow on the in vitro degradation kinetics of biodegradable scaffolds for tissue engineering. *Biomaterials* 21(23):2443-52.
- Alpert E, Gruzman A, Totary H, Kaiser N, Reich R, Sasson S. 2002a. A natural protective mechanism against hyperglycaemia in vascular endothelial and smooth-muscle cells: role of glucose and 12-hydroxyeicosatetraenoic acid. *Biochem J* 362(Pt 2):413-22.
- Alpert E, Gruzman A, Totary H, Kaiser N, Reich R, Sasson S. 2002b. A natural protective mechanism against hyperglycaemia in vascular endothelial and smooth-muscle cells: role of glucose and 12-hydroxyeicosatetraenoic acid. *Biochem. J.* 362(2):413-422.
- Altman GH, Lu HH, Horan RL, Calabro T, Ryder D, Kaplan DL, Stark P, Martin I, Richmond JC, Vunjak-Novakovic G. 2002. Advanced Bioreactor with Controlled Application of Multi-Dimensional Strain For Tissue Engineering. *Journal of Biomechanical Engineering* 124(6):742-749.
- Arrigoni C, Chitto A, Mantero S, Remuzzi A. 2008. Rotating versus perfusion bioreactor for the culture of engineered vascular constructs based on hyaluronic acid. *Biotechnol Bioeng.*
- Balis UJ, Behnia K, Dwarakanath B, Bhatia SN, Sullivan SJ, Yarmush ML, Toner M. 1999. Oxygen consumption characteristics of porcine hepatocytes. *Metab Eng* 1(1):49-62.
- Bilgen B bG. 2007. Location of scaffolds in bioreactors modulates the hydrodynamic environment experienced by engineered tissues. *Biotechnol Bioeng* 98(1):282-294.
- Blan NR, Birla RK. 2008. Design and fabrication of heart muscle using scaffold-based tissue engineering. *Journal of Biomedical Materials Research Part A* 86A(1):195-208.
- Bonfield W. 2006. Designing porous scaffolds for tissue engineering. *Philos Transact A Math Phys Eng Sci* 364(1838):227-32.
- Boschetti F, Raimondi MT, Migliavacca F, Dubini G. 2006. Prediction of the micro-fluid dynamic environment imposed to three-dimensional engineered cell systems in bioreactors. *Journal of Biomechanics* 39(3):418-425.
- Botchwey EA, Dupree MA, Pollack SR, Levine EM, Laurencin CT. 2003. Tissue engineered bone: measurement of nutrient transport in three-dimensional matrices. *J Biomed Mater Res A* 67(1):357-67.
- Brown A MB. 2007. Investigating the effects of fluid shear forces on cellular responses to profiled surfaces in-vitro: a computational and experimental investigation. *Conf Proc IEEE Eng Med Biol Soc*:5387-5390.
- Brown A, Meenan BJ. 2007. Investigating the effects of fluid shear forces on cellular responses to profiled surfaces in-vitro: a computational and experimental investigation. *Conf Proc IEEE Eng Med Biol Soc* 2007:5387-90.
- Butler DL, Goldstein SA, Guilak F. 2000. Functional tissue engineering: the role of biomechanics. *J Biomech Eng* 122(6):570-5.
- Capuani F, Frenkel D, Lowe CP. 2003. Velocity fluctuations and dispersion in a simple

- porous medium. *Phys Rev E Stat Nonlin Soft Matter Phys* 67(5 Pt 2):056306.
- Chandy T, Sharma CP. 1990. Chitosan-as a biomaterial. *Biomaterials Artificial Cells and Artificial Organs* 18(1):1-24.
- Chatzizisis YS, Coskun AU, Jonas M, Edelman ER, Feldman CL, Stone PH. 2007. Role of endothelial shear stress in the natural history of coronary atherosclerosis and vascular remodeling: molecular, cellular, and vascular behavior. *J Am Coll Cardiol* 49(25):2379-93.
- Chen H-C, Hu Y-C. 2006. Bioreactors for tissue engineering. *Biotechnology Letters* 28(18):1415-1423.
- Chen KD, Li YS, Kim M, Li S, Yuan S, Chien S, Shyy JYJ. 1999. Mechanotransduction in response to shear stress - Roles of receptor tyrosine kinases, integrins, and Shc. *Journal of Biological Chemistry* 274(26):18393-18400.
- Chung CA, Chen CP, Lin TH, Tseng CS. 2008. A compact computational model for cell construct development in perfusion culture. *Biotechnol Bioeng* 99(6):1535-41.
- Chung CA, Chen CW, Chen CP, Tseng CS. 2007. Enhancement of cell growth in tissue-engineering constructs under direct perfusion: Modeling and simulation. *Biotechnol Bioeng* 97(6):1603-16.
- Cioffi M, Boschetti F, Raimondi MT, Dubini G. 2006. Modeling evaluation of the fluid-dynamic microenvironment in tissue-engineered constructs: A micro-CT based model. *Biotechnology and Bioengineering* 93(3):500-510.
- Cooper JA, Jr., Li WJ, Bailey LO, Hudson SD, Lin-Gibson S, Anseth KS, Tuan RS, Washburn NR. 2007. Encapsulated chondrocyte response in a pulsatile flow bioreactor. *Acta Biomater* 3(1):13-21.
- Cukierman E, Pankov R, Stevens DR, Yamada KM. 2001. Taking cell-matrix adhesions to the third dimension. *Science* 294(5547):1708-1712.
- Cummings LJ, Waters SL. 2007. Tissue growth in a rotating bioreactor. Part II: fluid flow and nutrient transport problems. *Math Med Biol* 24(2):169-208.
- Fogler H. 2006a. *Elements of Chemical Reactor Engineering*. Upper Saddle River, NJ: Prentice Hall.
- Fogler HS. 2006b. *Elements of Chemical Reactor Engineering*. Upper Saddle River, NJ: Prentice Hall.
- Freed LE, Vunjaknovakovic G, Biron RJ, Eagles DB, Lesnoy DC, Barlow SK, Langer R. 1994. Biodegradable polymer scaffolds for tissue engineering. *Bio-Technology* 12(7):689-693.
- Freyman T YI, Gibson L. 2001. Cellular materials as porous scaffolds for tissue engineering. *Prog Mater Sci* 46:273-82.
- Goldstein AS, Juarez TM, Helmke CD, Gustin MC, Mikos AG. 2001. Effect of convection on osteoblastic cell growth and function in biodegradable polymer foam scaffolds. *Biomaterials* 22(11):1279-88.
- Gooch KJ, Kwon JH, Blunk T, Langer R, Freed L, Vunjak-Novakovic EG. 2001. Effects of mixing intensity on tissue-engineered cartilage. *Biotechnology and Bioengineering* 72(4):402-407.
- Grad S, Gorna K, Gogolewski S, Alini M. 2004. Scaffolds for Cartilage Tissue Engineering: Effect of Pore Size. *European Cells and Materials* 7(2).
- Grashow J, Yoganathan A, Sacks M. 2006. Biaxial Stress–Stretch Behavior of the Mitral Valve Anterior Leaflet at Physiologic Strain Rates. *Annals of Biomedical*

- Engineering 34(2):315-325.
- Gray ML, Pizzanelli AM, Grodzinsky AJ, Lee RC. 1988. Mechanical and physicochemical determinants of the chondrocyte biosynthetic response. *Journal of Orthopaedic Research* 6(6):777-792.
- Griffon DJ, Sedighi MR, Schaeffer DV, Eurell JA, Johnson AL. 2006. Chitosan scaffolds: Interconnective pore size and cartilage engineering. *Acta Biomaterialia* 2(3):313-320.
- Gutierrez RA, Crumpler ET. 2008. Potential effect of geometry on wall shear stress distribution across scaffold surfaces. *Ann Biomed Eng* 36(1):77-85.
- Hayashi T. 1994. Biodegradable polymers for biomedical uses. *Progress in Polymer Science* 19(4):663-702.
- Heydarkhan-Hagvall S, Esguerra M, Helenius G, Sapperberg R, Johansson BR, Risberg B. 2006. Production of Extracellular Matrix Components in Tissue-Engineered Blood Vessels. *Tissue Engineering* 12(4):831-842.
- Hoerstrup SP, Sodian R, Sperling JS, Vacanti JP, Mayer JE, Jr. 2000. New pulsatile bioreactor for in vitro formation of tissue engineered heart valves. *Tissue Eng* 6(1):75-9.
- Hollister SJ. 2006. Porous scaffold design for tissue engineering (vol 4, pg 518, 2005). *Nature Materials* 5(7):590-590.
- Huang Y, Onyeri S, Siewe M, Moshfeghian A, Madihally SV. 2005a. In vitro characterization of chitosan-gelatin scaffolds for tissue engineering. *Biomaterials* 26(36):7616-27.
- Huang Y, Onyeri S, Siewe M, Moshfeghian A, Madihally SV. 2005b. In vitro characterization of chitosan-gelatin scaffolds for tissue engineering. *Biomaterials* 26(36):7616-7627.
- Huang Y, Siewe M, Madihally SV. 2006. Effect of spatial architecture on cellular colonization. *Biotechnol Bioeng* 93(1):64-75.
- Hutmacher DW, Singh H. 2008. Computational fluid dynamics for improved bioreactor design and 3D culture. *Trends Biotechnol* 26(4):166-72.
- Ishaug-Riley SL, Crane-Kruger GM, Yaszemski MJ, Mikos AG. 1998. Three-dimensional culture of rat calvarial osteoblasts in porous biodegradable polymers. *Biomaterials* 19(15):1405-1412.
- Jaasma MJ, Plunkett NA, O'Brien FJ. 2008. Design and validation of a dynamic flow perfusion bioreactor for use with compliant tissue engineering scaffolds. *J Biotechnol* 133(4):490-6.
- Jeong SI, Kwon JH, Lim JI, Cho SW, Jung Y, Sung WJ, Kim SH, Kim YH, Lee YM, Kim BS and others. 2005. Mechano-active tissue engineering of vascular smooth muscle using pulsatile perfusion bioreactors and elastic PLCL scaffolds. *Biomaterials* 26(12):1405-11.
- Kannan RY, Salacinski HJ, Butler PE, Hamilton G, Seifalian AM. 2005. Current status of prosthetic bypass grafts: A review. *Journal of Biomedical Materials Research Part B-Applied Biomaterials* 74B(1):570-581.
- Kim BS, Nikolovski J, Bonadio J, Mooney DJ. 1999. Cyclic mechanical strain regulates the development of engineered smooth muscle tissue. *Nat Biotechnol* 17(10):979-83.
- Koller MR, Bender JG, Miller WM, Papoutsakis ET. 1993. Expansion of primitive

- human hematopoietic progenitors in a perfusion bioreactor system with IL-3, IL-6, and stem cell factor. *Biotechnology (N Y)* 11(3):358-63.
- Lawrence B, Beene J, Madihally S, Lewis R. 2004. Incorporating Nonideal Reactors in a Junior-Level Course using Computational Fluid Dynamics (CFD). *Chemical Engineering Education* 38(2):136-141.
- Lawrence BJ, Devarapalli M, Madihally SV. 2008. Flow dynamics in bioreactors containing tissue engineering scaffolds. *Biotechnol Bioeng*.
- Lawrence BJ DM, Madihally SV. 2008. Flow Dynamics in Bioreactors Containing Tissue Engineering Scaffolds. *Biotechnology/Bioengineering*.
- Lawrence BJ, Madihally SV. 2008. Cell colonization in degradable 3D porous matrices. *Cell Adhesion & Migration* 2-1:9-16.
- Lichtenberg A, Dumlu G, Walles T, Maringka M, Ringes-Lichtenberg S, Ruhparwar A, Mertsching H, Haverich A. 2005. A multifunctional bioreactor for three-dimensional cell (co)-culture. *Biomaterials* 26(5):555-62.
- Lisa Christenson AGM, Donald F. Gibbons, Grace Lee Picciolo. 1997. Biomaterials for Tissue Engineering: Summary. *Tissue Engineering* 3(1):71-76.
- Lo CM, Wang HB, Dembo M, Wang YL. 2000. Cell movement is guided by the rigidity of the substrate. *Biophys J* 79(1):144-52.
- Macario DK, Entersz I, Paul Abboud J, Nackman GB. 2007. Inhibition of Apoptosis Prevents Shear-Induced Detachment of Endothelial Cells. *J Surg Res*.
- Madihally SV, Matthew HWT. 1999. Porous chitosan scaffolds for tissue engineering. *Biomaterials* 20(12):1133-1142.
- Marois Y, Sigot-Luizard MF, Guidoin R. 1999. Endothelial cell behavior on vascular prosthetic grafts: Effect of polymer chemistry, surface structure, and surface treatment. *Asaio Journal* 45(4):272-280.
- Marolt D, Augst A, Freed LE, Vepari C, Fajardo R, Patel N, Gray M, Farley M, Kaplan D, Vunjak-Novakovic G. 2006. Bone and cartilage tissue constructs grown using human bone marrow stromal cells, silk scaffolds and rotating bioreactors. *Biomaterials* 27(36):6138-49.
- Martin I, Wendt D, Heberer M. 2004. The role of bioreactors in tissue engineering. *Trends in Biotechnology* 22(2):80-86.
- Martin Y, Vermette P. 2005. Bioreactors for tissue mass culture: Design, characterization, and recent advances. *Biomaterials* 26(35):7481-7503.
- Motterlini R, Kerger H, Green CJ, Winslow RM, Intaglietta M. 1998a. Depression of endothelial and smooth muscle cell oxygen consumption by endotoxin. *Am J Physiol* 275(3 Pt 2):H776-82.
- Motterlini R, Kerger H, Green CJ, Winslow RM, Intaglietta M. 1998b. Depression of endothelial and smooth muscle cell oxygen consumption by endotoxin. *Am J Physiol Heart Circ Physiol* 275(3):H776-782.
- Niklason LE, Gao J, Abbott WM, Hirschi KK, Houser S, Marini R, Langer R. 1999. Functional Arteries Grown in Vitro. *Science* 284(5413):489-493.
- Olteanu CE, Enescu D. 2007. Chitosan involved tissue engineering and regenerative medicine. *Romanian Biotechnological Letters* 12(3):3217-3233.
- Palsson BO, Paek SH, Schwartz RM, Palsson M, Lee GM, Silver S, Emerson SG. 1993. Expansion of human bone marrow progenitor cells in a high cell density continuous perfusion system. *Biotechnology (N Y)* 11(3):368-72.

- Palsson C-APaBO. 1996. Cell Growth and Differentiation on Feeder Layers Is Predicted to be influenced by Bioreactor Geometry. *Biotechnol Bioeng* 50:479-492.
- Papadaki M, Eskin SG, Ruef J, Runge MS, McIntire LV. Fluid shear stress as a regulator of gene expression in vascular cells: possible correlations with diabetic abnormalities; 1999. p 89-99.
- Phillips JE, Hutmacher DW, Guldberg RE, Garcia AJ. 2006. Mineralization capacity of Runx2/Cbfa1-genetically engineered fibroblasts is scaffold dependent. *Biomaterials* 27(32):5535-45.
- Porter B, Zauel R, Stockman H, Guldberg R, Fyhrie D. 2005a. 3-D computational modeling of media flow through scaffolds in a perfusion bioreactor. *Journal of Biomechanics* 38(3):543-549.
- Porter B, Zauel R, Stockman H, Guldberg R, Fyhrie D. 2005b. 3-D computational modeling of media flow through scaffolds in a perfusion bioreactor. *J Biomech* 38(3):543-9.
- Porter B ZR, Stockman H, Guldberg R, Fyhrie D. 2005. 3-D computational modelig of media flow through scaffolds in a perfusion bioreactor. *J Biomech* 38(3):543-549.
- Prabaharan M. 2008. Chitosan derivatives as promising materials for controlled drug delivery. *Journal of Biomaterials Applications* 23(1):5-36.
- Raghunath J, Rollo J, Sales KM, Butler PE, Seifalian AM. 2007. Biomaterials and scaffold design: key to tissue-engineering cartilage. *Biotechnology and Applied Biochemistry* 46:73-84.
- Raimondi MT, Moretti M, Cioffi M, Giordano C, Boschetti F, Lagana K, Pietrabissa R. 2006. The effect of hydrodynamic shear on 3D engineered chondrocyte systems subject to direct perfusion. *Biorheology* 43(3-4):215-22.
- S Grad KG, S.Gogolewski, M.Alini. 2004. Scaffolds for Cartilage Tissue Engineering: Effect of Pore Size. *European Cells and Materials* 7(2).
- Salerno A, Oliviero M, Di Maio E, Iannace S, Netti PA. 2007. Design and preparation of mu-bimodal porous scaffold for tissue engineering. *Journal of Applied Polymer Science* 106(5):3335-3342.
- Sander EA, Nauman EA. 2003. Permeability of musculoskeletal tissues and scaffolding materials: experimental results and theoretical predictions. *Critical Reviews in Biomedical Engineering* 31(1):1-26.
- Sander EA NE. 2003. Permeability of musculoskeletal tissues and scaffolding materials: Experimental results and theoretical predictions. *Crit Rrev Biomed Eng* 31(1):1-26.
- Sarasam A, Madihally SV. 2005. Characterization of chitosan-polycaprolactone blends for tissue engineering applications. *Biomaterials* 26(27):5500-5508.
- Sarasam AR, Krishnaswamy RK, Madihally SV. 2006. Blending chitosan with polycaprolactone: Effects on physicochemical and antibacterial properties. *Biomacromolecules* 7(4):1131-1138.
- Sengers BG, Heywood HK, Lee DA, Oomens CW, Bader DL. 2005a. Nutrient utilization by bovine articular chondrocytes: a combined experimental and theoretical approach. *J Biomech Eng* 127(5):758-66.
- Sengers BG, Heywood HK, Lee DA, Oomens CWJ, Bader DL. 2005b. Nutrient Utilization by Bovine Articular Chondrocytes: A Combined Experimental and Theoretical Approach. *Journal of Biomechanical Engineering* 127(5):758-766.

- Shito M, Kim NH, Baskaran H, Tilles AW, Tompkins RG, Yarmush ML, Toner M. 2001. In vitro and in vivo evaluation of albumin synthesis rate of porcine hepatocytes in a flat-plate bioreactor. *Artif Organs* 25(7):571-8.
- Sikavitsas VI, Bancroft GN, Holtorf HL, Jansen JA, Mikos AG. 2003. Mineralized matrix deposition by marrow stromal osteoblasts in 3D perfusion culture increases with increasing fluid shear forces. *Proc Natl Acad Sci U S A* 100(25):14683-8.
- Sikavitsas VI, Bancroft GN, Lemoine JJ, Liebschner MA, Dauner M, Mikos AG. 2005. Flow perfusion enhances the calcified matrix deposition of marrow stromal cells in biodegradable nonwoven fiber mesh scaffolds. *Ann Biomed Eng* 33(1):63-70.
- Sodian R, Hoerstrup SP, Sperling JS, Daebritz SH, Martin DP, Schoen FJ, Vacanti JP, Mayer JE. 2000. Tissue engineering of heart valves: in vitro experiences. *The Annals of Thoracic Surgery* 70(1):140-144.
- Stephens JS, Cooper JA, Phelan FR, Jr., Dunkers JP. 2007. Perfusion flow bioreactor for 3D in situ imaging: investigating cell/biomaterials interactions. *Biotechnol Bioeng* 97(4):952-61.
- Takahashi M, Berk BC. 1996. Mitogen-activated protein kinase (ERK1/2) activation by shear stress and adhesion in endothelial cells. Essential role for a herbimycin-sensitive kinase. *J Clin Invest* 98(11):2623-31.
- Thomson RC, Yaszemski MJ, Powers JM, Mikos AG. 1995. Fabrication of biodegradable polymer scaffolds to engineer trabecular bone. *Journal of Biomaterials Science-Polymer Edition* 7(1):23-38.
- Tillman J, Ullm A, Madihally SV. 2006a. Three-dimensional cell colonization in a sulfate rich environment. *Biomaterials* 27(32):5618-5626.
- Tillman J, Ullm A, Madihally SV. 2006b. Three-dimensional cell colonization in a sulfate rich environment. *Biomaterials* 27(32):5618-26.
- Timmins NE, Scherberich A, Fruh J-A, Heberer M, Martin I, Jakob M. 2007. Three-Dimensional Cell Culture and Tissue Engineering in a T-CUP (Tissue Culture Under Perfusion). *Tissue Engineering* 13(8):2021-2028.
- Truskey GA, Yuan F, Katz DF. 2004. *Transport Phenomena in Biological Systems*. Upper Saddle River, NJ: Pearson Prentice Hall. p 317-321.
- Waters SL, Cummings LJ, Shakesheff KM, Rose FR. 2006. Tissue growth in a rotating bioreactor. Part I: mechanical stability. *Math Med Biol* 23(4):311-37.
- Williams KA, Saini S, Wick TM. 2002. Computational Fluid Dynamics Modeling of Steady-State Momentum and Mass Transport in a Bioreactor for Cartilage Tissue Engineering. *Biotechnol. Prog.* 18(5):951-963.
- Williams KA SS, Wick TM. 2002. Computational fluid dynamics modeling of steady-state momentum and mass transport in a bioreactor for cartilage tissue engineering. *Biotechnol Prog* 18(5):951-963.
- Yannas IV, Lee E, Orgill DP, Skrabut EM, Murphy GF. 1989. Synthesis and characterization of a model extracellular matrix that induces partial regeneration of adult mammalian skin. *Proc Natl Acad Sci U S A* 86(3):933-7.

## APPENDICES

### APPENDIX A: CFX Manual

This is a modified version of “building and running a CFX model” from Benjamin J. Lawrence.

#### A.1. Creating Geometry:

1. **Start > All programs > Select ANSYS Workbench.**
2. From the **New** section, Click on **Empty project**. Project page will appear containing **unsaved project**.
3. Go to **File > Save** and save the project as **DiscReactor.wbdb** in a new directory.  
(Make sure to create a new working directory. The directory should not be located on desktop or contain spaces.)
4. At the left side of the project page, Click on **New geometry**. This will open up a designer modeler page. In the pop up window select millimeters as the desired units.  
The designer Modeler window has four main areas as show below:

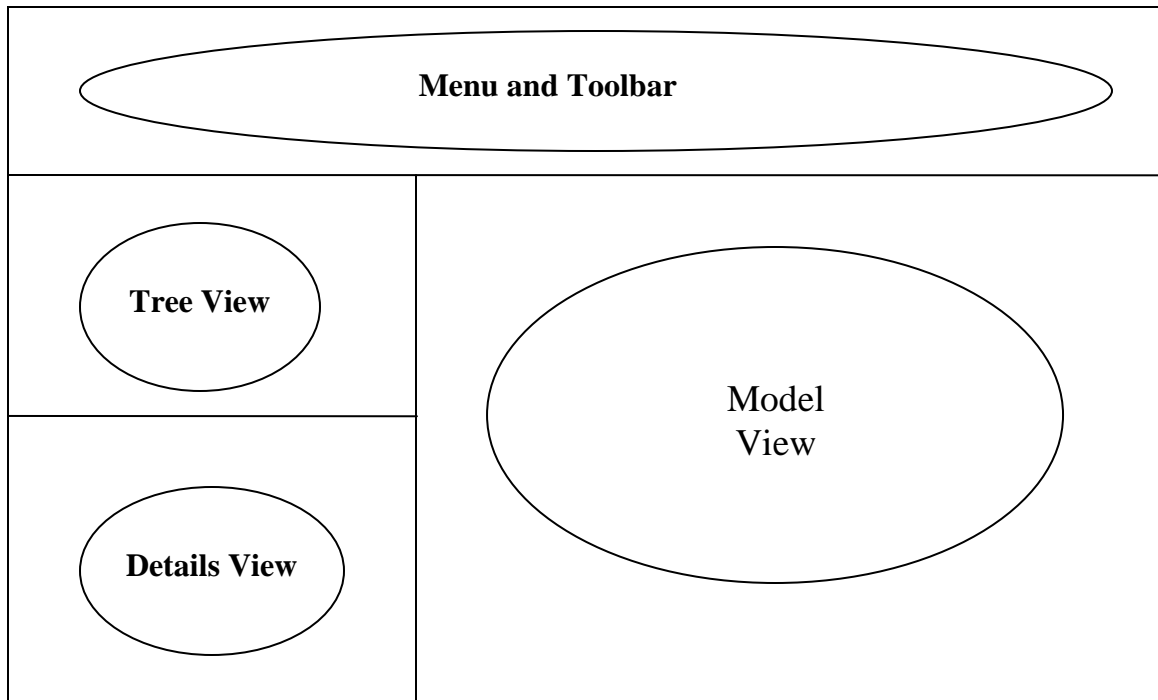


**Figure A.1:** Outline of the CFX designer modeler window.

5. Select the **ZX plane** in the **Tree View** (**Figure A 1**) on which the sketch is based.
6. **Sketching> Settings>Grid> turn on 2D & Snap.**
7. **Major grid spacing: 20 mm**
8. **Minor-Steps per each major: 10**
9. **Sketching> draw> circle**
10. Create a circle of 100 mm diameter.
11. **Sketching>dimension>Click on diameter.** Now, click on the circle and then anywhere inside the circle. The diameter of the circle is labeled as **D1**, this doesn't affect the design, and it's just to indicate the dimensions. In modeling adjust **D1: 100mm** press **Enter** in the keyboard to change the D1 value.

12. Click on **Extrude** from the 3D feature toolbar. In the **Details View** which is to the bottom left of the window, change the **depth** to **2 mm**. click on **generate** button (which is to the left of the Extrude button in the 3D Feature toolbar.)to extrude the operation.( other way of extruding is to right click on the **Extrude1** in **Tree View** and click on **Generate**)
13. To the left side, in the **Tree View** click on the plus sign next to **1 part, 1 body**. Position the cursor on **Solid**. Now, **right click** and select **hide body**.
14. Select **ZX Plane** in the tree view, create a **new sketch** by click on the new sketch button (this new sketch button is to the left of the extrude button in the 3D feature toolbar).
15. Create a circle with center at  $x = 24$  mm,  $z = 28$  mm from the origin. The diameter of the circle is 6 mm. set the diameter as done before. Click **Extrude** button in the 3D feature toolbar.
16. Click on **Extrude2** in the tree view, at the bottom left corner we can see **Details View**, Select **Base Object** and change to **Sketch2**, change the **depth** to **10 mm**.Click on **directions** and select **Reverse**. Click on generate button to extrude the operation
17. Similarly, select **ZX plane** again, select **new sketch** and **draw a circle** with the center at  $x = -28$  mm and  $z = -28$  mm. Adjust the diameter of the circle to 6 mm. Click Extrude. Click on **Extrude3** in the **Tree View**, to the bottom left corner select **Details View, Base Object> Sketch3** set the **depth 10mm**, change the **direction** to **Normal** and click on **generate**.
18. Click on the plus sign beside the **(1 part, 1 Body)> Solid> Show Body**.
19. The geometry is now complete. Click on **File> Save**.(save the file as DiscReactor)

## A.2. Generating CFX Mesh:

1. On the ANSYS Workbench window now we can see two tabs **DiscReactor (Project)**, **DiscReactor (DesignerModeler)**. Click on the **DiscReactor (Project)** and go to the project page, to the left side of this page now we can see a new entry called as **Generate CFX Mesh**. Click on this.
2. A new tab will be opened as CFXMesh; this will look somewhat similar to the designer modeler. But, if we see the tree view to the top left side we would feel the difference between designer modeler and CFX Mesh.
3. Set up the 2D Regions. **Right click** over **Regions** in **Tree View**. Select **Insert> Composite 2D Region**. A new object, **composite 2D Region1** will be inserted under regions in Tree View. In **Details View**, We can see two buttons next to the **location**, **Apply** and **Cancel**. Click on the circular face that is extruded normal to the ZX plane. Now click **Apply**. **Right click** on the **composite 2D region1** in the **Tree View** and select **Rename**. Name the region as **inlet**.
4. Similarly create another Composite 2D region for the circular face that is extruded reverse to the ZX plane and name it as **outlet**.
5. The remaining faces will be automatically assigned to the 2D region names as **Default 2D Region**.
6. Click on **Mesh>Spacing>Default Body Spacing >** In the Details View change **Maximum Spacing: 1** and press **Enter** in the keyboard to see the change. Select **Inflation** and change the value to 1.2
7. Leave the remaining settings as default.

8. In the toolbar Click on **Go> Generate All surface Meshes**. After all the surface meshes are created. Click on **Go> generate Volume Mesh**.
9. Click on **Options** in **Tree View** change the name of the file from **unnamed.gtm** to **DiscReactor.gtm**. Go to **File > Save**.
10. The mesh is now complete(**Figure A.2 and Figure A.3**).

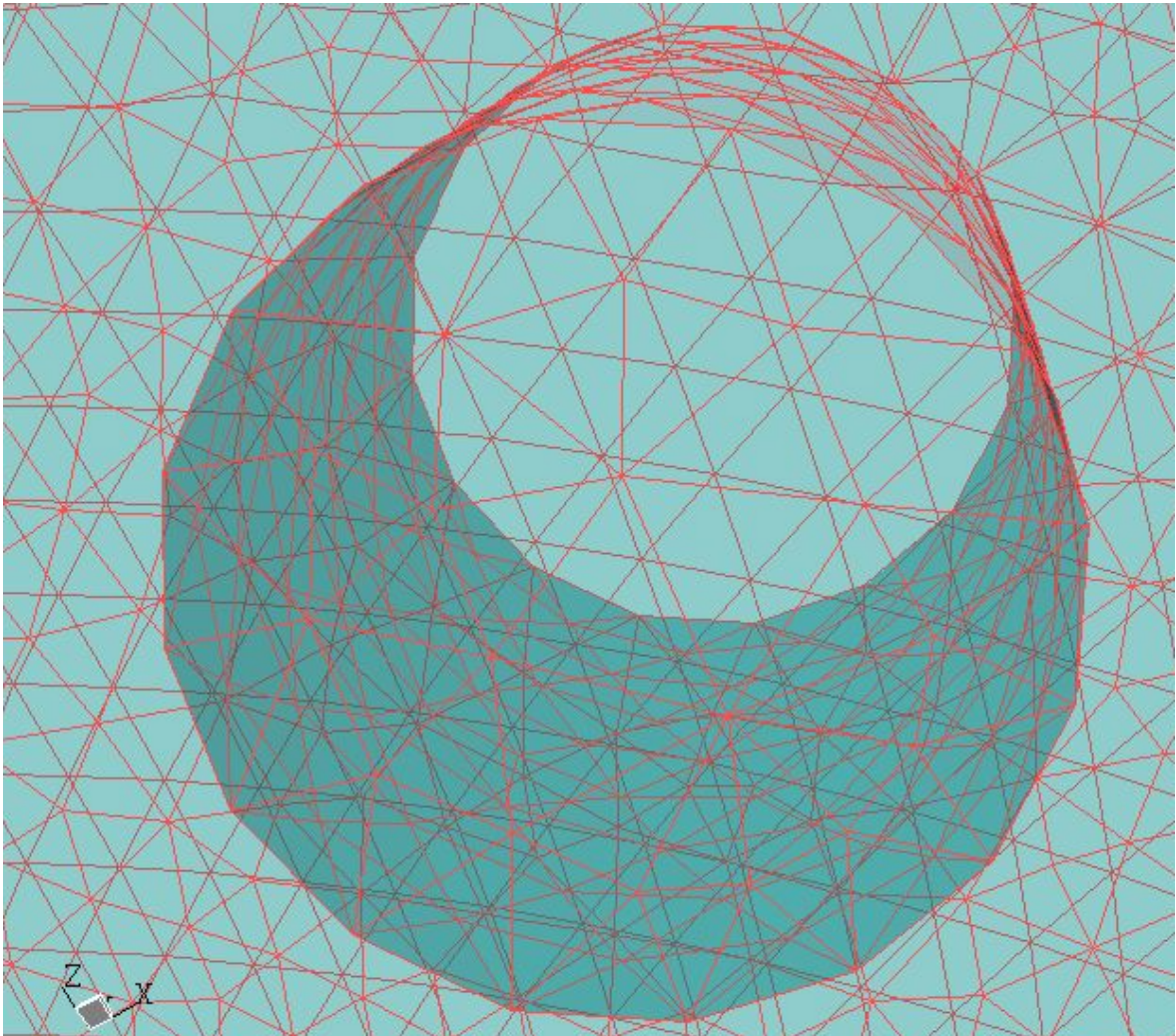


**Figure A.2:** Snapshot of the reactor mesh in the CFX Mesh. The Maximum body spacing is 1 mm, Angular resolution is 30°, and Minimum edge length is 0.265 mm and maximum edge length is 5.3 mm.

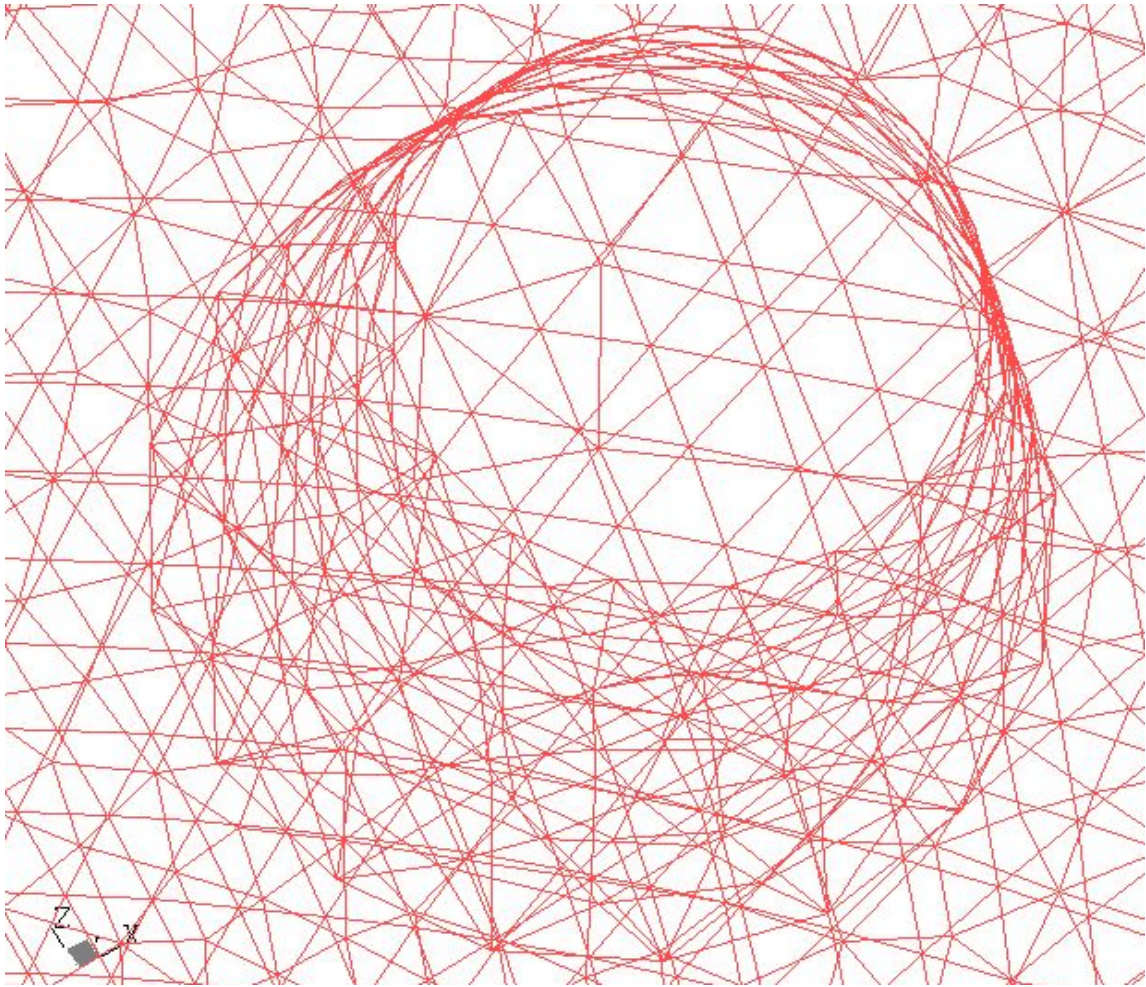


**Figure A.3:** Snapshot of the reactor wire mesh.

11. Go back to the project window and select **File> Save** to save the CFX-Mesh database as **DiscReactor.cmdb** in the same directory as the other project files.

12. Now, we can see three tabs at the top of the ANSYS Workbench: **DiscReactor [Project]**, **DiscReactor [DesignerModeler]** and **DiscReactor [CFXMesh]**.

13. In the project window Select **File> Save all** and then **Exit**.

### **1.3. Creating boundary conditions in CFX Pre:**

1. Click on **Open Simulation** file. Select the **DiscReactor.gtm** file and then Click **Open**.

2. Click on **Materials** tab, select Water and then Click on the **Duplicate** button( it will be similar to the copy button that we see in MS Word)
3. Click on **Physics** tab, Define the **Simulation Type** as **Steady State** and Click **OK**.
4. On the top in the toolbar click on  icon to **create a domain**. A window pops up. Name the domain(say Domain1) and click OK.
5. In the **Physics** tab we can see **Domain** in the **Tree View**, click on it. A window pops up. Click **General Options> Fluid List>** Choose **Water** and **Tracer**. Click on **Fluid Models> Check Homogeneous Model for both Multiphase and Heat transfer Model**. Leave the rest as default values. Click OK.

### 1.3.1. Inlet boundary condition:

1. Click on  icon in the toolbar to Create inlet Boundary condition. Name the Boundary as Inlet and Click OK. A Inlet boundary conditions window will pop up.
2. In **Basic Settings** tab > Select **Boundary type > Inlet** and **Location> Inlet**.
3. In **Boundary Details** tab> **Flow Regime>subsonic. Mass and momentum>** Select **Bulk mass flow rate** (set the mass flow rate as 0.0026 kg/s). Leave the rest as default.
4. In Fluid values tab > click on Tracer volume fraction> set automatic with value as 0 and water volume fraction> set automatic with value as 1. Click OK.

### 1.3.2. Outlet boundary condition:

1. Click on  icon in the toolbar to Create outlet Boundary condition. A window will pop up. Name the boundary as Outlet and Click OK. A outlet boundary conditions window will pop up.
2. In **Basic Settings** tab > select **Boundary type**> **Outlet** and **Location** > **Outlet**.
3. In **Boundary Details** tab> **Flow Regime**> **Subsonic. Mass and momentum**> **bulk mass flow rate** (set the mass flow rate to 0.0026 kg/s). Click OK.

### 1.3.3. Wall boundary condition:

1. Click on  icon in the toolbar to Create Boundary condition. Name the boundary as wall. Click OK. A Wall Boundary conditions window will pop up.
2. In **Basic Settings** tab> **Boundary type**> **Wall** and select **location**>**Default Boundary conditions**.
3. In **Boundary Details** tab > Select **No Slip, Smooth wall**. Click OK.

### 1.3.4. Global Initialization:

1. Click on  icon in the toolbar to do Global Initialization.
2. In **Global Settings** tab> Turn on **Turbulent Eddy Dissipation**. Leave the rest as defaults.
3. In **Fluid Settings** tab > Select **Tracer Volume Fraction as 0** and Select **Water Volume Fraction as 1**.
4. Leave the rest as defaults( i.e.; **Solver Control, Results**)

5. Go to **File > Click on Write Solver File**. Add a file name as “**DiscReactor.def**” and Click OK. Solver manager window will pop up. Click OK and start the run.(make sure that the DiscReactor.def file is loaded in the Solver Manager before running the solver)
6. After the solver runs the simulations successfully the results file is saved in the working directory with **.res** extension.( the file name would probably be DiscReactor\_001.res)

#### **A.4. Modifying the Simulation for Transient Flow:**

1. In CFX Pre, go to **File> Open> DiscReactor.def. File > Save As> DiscReactor\_trans.def**
2. Change **Simulation type > Basic Settings> Options> Transient**.
3. Set the **time duration** as 20 s. **number of time steps** as 12 and **time duration between each time step** as 1 s.
4. **Physics tab > In Inlet boundary Conditions > Change Volume fraction of tracer as 1 and Volume fraction of water as 0.**
5. **Global Initialization > Fluid Settings> Change the volume fractions of water and tracer as automatic.**
6. **Physics tab> Results > Output Control> Transient Results> Create Transient Results File.** Select **time interval** as 1sec. (this will allow us to record the data for each time step)
7. Go to File > write solver file. Add file name as DiscReactor\_trans.def , Click OK.

#### A.5. Write a Solver file:

1. Open the CFX Solver Browse **DiscReactor\_trans.def** file
2. **Initial Values file** > Browse the **Steady State results file** from the working directory
3. Click OK and start the Run.
4. The Transient results file is saved in the working directory as DiscReactor\_trans\_001.res

#### A.6. Posting the Results in CFX Post:

1. File > Load Results
2. In the toolbar search for  icon. Click on it to “create a line”. To the right of this icon there is “create a plane” icon. Click on it to create a plane. In the same row we can see icons like “contour plot”, “streamlines” et al.
3. After clicking on “**create a plane**” icon, a window will pop up. Name the plane (say **Plane1**) and Click OK. Create a ZX plane near the exit at  $y=-9\text{mm}$  distance.
4. To create a contour plot. Click on Contour plot icon in the toolbar. Then Select the domain as Domain1. Select the plane as Plane1. Select the variable for which a contour plot is to be drawn (say tracer.volumefraction). In the toolbar search for an icon that looks like a “clock”. Click on it. A window will pop up with 20 time steps, to see the contour plot for different time steps click on a particular time step and then click OK. We can see the colors changing in the Model view for each time step.
5. Go to **File> Export**. Name the file (say DiscReactor\_20.csv for 20<sup>th</sup> time step) Select **Plane1**. Select the variables (say tracer.superficial velocity, tracer.volumefraction). Click OK.

6. A .csv file will be created and saved in the working directory. Go to the working directory and click on this file to see the results in MS Excel. In order to do any modifications and further calculations save the file using “Save As” and Save the .csv file as .xls file)
7. Do the same for the rest of the time steps to export the data for each time step.

### **A.7. Taking Pictures:**

To take pictures in CFX ( In CFX Pre / CFX Post).

1. Go to **File> Print**.
2. Select **Format – JPEG**
3. **File** – Click on the browse button and select the directory in which u want to save this image and then give the file name and save.
4. To print the image on a paper, check on “**use white backgkground**”.

## **APPENDIX B. DETERMINATION OF RTD FOR A CIRCULAR REACTOR USING THE CFX SIMULATION (SAMPLE CALCULATIONS)**

### **B.1. Introduction**

CFX is a commercial Computational Fluid Dynamics (CFD) program used to simulate fluid flow in a wide variety of applications. It allows engineers to test systems in a virtual environment. It is used by companies around the world in a wide range of industries including aerospace, chemical processing, power generation, automotive, oil and gas, heating, ventilation and air conditioning, and many others to improve processes, solve performance issues and vastly reduce product time to market.

The six steps that are to be followed to do simulations in CFX are:

1. Creating a geometry in CAD Mesh
2. Meshing the geometry in Designer Modular
3. Creating the boundary conditions in CFX Pre
4. Solving for the flow in CFX Solver
5. Posting the results in the CFX Post
6. Exporting the data from CFX Post to Excel sheet for further calculations.

### **B.2. DESIGNING OF A CIRCULAR REACTOR:**

Three reactors have been designed in CFX. **APPENDIX2** explains in detail about the designing of the circular reactor in CFX. For both the cases, the axis is considered at the center of the circular region where the cells grow on the porous structure. . In Case1, the reactor has the inlet to the center and outlet to the side. The outlet with a diameter of 6mm is in the negative ZX direction and is extruded to a length

of 10mm in the negative Y direction. In Case2, the reactor has both the inlet and outlet to the sides. The inlet with a diameter of 6 mm is in the negative ZX direction and is extruded to a length of 10 mm in the positive Y direction, whereas, the outlet with a diameter of 6mm is in the positive ZX direction and is extruded to a length of 10 mm in the negative Y direction Case 3 is same as Case 2 except for the fact that both the inlet and outlet are extruded on the same side in the positive Y direction. **Figure1(Chapter 3)** Shows the schematics of circular reactor with different inlet and outlet positions

**B.2.1. Calculation of RTD function:**

The RTD is obtained for circular reactor by applying a step change in the concentration of a tracer flowing into the reactor (Co) and evaluating the temporal mixing cup tracer concentration at the reactor outlet (C<sub>mix</sub>). Since, the direction of flow changes in the circular reactor, concentration and velocity both vary with r and θ. At the outlet, variation in velocity and trace volume fraction with respect to x, y and z co-ordinates are obtained from the simulations done in CFX for each time step. From these values we need to find out r, θ, concentration.

Since, the reactor is based on the ZX plane,  $r = \sqrt{x^2 + z^2}$  and  $\theta = \tan^{-1}\left(\frac{x}{z}\right)$

$$C_{mix} = \frac{\int_0^R C(r, \theta) \cdot 2\pi r \cdot dr}{\int_0^R 2\pi r \cdot dr} \times 1000$$

Calculations of r, θ, concentration are show below for some data points, these data points correspond to the 20<sup>th</sup> second simulation: (Case2):

**Table B1. Output Results from CFX for a Time point**

<b>X [m]</b>	<b>Y [m]</b>	<b>Z [m]</b>	<b>tracer. Superficial Velocity</b>	<b>tracer Volume Fraction</b>
			<b>[m/s]</b>	
$2.442 \times 10^{-2}$	$-9.00 \times 10^{-3}$	$2.526 \times 10^{-2}$	$7.930 \times 10^{-2}$	1.000
$2.467 \times 10^{-2}$	$-9.00 \times 10^{-3}$	$2.506 \times 10^{-2}$	$7.708 \times 10^{-2}$	1.000
$2.353 \times 10^{-2}$	$-9.00 \times 10^{-3}$	$2.504 \times 10^{-2}$	$7.567 \times 10^{-2}$	1.000
$2.353 \times 10^{-2}$	$-9.00 \times 10^{-3}$	$2.524 \times 10^{-2}$	$7.811 \times 10^{-2}$	1.000
$2.255 \times 10^{-2}$	$-9.00 \times 10^{-3}$	$2.558 \times 10^{-2}$	$7.573 \times 10^{-2}$	1.000
$2.243 \times 10^{-2}$	$-9.00 \times 10^{-3}$	$2.545 \times 10^{-2}$	$7.428 \times 10^{-2}$	1.000
$2.233 \times 10^{-2}$	$-9.00 \times 10^{-3}$	$2.552 \times 10^{-2}$	$7.439 \times 10^{-2}$	1.000
$2.681 \times 10^{-2}$	$-9.00 \times 10^{-3}$	$2.861 \times 10^{-2}$	$8.735 \times 10^{-2}$	1.000
$2.692 \times 10^{-2}$	$-9.00 \times 10^{-3}$	$2.866 \times 10^{-2}$	$8.609 \times 10^{-2}$	1.000
$2.694 \times 10^{-2}$	$-9.00 \times 10^{-3}$	$2.854 \times 10^{-2}$	$8.597 \times 10^{-2}$	1.000
$2.160 \times 10^{-2}$	$-9.00 \times 10^{-3}$	$2.960 \times 10^{-2}$	$8.121 \times 10^{-2}$	1.000
$2.159 \times 10^{-2}$	$-9.00 \times 10^{-3}$	$2.963 \times 10^{-2}$	$7.991 \times 10^{-2}$	1.000
$2.165 \times 10^{-2}$	$-9.00 \times 10^{-3}$	$2.973 \times 10^{-2}$	$8.016 \times 10^{-2}$	1.000
$2.240 \times 10^{-2}$	$-9.00 \times 10^{-3}$	$3.053 \times 10^{-2}$	$8.275 \times 10^{-2}$	1.000
$2.240 \times 10^{-2}$	$-9.00 \times 10^{-3}$	$3.043 \times 10^{-2}$	$8.361 \times 10^{-2}$	1.000
$2.231 \times 10^{-2}$	$-9.00 \times 10^{-3}$	$3.047 \times 10^{-2}$	$8.251 \times 10^{-2}$	1.000
$2.463 \times 10^{-2}$	$-9.00 \times 10^{-3}$	$3.093 \times 10^{-2}$	$8.793 \times 10^{-2}$	1.000
$2.453 \times 10^{-2}$	$-9.00 \times 10^{-3}$	$3.083 \times 10^{-2}$	$8.893 \times 10^{-2}$	1.000
$2.452 \times 10^{-2}$	$-9.00 \times 10^{-3}$	$3.095 \times 10^{-2}$	$8.774 \times 10^{-2}$	1.000
$2.558 \times 10^{-2}$	$-9.00 \times 10^{-3}$	$3.041 \times 10^{-2}$	$8.979 \times 10^{-2}$	1.000

These above values are the data that we got from the simulations done in CFX.

The X, Y, Z co-ordinates are with respect to the axes to the center of the disc. But, we need the distance from the center of the outlet tube.

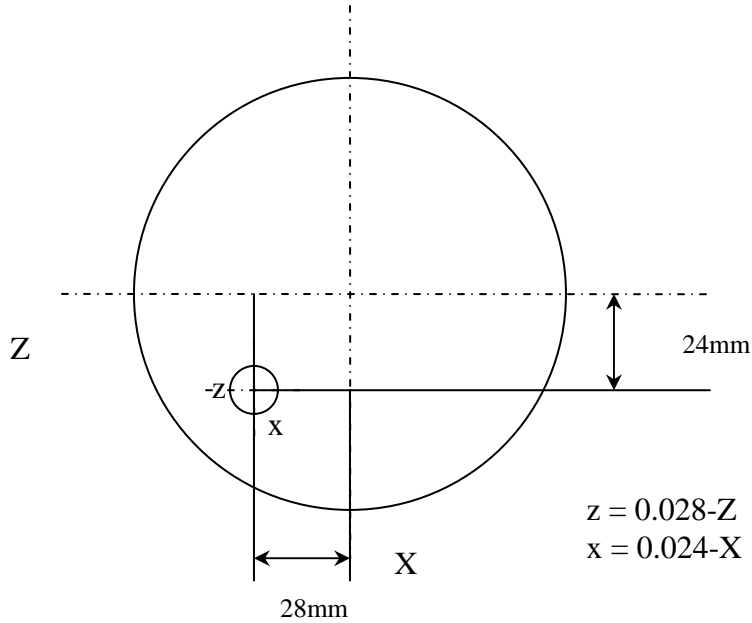


**Figure B.1:** Shifting the ZX axis to the center of the outlet from the center of the circular reactor.

**Figure B.1** shows that the center of the outlet tube is at a distance of  $x = 24\text{mm}$  and  $z = 28\text{mm}$  from the center of the circular region where the cells grow. Thus, to get the distance of a point in the outlet with respect to the center of the outlet the  $X, Z$  values are to be subtracted from  $0.024, 0.028$  respectively to get  $x, z$  in meters. For example, consider the first point,

$X = 0.02442 \text{ m}$  and  $Z = 0.02526 \text{ m}$  then  $x = 0.024 - 0.02442 = -0.00042$  and  $z = 0.028 - 0.02526 = 0.00274$ .  $r, \theta$  and concentration are calculated from the formulas shown above.

**Table B2. Conversion into Cylindrical coordinates**

<b>x(m)</b>	<b>z(m)</b>	<b>R</b>	<b><math>\theta</math>(radians)</b>	<b>dr</b>	<b>d<math>\theta</math></b>
$-4.200 \times 10^{-4}$	$2.740 \times 10^{-3}$	$2.770 \times 10^{-3}$	$-1.518 \times 10^{-1}$		
$-5.700 \times 10^{-4}$	$2.940 \times 10^{-3}$	$2.990 \times 10^{-3}$	$-1.929 \times 10^{-1}$	$2.200 \times 10^{-4}$	$4.104 \times 10^{-2}$
$4.700 \times 10^{-4}$	$2.960 \times 10^{-3}$	$3.000 \times 10^{-3}$	$1.582 \times 10^{-1}$	0.000	$3.510 \times 10^{-1}$
$4.700 \times 10^{-4}$	$2.760 \times 10^{-3}$	$2.800 \times 10^{-3}$	$1.698 \times 10^{-1}$	2.000E-04	$1.164 \times 10^{-2}$
$1.550 \times 10^{-3}$	$2.420 \times 10^{-3}$	$2.880 \times 10^{-3}$	$5.693 \times 10^{-1}$	$8.000 \times 10^{-5}$	$3.995 \times 10^{-1}$
$1.570 \times 10^{-3}$	$2.550 \times 10^{-3}$	$3.000 \times 10^{-3}$	$5.528 \times 10^{-1}$	$1.200 \times 10^{-4}$	$1.653 \times 10^{-2}$
$1.670 \times 10^{-3}$	$2.480 \times 10^{-3}$	$2.990 \times 10^{-3}$	$5.934 \times 10^{-1}$	0.000	$4.061 \times 10^{-2}$
$-2.810 \times 10^{-3}$	$-6.100 \times 10^{-3}$	$2.870 \times 10^{-3}$	-1.785	$1.200 \times 10^{-4}$	2.379
$-2.920 \times 10^{-3}$	$-6.600 \times 10^{-3}$	$2.990 \times 10^{-3}$	-1.794	$1.200 \times 10^{-4}$	$8.740 \times 10^{-3}$
$-2.940 \times 10^{-3}$	$-5.400 \times 10^{-4}$	$2.990 \times 10^{-3}$	-1.753	0.000	$4.107 \times 10^{-2}$
$2.400 \times 10^{-3}$	$-1.600 \times 10^{-3}$	$2.880 \times 10^{-3}$	2.159	$1.100 \times 10^{-4}$	3.912
$2.510 \times 10^{-3}$	$-1.630 \times 10^{-3}$	$2.990 \times 10^{-3}$	2.148	$1.100 \times 10^{-4}$	$1.085 \times 10^{-2}$
$2.450 \times 10^{-3}$	$-1.730 \times 10^{-3}$	$3.000 \times 10^{-3}$	2.187	0.000	$3.863 \times 10^{-2}$
$1.600 \times 10^{-3}$	$-2.530 \times 10^{-3}$	$3.000 \times 10^{-3}$	2.579	0.000	$3.924 \times 10^{-1}$
$1.600 \times 10^{-3}$	$-2.430 \times 10^{-3}$	$2.910 \times 10^{-3}$	2.559	8.000	$1.963 \times 10^{-2}$
$1.690 \times 10^{-3}$	$-2.470 \times 10^{-3}$	$2.990 \times 10^{-3}$	2.541	8.000	$1.849 \times 10^{-2}$
$-6.300 \times 10^{-4}$	$-2.930 \times 10^{-3}$	$2.990 \times 10^{-3}$	-2.929	0.000	5.470
$-5.300 \times 10^{-4}$	$-2.830 \times 10^{-3}$	$2.880 \times 10^{-3}$	-2.958	1.200	$2.914 \times 10^{-2}$
$-5.200 \times 10^{-4}$	$-2.950 \times 10^{-3}$	$3.000 \times 10^{-3}$	-2.967	1.200	$8.550 \times 10^{-3}$
$-1.580 \times 10^{-3}$	$-2.410 \times 10^{-3}$	$2.880 \times 10^{-3}$	-2.562	1.200	$4.049 \times 10^{-1}$

**Table B3. Calculation of Concentration at each time point**

Conc (mol/m <sup>3</sup> )	c*v*r	avg(cvr)	v*r	avg(vr)	cvrdrdθ	vrdrdθ
2.174×10 <sup>-4</sup>	4.780		2.200×10 <sup>-4</sup>			
2.174×10 <sup>-4</sup>	5.017	4.899	2.300×10 <sup>-4</sup>	2.300×10 <sup>-4</sup>	4.000×10 <sup>-5</sup>	1.000×10 <sup>-5</sup>
2.174×10 <sup>-4</sup>	4.928	4.973	2.300×10 <sup>-4</sup>	2.300×10 <sup>-4</sup>	0.000	1.000×10 <sup>-5</sup>
2.174×10 <sup>-4</sup>	4.750	4.839	2.200×10 <sup>-4</sup>	2.200×10 <sup>-4</sup>	1.000×10 <sup>-5</sup>	1.000×10 <sup>-5</sup>
2.174×10 <sup>-4</sup>	4.735	4.742	2.200×10 <sup>-4</sup>	2.200×10 <sup>-4</sup>	1.500×10 <sup>-4</sup>	1.000×10 <sup>-5</sup>
2.174×10 <sup>-4</sup>	4.837	4.786	2.200×10 <sup>-4</sup>	2.200×10 <sup>-4</sup>	1.000×10 <sup>-5</sup>	1.000×10 <sup>-5</sup>
2.174×10 <sup>-4</sup>	4.841	4.839	2.200×10 <sup>-4</sup>	2.200×10 <sup>-4</sup>	0.000	1.000×10 <sup>-5</sup>
2.174×10 <sup>-4</sup>	5.459	5.150	2.500×10 <sup>-4</sup>	2.400×10 <sup>-4</sup>	1.450×10 <sup>-3</sup>	1.000×10 <sup>-5</sup>
2.174×10 <sup>-4</sup>	5.605	5.532	2.600×10 <sup>-4</sup>	2.500×10 <sup>-4</sup>	1.000×10 <sup>-5</sup>	1.000×10 <sup>-5</sup>
2.174×10 <sup>-4</sup>	5.596	5.601	2.600×10 <sup>-4</sup>	2.600×10 <sup>-4</sup>	0.000	1.000×10 <sup>-5</sup>
2.174×10 <sup>-4</sup>	5.084	5.340	2.300×10 <sup>-4</sup>	2.500×10 <sup>-4</sup>	2.390×10 <sup>-3</sup>	1.000×10 <sup>-5</sup>
2.174×10 <sup>-4</sup>	5.202	5.143	2.400×10 <sup>-4</sup>	2.400×10 <sup>-4</sup>	1.000×10 <sup>-5</sup>	1.000×10 <sup>-5</sup>
2.174×10 <sup>-4</sup>	5.219	5.211	2.400×10 <sup>-4</sup>	2.400×10 <sup>-4</sup>	0.000	1.000×10 <sup>-5</sup>
2.174×10 <sup>-4</sup>	5.388	5.304	2.500×10 <sup>-4</sup>	2.400×10 <sup>-4</sup>	0.000	1.000×10 <sup>-5</sup>
2.174×10 <sup>-4</sup>	5.297	5.343	2.400×10 <sup>-4</sup>	2.500×10 <sup>-4</sup>	1.000×10 <sup>-5</sup>	1.000×10 <sup>-5</sup>
2.174×10 <sup>-4</sup>	5.371	5.334	2.500×10 <sup>-4</sup>	2.500×10 <sup>-4</sup>	1.000E-05	1.000×10 <sup>-5</sup>
2.174×10 <sup>-4</sup>	5.725	5.548	2.600×10 <sup>-4</sup>	2.600×10 <sup>-4</sup>	1.000E-05	1.000×10 <sup>-5</sup>
2.174×10 <sup>-4</sup>	5.565	5.645	2.600×10 <sup>-4</sup>	2.600×10 <sup>-4</sup>	2.000E-05	1.000×10 <sup>-5</sup>
2.174×10 <sup>-4</sup>	5.713	5.639	2.600×10 <sup>-4</sup>	2.600×10 <sup>-4</sup>	1.000E-05	1.000×10 <sup>-5</sup>
2.174×10 <sup>-4</sup>	5.614	5.663	2.600×10 <sup>-4</sup>	2.600×10 <sup>-4</sup>	2.700E-04	1.000×10 <sup>-5</sup>

As, the flow of the fluid is radial in the reactor,  $C_{mix}$  for each time step would be:

$$C_{mix} = \frac{\int_0^{2\pi R} \int_0^{2\pi R} C(r, \theta) \cdot V(r, \theta) \cdot r \cdot dr \cdot d\theta}{\int_0^{2\pi R} \int_0^{2\pi R} V(r, \theta) \cdot r \cdot dr \cdot d\theta}$$

To solve the double integral in this equation and get the  $C_{mix}$  values, first an equation for concentration and velocity are to be obtained in terms of  $r$  and  $\theta$ .

There are the two ways of getting an equation for a set of data points:

1. Graphical method.

2. Regression.

The graphical method was not useful as the data points that we got for a plane near the outlet has all the points scattered and thus, fitting these data points into a curve was neither advisable nor possible. Below in Figure 2 are the graphs shown for circular reactor with inlet and outlet to the sides:

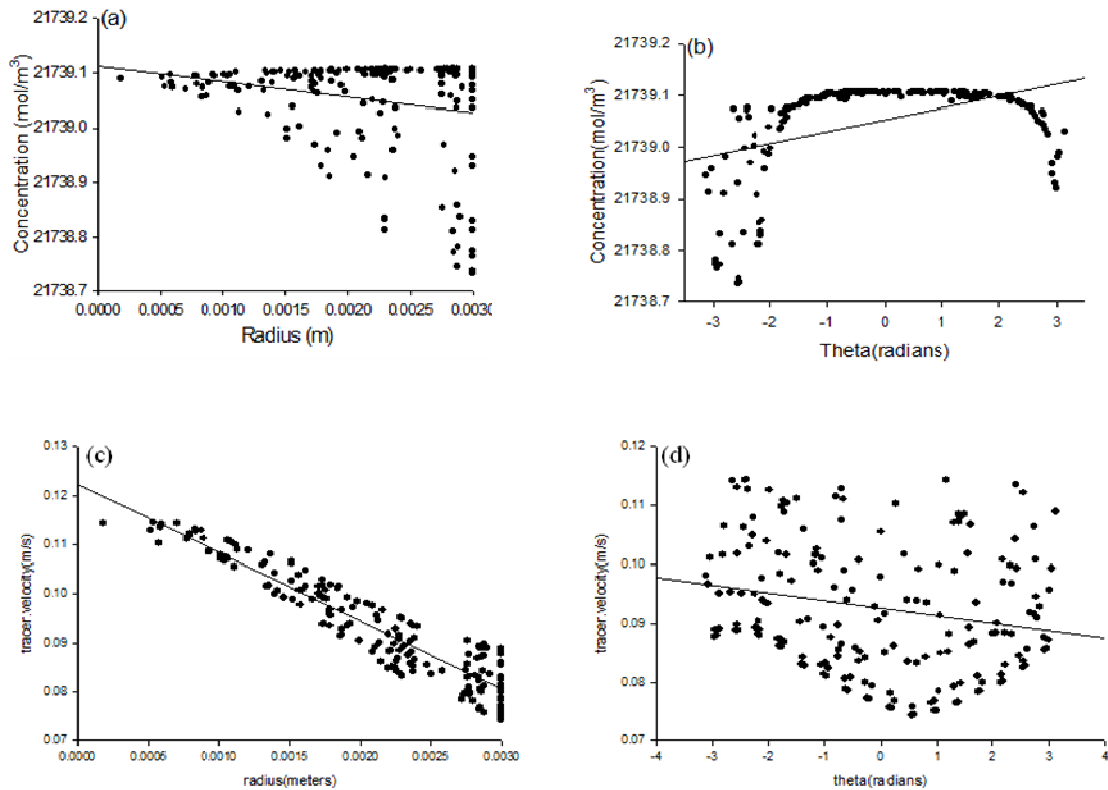


**Figure B.2:** (a) Variation of concentration( $C$ ) with respect to the radius( $r$ ) at the outlet of the reactor. (b) Variation of concentration( $C$ ) with respect to the cylindrical co-ordinate theta ( $\theta$ ) (c) Variation of tracer velocity with respect to the radius ( $r$ ) (d) Variation of tracer velocity with respect to the cylindrical co-ordinate theta ( $\theta$ ). The concentration and velocity values plotted are end the end of 20<sup>th</sup> time step.

The second way of fitting these data points into an equation was regression which was also of not much use as the concentration and velocity values that were calculated using the equation that was obtained from regression were much greater than the actual values. The error was around more than 150% and went up to 300% for some data points.

Thus, it's clear that the data points cannot fit into any particular equation and this double integration is to be solved by doing some numerical analysis.

Hence, to find out the outlet concentrations for each time step the  $C_{mix}$  equation was modified by applying the concept of discrete integration as follows:

$$C_{mix} = \frac{\sum C_{avg} V_{avg} r \Delta r \Delta \theta}{\sum V_{avg} r \Delta r \Delta \theta}$$

where  $C_{mix}(t)$  is the measured tracer concentration from the experiments at a given time when collecting samples at the reactor exit. For circular reactor the simulations was run using 5 s time-steps until the volume fraction reached 0.99 (20 steps, 120 s). Transient results were written for every 5 s ( Flow rate : 20 ml/min).

Assuming that all the set of data points in the plane are uniform,  $dr$  and  $d\theta$  is found by taking the difference between two consecutive points. For better accuracy, instead of taking just  $c*v*r$  to find out  $cvrdrd\theta$  average of  $cvr$  has been taken. Thus,  $cvr.dr.d\theta$  is found in between two consecutive data points and summation of all the  $cvrdrd\theta$  values would give us the numerator value in the  $C_{mix}$  equation. The same rule has been applied to find out the value of denominator in the  $C_{mix}$  equation. Hence, by dividing the numerator value with the denominator value  $C_{mix}$  is found for each time step.

**Table B4. Calculation of Average Concentration**

time	Cvrdrd0	Vrdrd0	Cmix
0	0.000	$1.000 \times 10^{-5}$	$5.290 \times 10^{-3}$
1	$1.160 \times 10^{-3}$	$1.000 \times 10^{-5}$	$1.294 \times 10^2$
2	$3.960 \times 10^{-3}$	$1.000 \times 10^{-5}$	$4.417 \times 10^2$
3	$1.082 \times 10^{-2}$	$1.000 \times 10^{-5}$	$1.207 \times 10^3$
4	$2.469 \times 10^{-2}$	$1.000 \times 10^{-5}$	$2.756 \times 10^3$
5	$4.827 \times 10^{-2}$	$1.000 \times 10^{-5}$	$5.387 \times 10^3$
6	$8.146 \times 10^{-2}$	$1.000 \times 10^{-5}$	$9.091 \times 10^3$
7	$1.175 \times 10^{-1}$	$1.000 \times 10^{-5}$	$1.311 \times 10^4$
8	$1.442 \times 10^{-1}$	$1.000 \times 10^{-5}$	$1.610 \times 10^4$
9	$1.622 \times 10^{-1}$	$1.000 \times 10^{-5}$	$1.810 \times 10^4$
10	$1.755 \times 10^{-1}$	$1.000 \times 10^{-5}$	$1.958 \times 10^4$
11	$1.846 \times 10^{-1}$	$1.000 \times 10^{-5}$	$2.060 \times 10^4$
12	$1.901 \times 10^{-1}$	$1.000 \times 10^{-5}$	$2.122 \times 10^4$
13	$1.930 \times 10^{-1}$	$1.000 \times 10^{-5}$	$2.154 \times 10^4$
14	$1.942 \times 10^{-1}$	$1.000 \times 10^{-5}$	$2.167 \times 10^4$
15	$1.946 \times 10^{-1}$	$1.000 \times 10^{-5}$	$2.172 \times 10^4$
16	$1.947 \times 10^{-1}$	$1.000 \times 10^{-5}$	$2.173 \times 10^4$
17	$1.948 \times 10^{-1}$	$1.000 \times 10^{-5}$	$2.174 \times 10^4$
18	$1.948 \times 10^{-1}$	$1.000 \times 10^{-5}$	$2.174 \times 10^4$
19	$1.948 \times 10^{-1}$	$1.000 \times 10^{-5}$	$2.174 \times 10^4$
20	$1.948 \times 10^{-1}$	$1.000 \times 10^{-5}$	$2.174 \times 10^4$

Once,  $C_{mix}$  is determined, the RTD function  $E(t)$  is determined. For a positive step change in the tracer concentration,  $E(t)$  is evaluated from  $C_{mix}(t)$  according to:

$$E(t) = \frac{1}{C_o} \cdot \frac{dC_{mix}(t)}{dt}$$

While doing the simulations in CFX, the tracer volume fraction is given as 1

$$\Rightarrow C_o = \frac{1m^3 / m^3 \cdot 1000kg / m^3 \cdot 1000gm / kg}{46} = 21,739.13 \text{ mol/m}^3$$

$$dC_{mix} / dt = \frac{C(t) - C(t-1)}{t - (t-1)}$$

$$t_{avg} = \frac{t - (t-1)}{2}$$

Using the above equations  $dc/dt$ ,  $t_{avg}$  is found. Thus, substituting all these values in the  $E(t)$  equation we get the RTD function for disc reactor with inlet and outlet to the sides.

Similarly, The RTD function has been determined for disc reactor with inlet to the center and outlet to the side

**Table B5. The  $E(t)$  values are tabulated as below (Case2)**

Time	Cmix	dc/dt	Tavg	E
0	$5.290 \times 10^{-3}$			
1	$1.294 \times 10^2$	$1.294 \times 10^2$	$5.000 \times 10^{-1}$	$5.950 \times 10^{-3}$
2	$4.417 \times 10^2$	$3.123 \times 10^2$	1.500	$1.437 \times 10^{-2}$
3	$1.207 \times 10^3$	$7.658 \times 10^2$	2.500	$3.523 \times 10^{-2}$
4	$2.756 \times 10^3$	$1.548 \times 10^3$	3.500	$7.122 \times 10^{-2}$
5	$5.387 \times 10^3$	$2.632 \times 10^3$	4.500	$1.211 \times 10^{-1}$
6	$9.091 \times 10^3$	$3.704 \times 10^3$	5.500	$1.704 \times 10^{-1}$
7	$1.311 \times 10^3$	$4.023 \times 10^3$	6.500	$1.850 \times 10^{-1}$
8	$1.610 \times 10^3$	$2.982 \times 10^3$	7.500	$1.372 \times 10^{-1}$
9	$1.810 \times 10^4$	$2.009 \times 10^3$	8.500	$9.240 \times 10^{-2}$
10	$1.958 \times 10^4$	$1.479 \times 10^3$	9.500	$6.801 \times 10^{-2}$
11	$2.060 \times 10^4$	$1.018 \times 10^3$	$1.050 \times 10^1$	$4.682 \times 10^{-2}$
12	$2.122 \times 10^4$	$6.193 \times 10^2$	$1.150 \times 10^1$	$2.849 \times 10^{-2}$
13	$2.154 \times 10^4$	$3.188 \times 10^2$	$1.250 \times 10^1$	$1.467 \times 10^{-2}$
14	$2.167 \times 10^4$	$1.312 \times 10^2$	$1.350 \times 10^1$	$6.040 \times 10^{-3}$
15	$2.172 \times 10^4$	$4.648 \times 10^1$	$1.450 \times 10^1$	$2.140 \times 10^{-3}$
16	$2.173 \times 10^4$	$1.520 \times 10^1$	$1.550 \times 10^1$	$7.000 \times 10^{-4}$
17	$2.174 \times 10^4$	4.916	$1.650 \times 10^1$	$2.300 \times 10^{-4}$
18	$2.174 \times 10^4$	1.620	$1.750 \times 10^1$	$7.000 \times 10^{-5}$
19	$2.174 \times 10^4$	$4.902 \times 10^{-1}$	$1.850 \times 10^1$	$2.000 \times 10^{-5}$
20	$2.174 \times 10^4$	$1.528 \times 10^{-1}$	$1.950 \times 10^1$	$1.000 \times 10^{-5}$

**Theoretical calculation of residence time:**

The bulk mass flow rate is 0.0026kg/s

The volumetric flow rate is mass flow rate/density =  $\frac{0.0026(\text{kg} / \text{s})}{1(\text{kg} / \text{lt})} = 0.0026 \text{ lt/s}$

Since, the diameter and thickness of the disc are 10cm and 2mm respectively,

The volume of the reactor is  $\frac{\pi D^2}{4} \cdot W = \pi \cdot (10)^2 \cdot (0.2)/4 = 15.71 \text{ cc.} = 15.71 * 10^{-3} \text{ lt}$

Residence time =  $\frac{\text{Volume of the reactor}}{\text{volumetric flow rate}}$

Residence time =  $\frac{15.71 \times 10^{-3}(\text{lt})}{0.0026(\text{lt} / \text{s})} = 6 \text{ s}$

## APPENDIX C: USING COMSOL 3.4

This is a quick manual for learning COMSOL 3.4 Chemical Engineering Module.

C.1. Momentum Balance of Circular Reactor with porous structure:

### C.1.1. Creating Geometry:

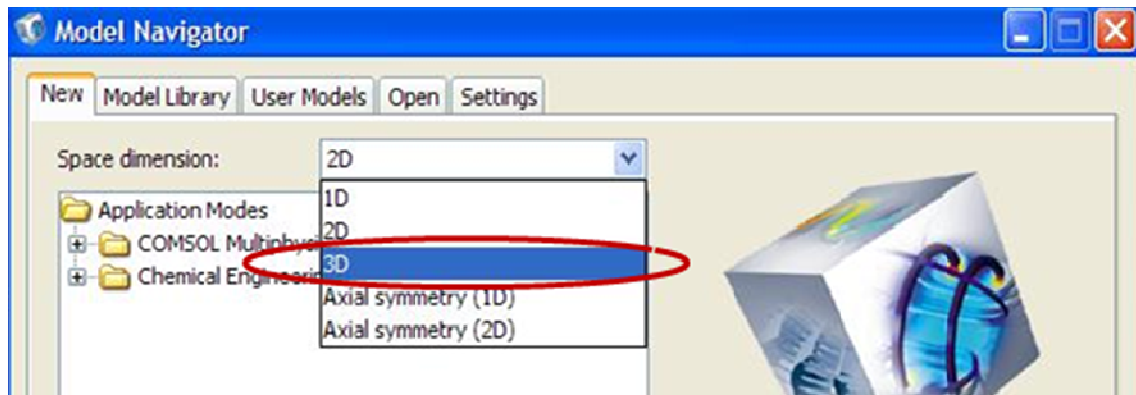
1. **Start > All Programs > COMSOL 3.4 > Click on COMSOL Multiphysics 3.4.**

Model

2. Navigator window will pop up.

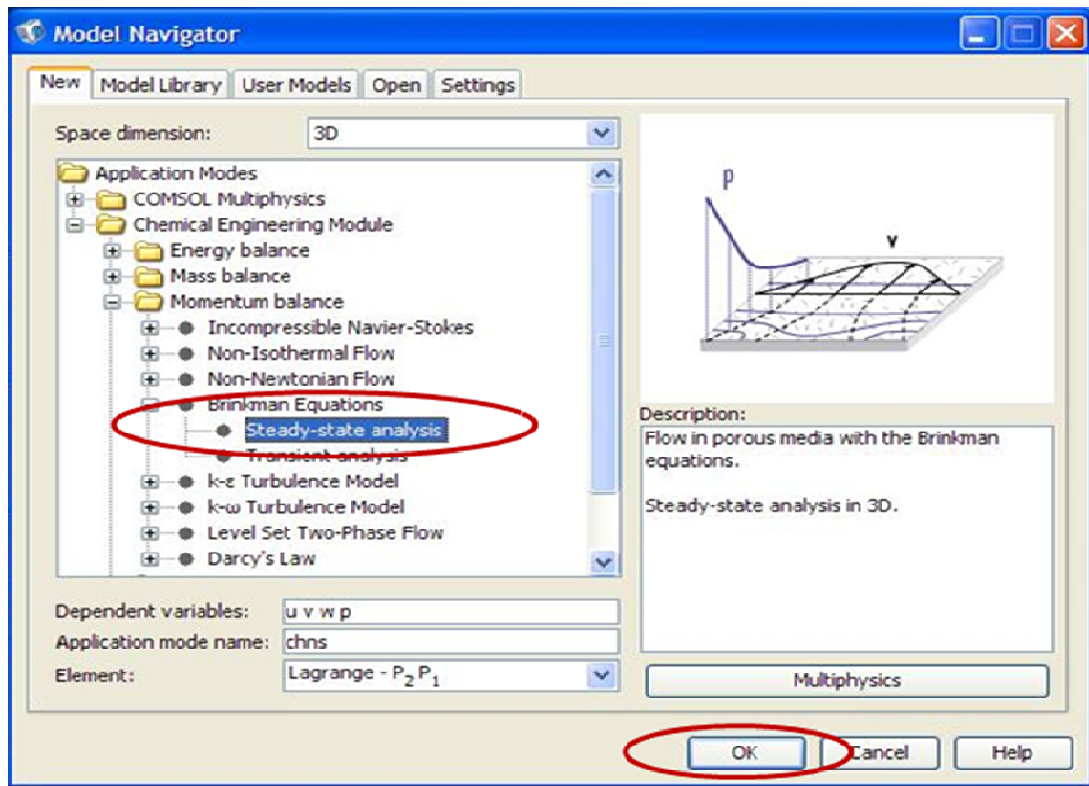


3. In **Model Navigator > Set Space Dimension as 3D**

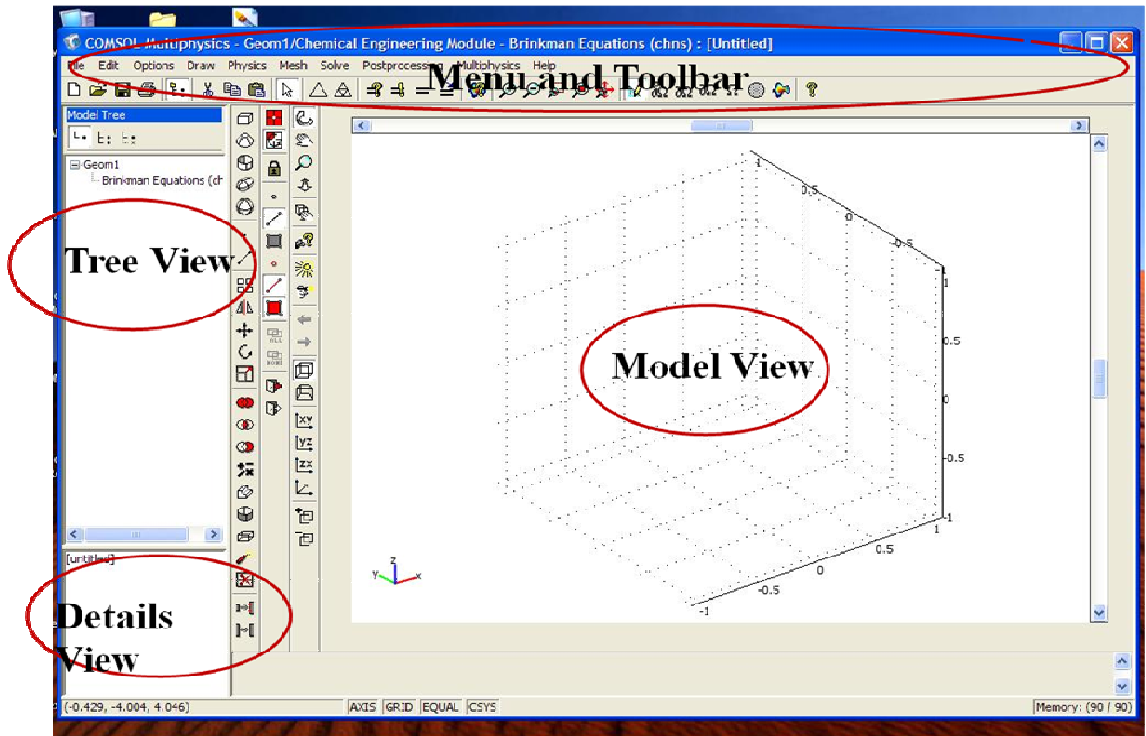


4. In the **Application Modes** section Click on **Chemical Engineering Module >**

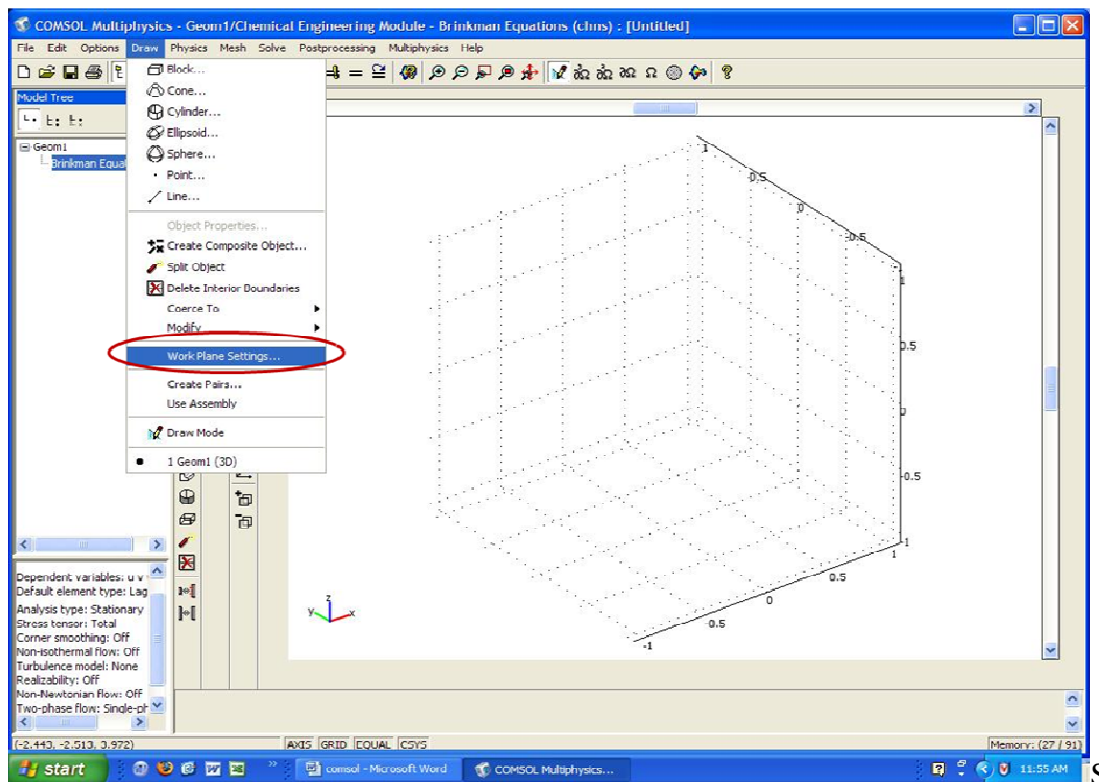
**Momentum Balance**> **Brinkman Equation**> Select **Steady State Analysis**. Click **OK**.



COMSOL Multiphysics Window will pop up.

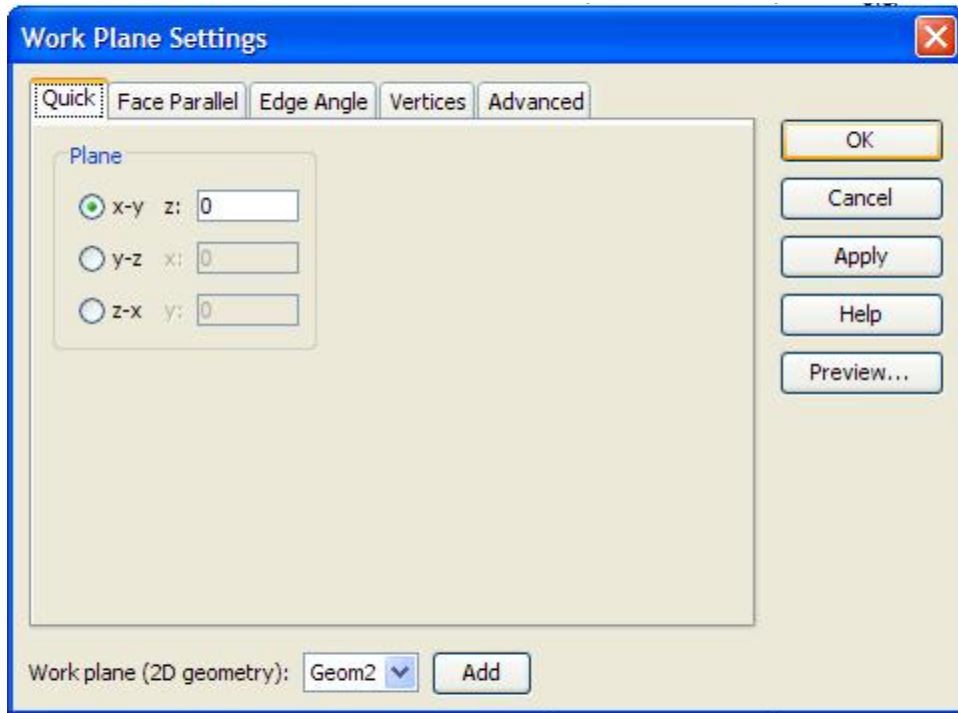


5. In the **Menu bar** go to **file > Save**. And save the file with a desired name, say, circular\_reactor.mph

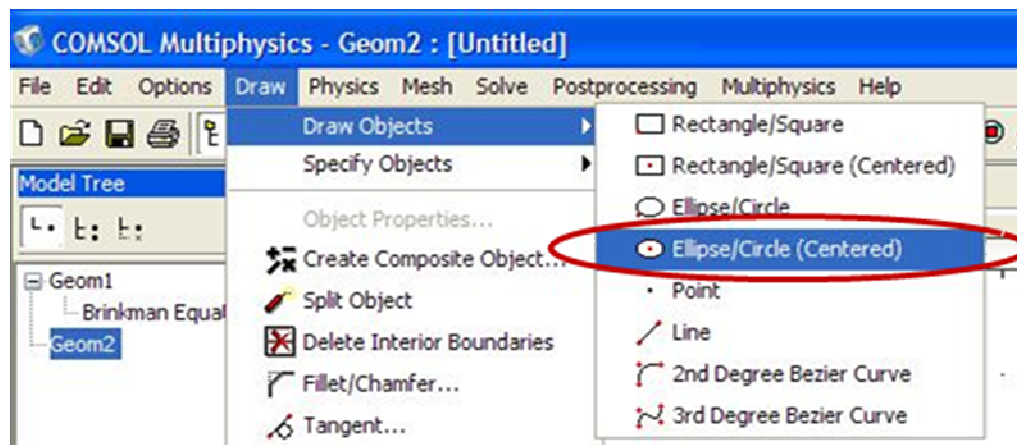


elect **Draw** tab > Click on **Work Place Settings**. Work plane settings A window will pop up.

6. Select **Quick** tab > Check on **x-y** and set **z = 0**. Click **OK**.

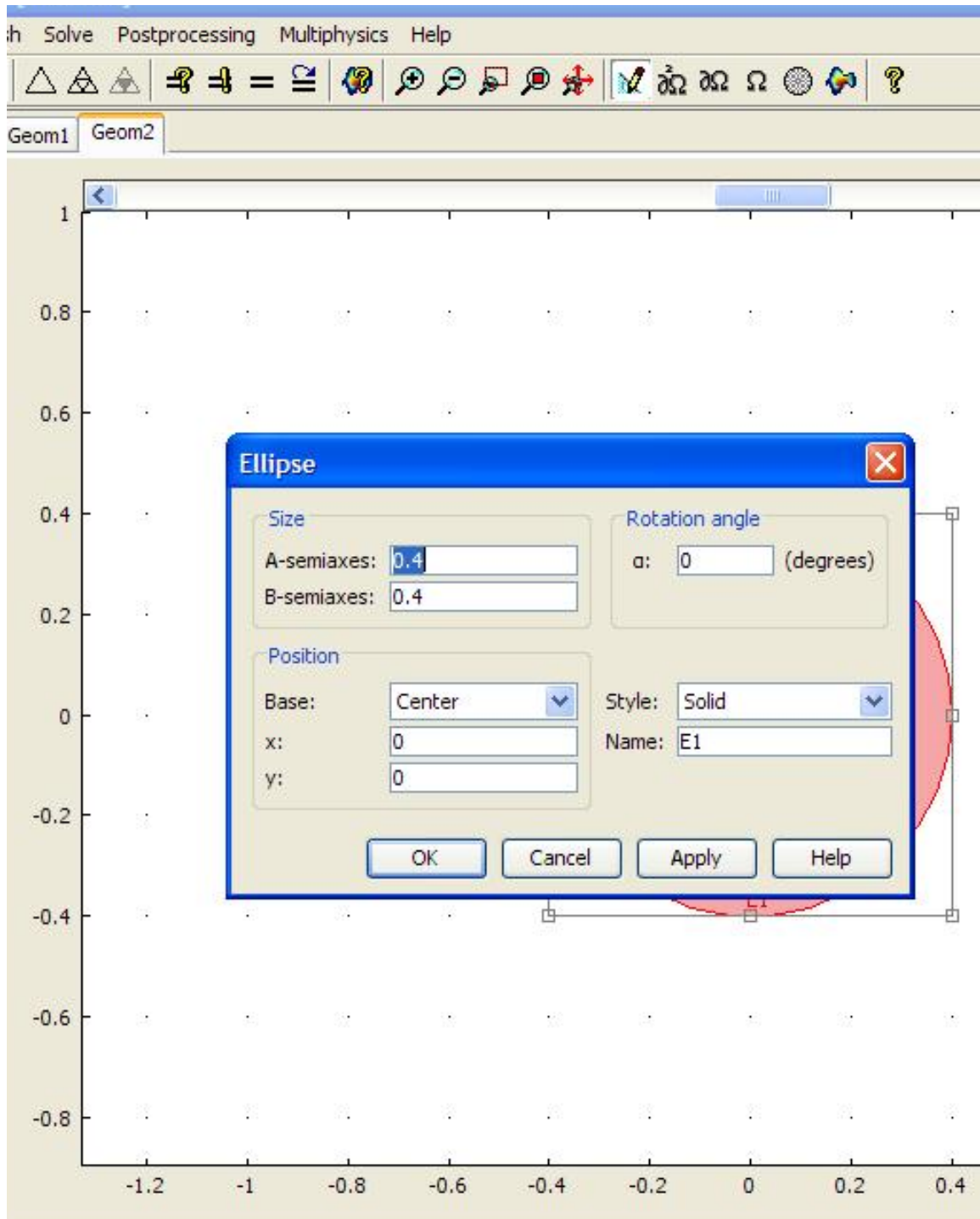


7. Select **Draw** tab > **Draw Objects** > Click on **Ellipse/ Circle (centered)** and create a circle in the Model View. To draw a circle Select a point in the model view and move the mouse to some extent and then click the left button of the mouse once.



8. To Change the dimensions of the object created (say Circle), double click on that

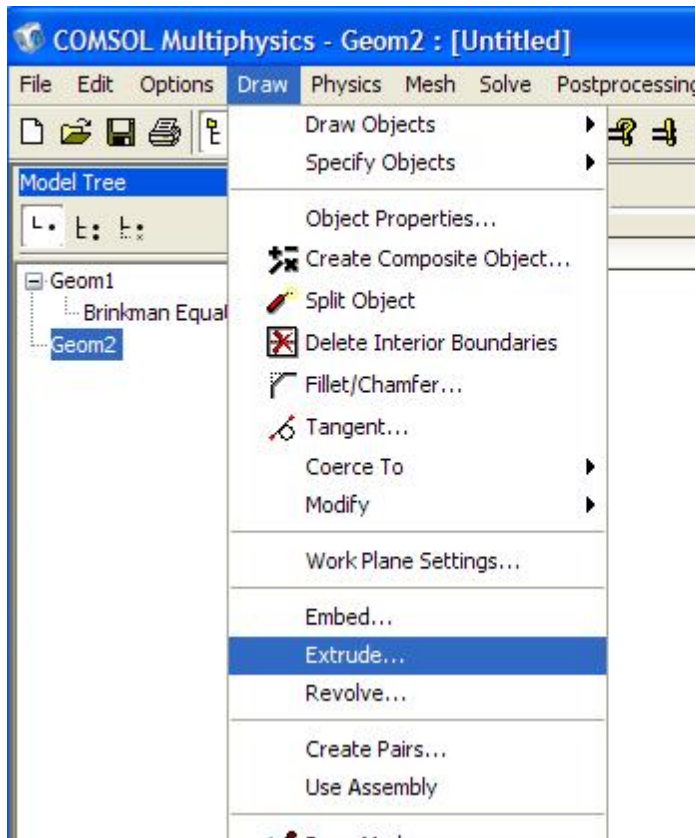
particular object a window will pop up. In **Size section**> Change **A semi-axes: 0.5**;  
Change **B semi-axes: 0.5**. Leave the rest as it is.



9. To extrude 2D Geometry object to 3D, select the object that is to be extruded.( In our

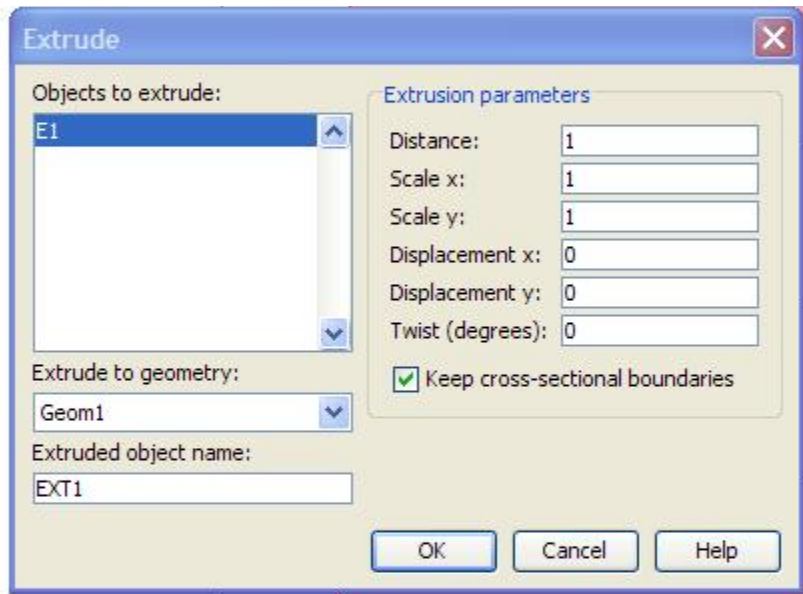
Case, it is the circle)

10. In the Menu bar Select **Draw tab> Extrude**.

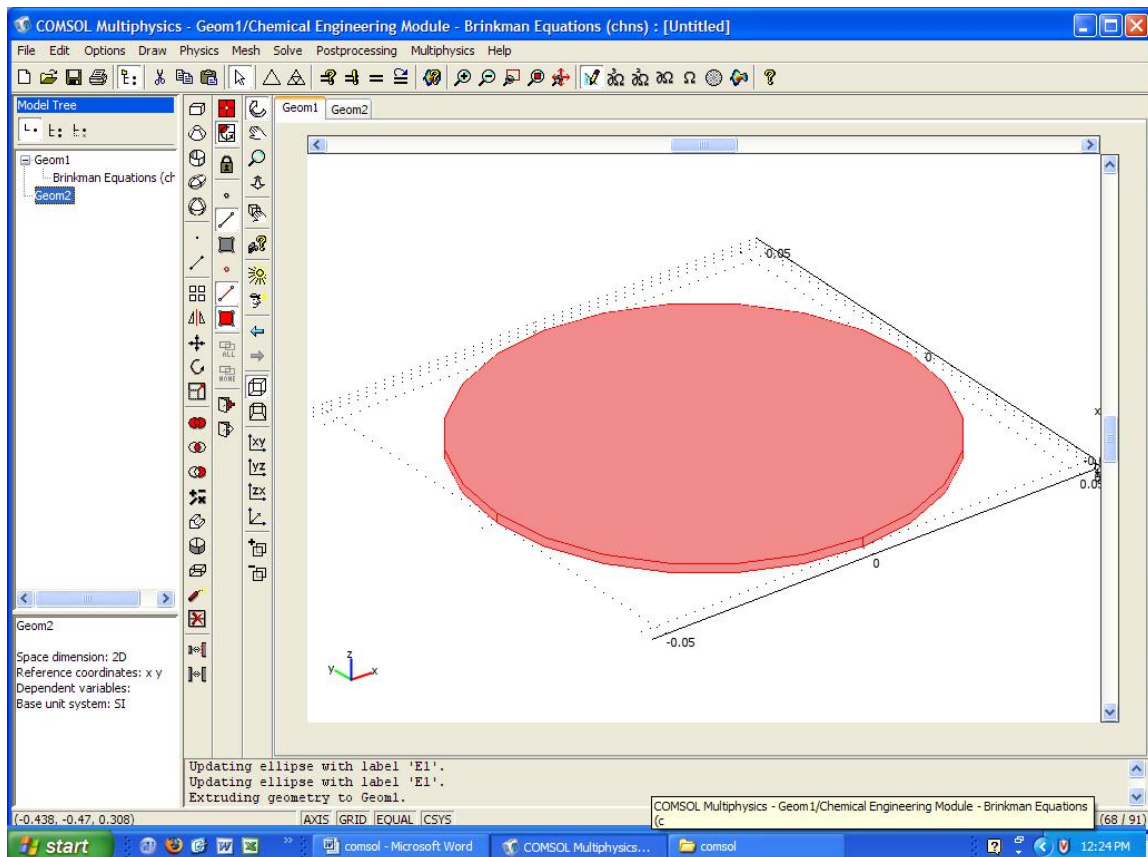


A window will pop up.

11. In the Extrusion parameters section > Change **Distance:** 0.002. Leave the rest as it is for Straight Extrusion. Click **OK**.

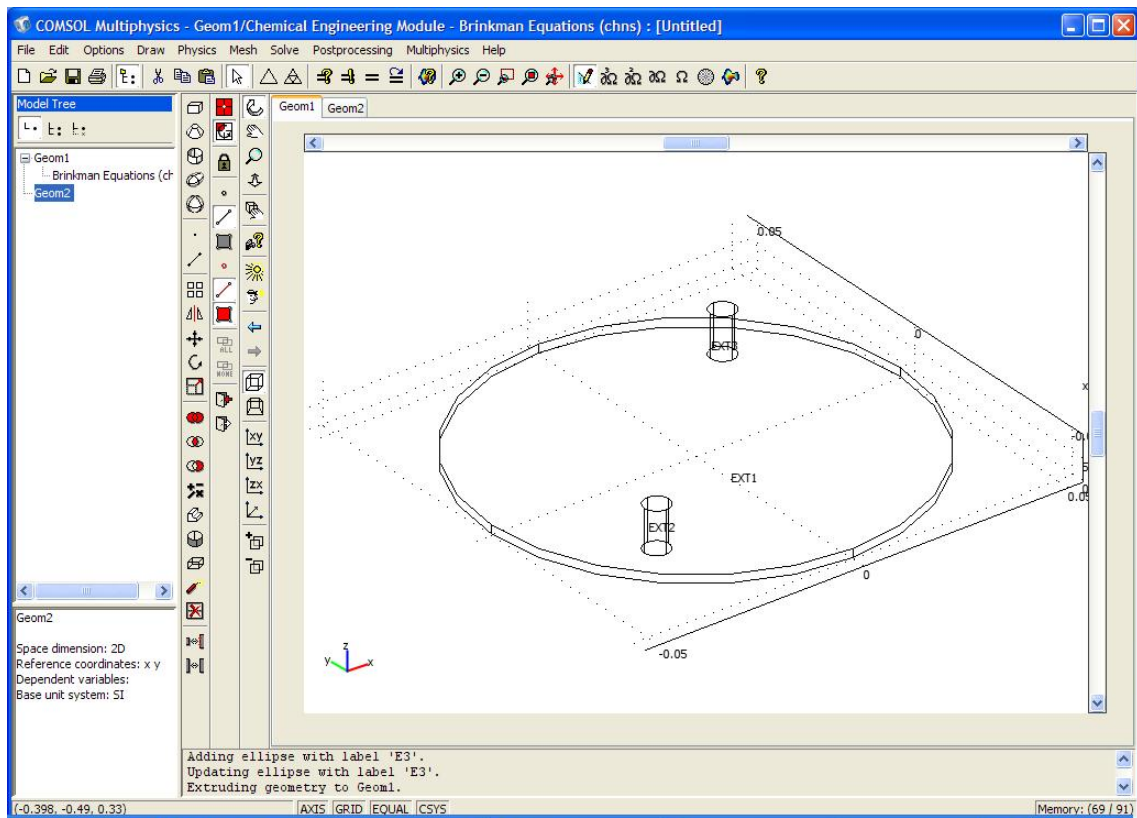


In the **Model View**> **Geom1 Tab** a circle with diameter 10cm and thickness of 2mm will be seen.



12. Click on **Geom2 tab** in the Model View. Repeat Step 6 and create a circle in the

- Fourth quadrant (i.e.; quadrant in which both x & y are negative).
13. Repeat Step 7 to Change the dimensions of the circle. In **size** section > Change **A semi-axes: 0.003** and **B semi-axes: 0.003**. In the **Position** Section> Change **x: -0.028** and **y: - 0.028**. (This is to create the inlet of 6 mm diameter for the circular reactor).
  14. Repeat Step 9 to extrude. In the **Extrusion parameters** section > Change **Distance: 0.01**. Click **Ok**. In the **Model View> Geom1 tab** an inlet of 1cm length with a diameter of 6 mm is extruded.
  15. In the similar way to create an outlet in the first quadrant(i.e.; quadrant in which both x & y are positive) Repeat Steps 6, 12 and 13.
  16. The circular reactor is created.



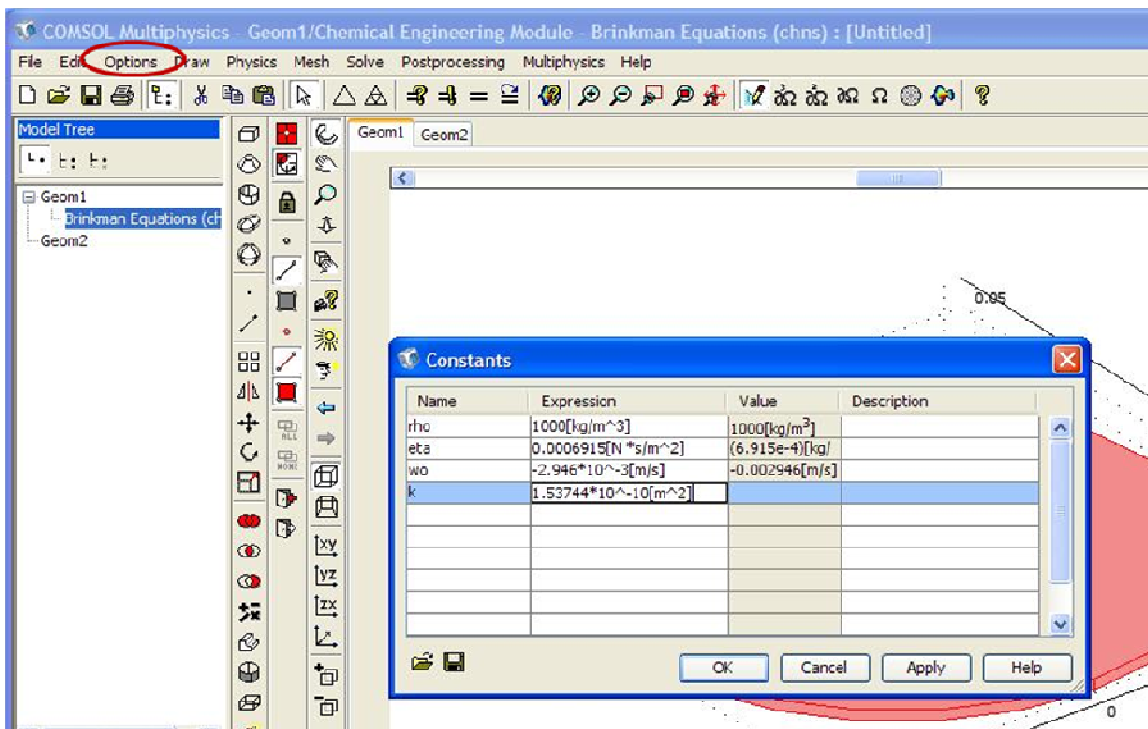
17. To clear an object. Select that particular object, Go to **Edit > Select Undo**  
**Circle/Ellipse** ( whatever object is to be cleared)

18. To zoom Click on the  in the toolbar and move the side bars in the model view to adjust the object in the model view to the center of the window.

### C.1.2. Creating a constants list:

Creating a constants list is safe and an easier way to input the parameters which might be used multiple times while writing the boundary conditions.

1. In the **Menu bar** > Select **Options** > click on **Constants**. A window will pop up.



2. In the window that pops up. There will be four columns. **Name**, **Expression**, **Value** and **Description**. In the Name column type in the name for the parameter. For example, Density can be named as rho. In the Expression column enter the values of the constant with units. And then Click **Enter**, the Value will be automatically shown in the Value column. In the Description column we can write comments for the users to understand about a particular constant.

- Input the below data in the Constants window that pops up.(the below values are for water flowing through the circular reactor completely filled with chitosan porous structure having around 120 pores/mm<sup>2</sup> , 85 μm pore size and the volumetric flow rate maintained at 5 mL/min)

**Table C.1. Property Selection Table.**

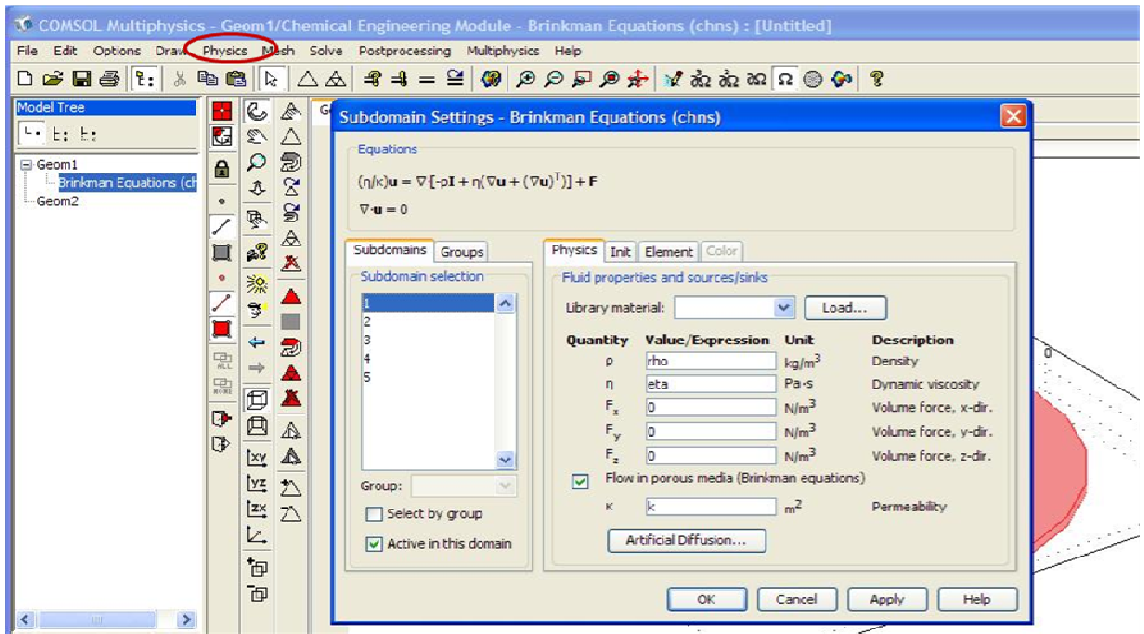
<b>Name</b>	<b>Expression</b>
Rho	1000[kg/m <sup>3</sup> ]
Eta	0.0006915[N*s/m <sup>2</sup> ]
w0	-2.946*10 <sup>-3</sup> [m/s]
K	1.53744*10 <sup>-10</sup> [m <sup>2</sup> ]

Click **OK**.

#### **4. Setting up the boundary conditions:**

##### **Subdomain settings:**

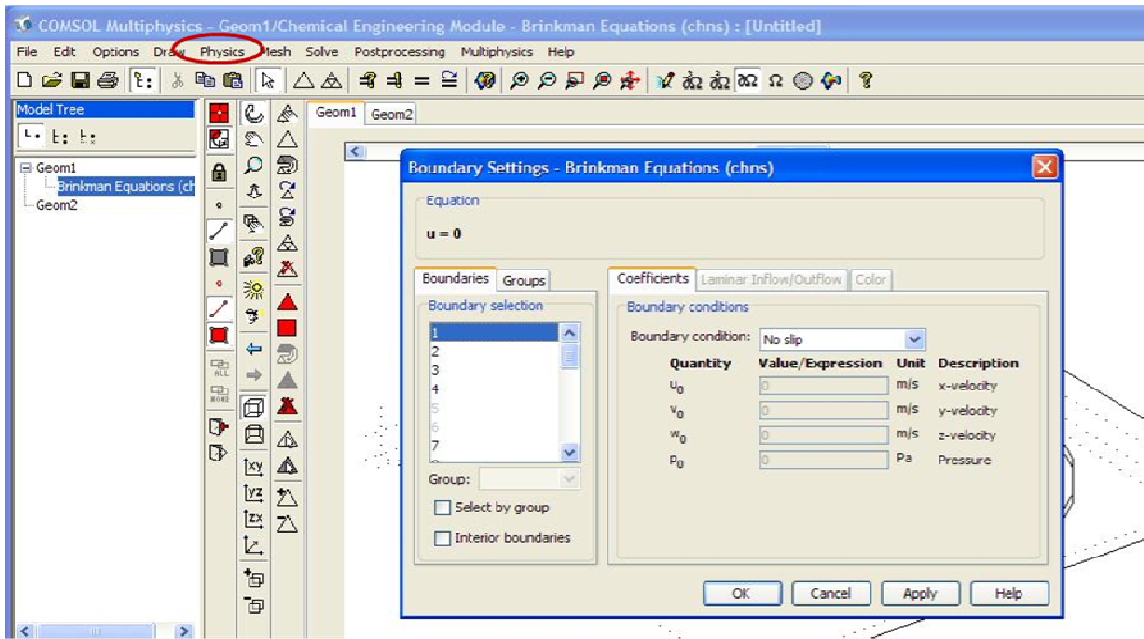
- In the **Menu bar** > Select **Physics**> Click on **Subdomain Settings**. A window will pop up



2. Select **subdomain tab**> In the **subdomain selection**> select **1**.
3. Select the **physics tab** and Input the fluid properties. For  $\rho$ : give the input as *rho*  
Similarly for  $\eta$ : give the input as *eta*. Leave the remaining as it is.
4. **Check on the flow in porous media** (brinkman equation) option.  $\epsilon_p$ : Input the value as 0.85 and  $k$  : give the input as *k*.  
Repeat the same for Subdomain selections 2 & 4.
5. For **3, 5** subdomain selections repeat step 3 and **do not check** the flow in porous media option. Click OK.

### C.1.3. Boundary Settings:

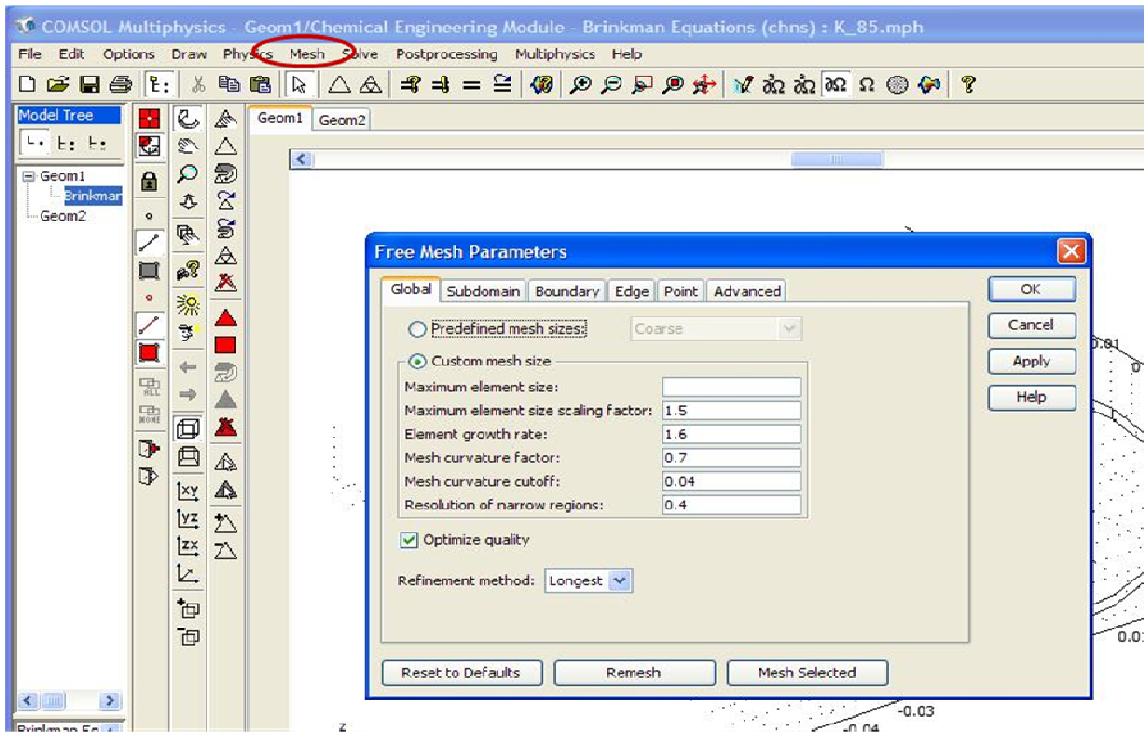
1. In the **Menu bar**> Select the **Physics tab**> Click on **Boundary settings**. A window will pop up.



2. In the **Boundaries tab** > Select **11**.(it is the inlet Boundary)
3. In the **Boundary conditions section, Boundary type**> Select **Inlet** and **Boundary condition**> Select **velocity**
4. In the **Quantity select section** > **Check mark** on the option for lower case  $u_0, v_0, w_0$ . set  $u_0, v_0$  to *zero* and set  $w_0$  as  $w_0$ .
5. In **Boundaries tab**> select **24**
6. In the **Boundary conditions section, Boundary type**> Select **Outlet** and **Boundary condition**> select **Pressure** and set Pressure  $P_0$  to *zero*.
7. Leave the rest of the Boundaries as wall and with no slip condition

#### C.1.4. Creating the Mesh:

1. In the **Menu bar** > Select **Mesh** > **Free Mesh Parameter**. A window will pop up.



2. In the **Global tab** > we can either check on the **Predefined Mesh sizes** and vary the mesh size from **coarser** to **finer** mesh size Or custom mesh size. For our purpose let us check on custom mesh size.

Enter the below values for the following:

**Maximum element size scaling factor: 1.5**

**Element growth rate: 1.6**

**Mesh curvature factor: 0.7**

**Mesh curvature cut off : 0.04**

**Resolution of narrow regions: 0.4**

Check on the optimum quality

In the **Boundary tab**> For **Boundary selections:** 1,2,5,6,12,14,16,17,18,19,25,27. In the **Boundary mesh parameter** section> set **maximum element size** to 0.001. (This is done in order to increase the number of volume elements on the edges of the reactor which is

very thin).

Click **Remesh**.

After Remeshing is done Click **Ok**.

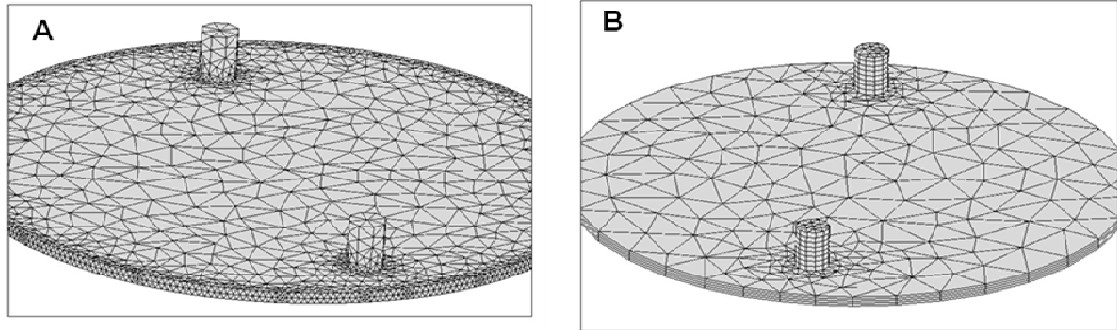


**Figure1 :** The above two figures show different kinds of meshing (A) Free meshing (B) Swept Meshing

### **C.1.5. Solving in COMSOL:**

In the **Menu bar**> select **Solve tab**> Click on **Solve**.

### **Posting Results in COMSOL:**

#### **Cross-Section Plots:**

In the **Menu bar** > Select **Post Processing** > Click on **Cross-Section Plot Parameters**.

A window will pop up.

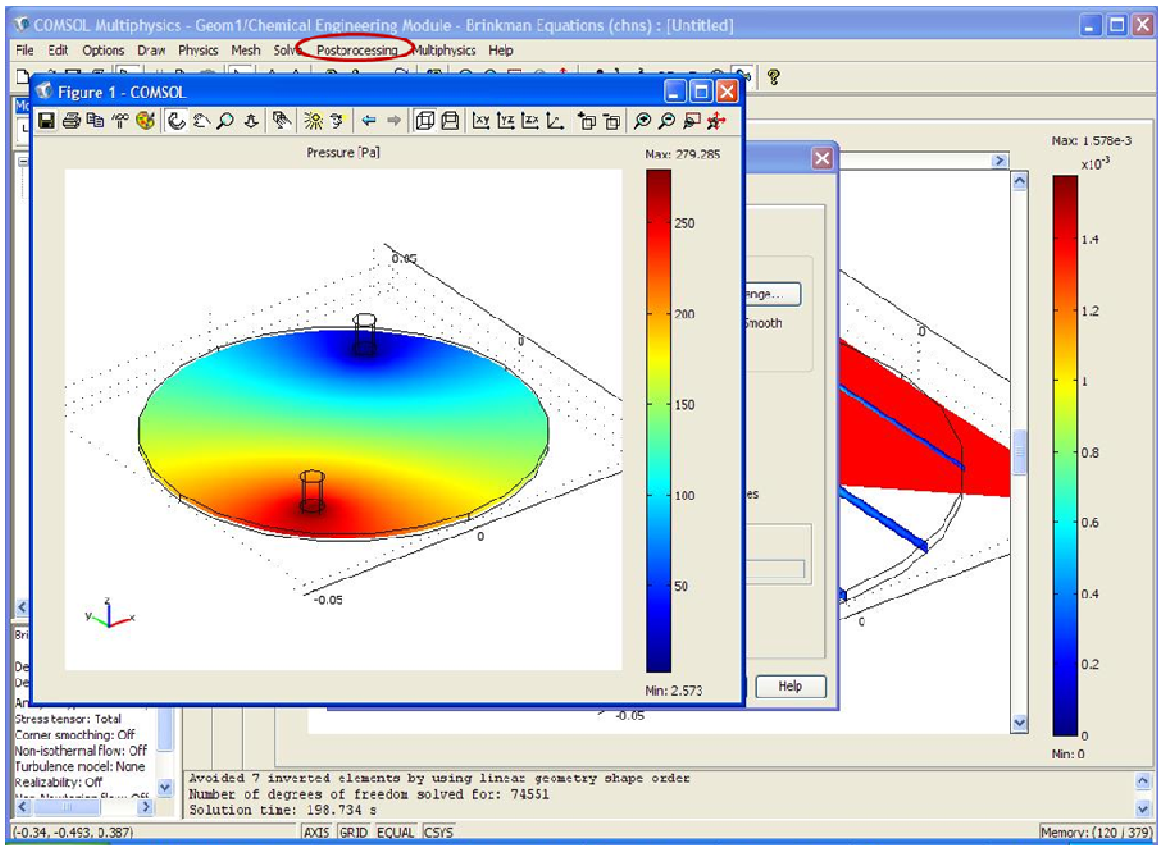
Select **slice plot tab**> **Predefined quantities:** Select **Pressure**.

In the **plane through 3 points** sections: input the three co-ordinates as ( 0.05, 0.05, 0.001); (-0.05, 0.05, 0.001) & (0.05, -0.05, 0.001) respectively.

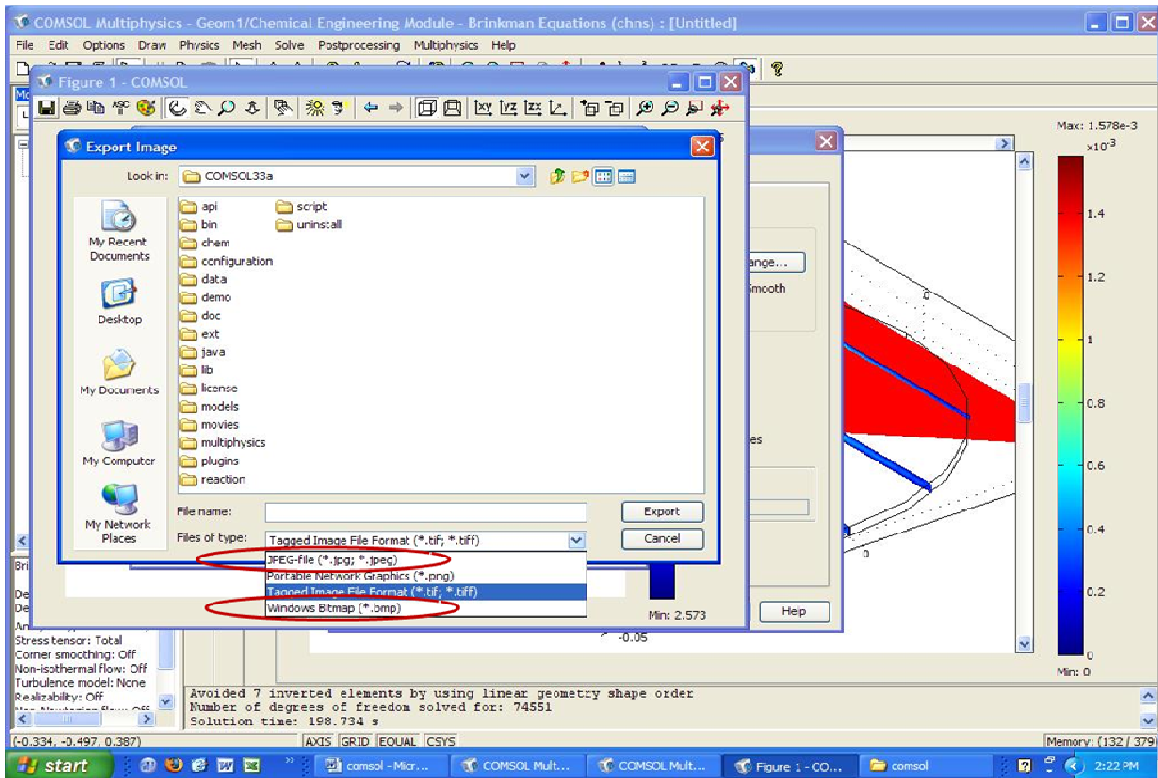
**Uncheck** the display cross – section in main axes.

Click **Apply**.

A window would pop up with pressure cross section plot.



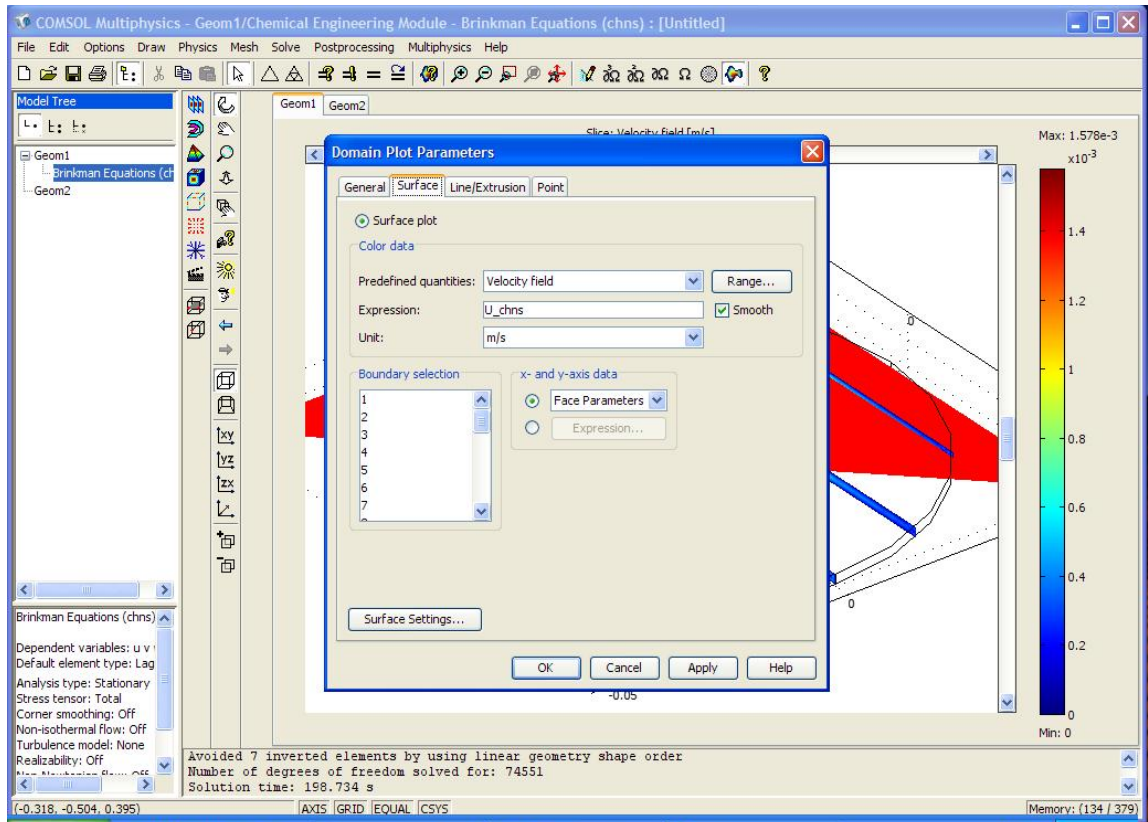
To save the plot obtained click on the **save icon** in the toolbar. A window will pop up click on **Export** > Select **file** of type as either **.jpeg** or **bmp**. Given a desired name for the file and save in the desired directory.



Similarly cross section plots can be drawn for different predefined quantities.

### Domain Plots:

**Post Processing** tab> select **Domain plot** parameters. A window will pop up.



Select **Surface tab** > In **Boundary selection**, Press **CTRL** & select the boundaries; from 1 to 7, 10, 12, 14, 16, 17, 18, 19, 20, 23, 25 & 27.

**Predefined quantities** > Select **viscous force per area, x component**. Click **Apply**.

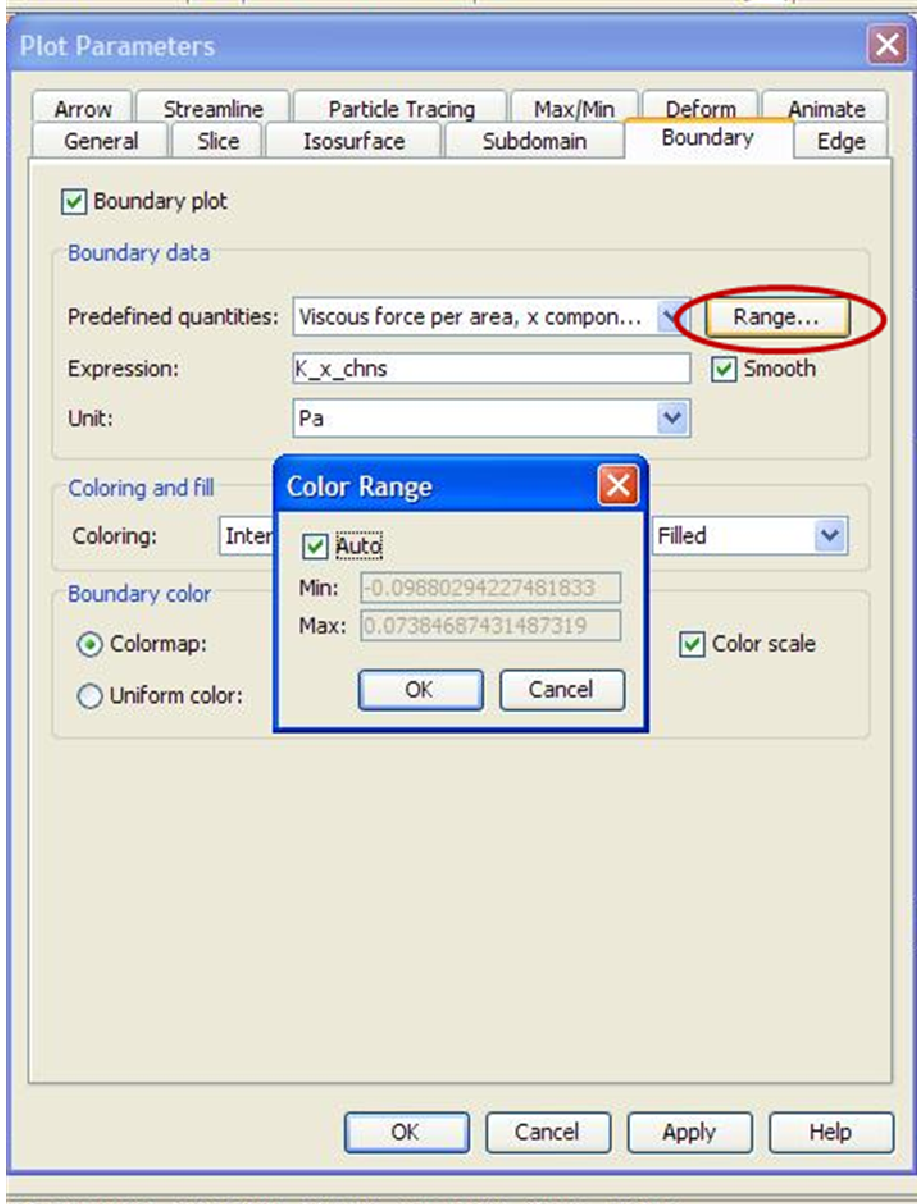
This would give us the maximum shear stress within the reactor.

To get the shear stress plots:

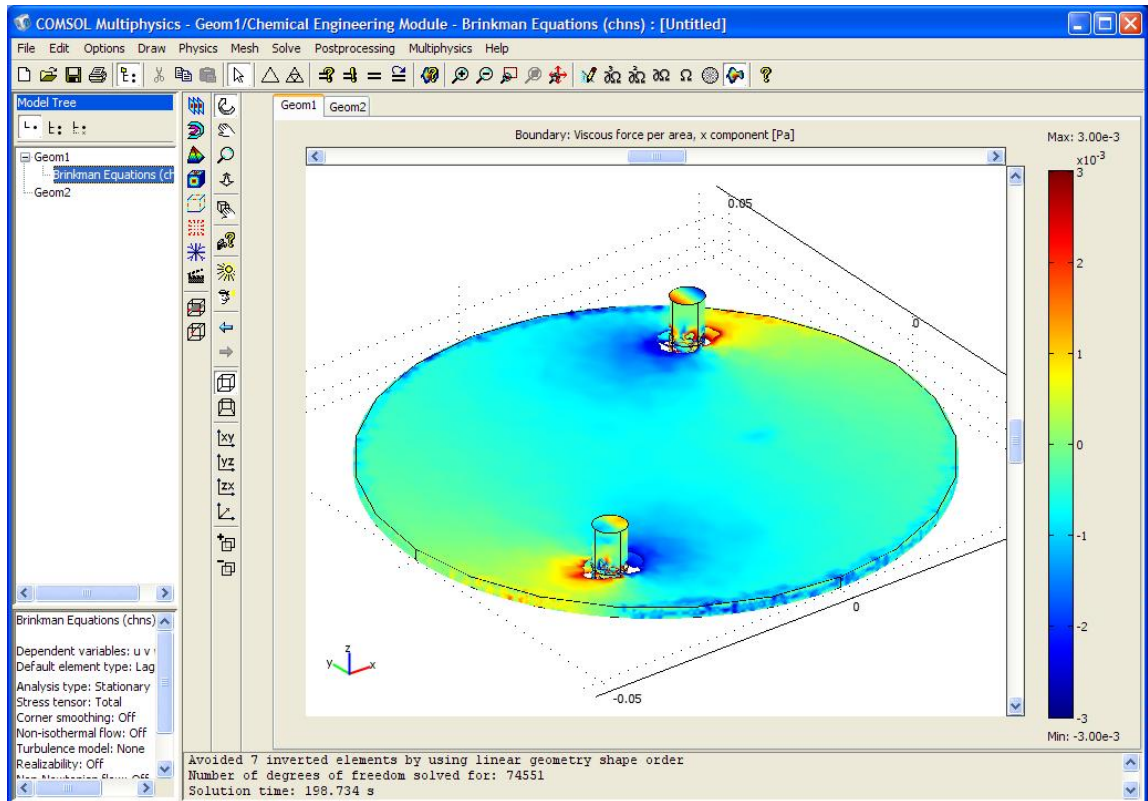
**Post Processing** > **Plot Parameters**

Select **Boundary plots tab** > Check **Boundary Plot**. (when one plot parameter is on make sure that the other plot parameters are off or unchecked).

**Predefined quantities: viscous force per area, x component**.



To change the **Range** of any parameter that is being analyzed ( say viscous force, Pressure et.al) click on the **Range** button and change the Max. and Min. values. Click **Apply**.



In the **Model View** , we can see the plot. To save the plot go to **file > Export** click on **Image**. A window will pop up . Click on **Export**. Select file type as **.jpeg** or **.bmp** give a name to the file and save in the desired directory.

## **C.2. Concentration distribution in the circular reactor with porous structure:**

### **C.2.1. Creating Geometry:**

1. If the desired geometry is already created then go to the **Multiphysics tab** in the Menu bar and Click on **Model Navigator**. A window will pop up.

- In the window that popped up. **Multiphysics tab** > Click on '+' sign beside **Fluid-Chemical Reaction Interaction** > Select **Reacting Flow**.
- **Dependent variables:** Keep the rest of the variables  $u$   $v$   $p$  as it is and Enter  $c_1$  and  $c_2$  in place of  $c$  (1, 2 specify the two species say 1- oxygen and 2- glucose in our case)
- Click on the "Add" button and then Click OK. Now u can see Brinkman , Incompressible Navier – Stokes equation and convection & diffusion under Geom1 in the Model Tree. Incompressible Navier-Stokes equation is coupled with convection and diffusion hence we need specifcy Brinkman equation again to solve the momentum balance. To delete the Brinkman equation right click on brinkman equation in the model tree and then click on Remove. The incompressible Navier-Stokes can be changed to Brinkman anytime by selecting the flow through porous media option while setting up the subdomain boundary conditions.

2. To create a new geometry:

- **Start** > **All Programs** > **COMSOL 3.4** > Click on **COMSOL Multiphysics 3.4**. Model Navigator window will pop up.
- In **Model Navigator** > Set **Space Dimension** as 3D

- **Application Modes** > Click on ‘+’ sign beside **Chemical Engineering Module**> Click on ‘+’ sign beside **Fluid Chemical Reaction Interaction** > Select “**Reacting Flow**”
- **Dependent variables** : change u v p c to u v p c1 c2 ( as said earlier 1, 2 indicated species 1 and 2 respectively). Click OK. A window will pop up.
- Draw the geometry as described from step 5 to 18 in Create Geometry at the beginning of this Manual in Momentum balance for circular reactor with porous structure section.

### C.2.2. Create a Constant list:

1. Go to **Option** tab in the Menu bar > Click on **Constants**. A window will pop up.

Enter the data given below.

Table C.2

Name	Expression
Rho	1000[kg/m <sup>3</sup> ]
Eta	0.0006915[N*s/m <sup>2</sup> ]
w0	-2.946*10 <sup>-3</sup> [m/s]
K	1.53744*10 <sup>-10</sup> [m <sup>2</sup> ]
V_g	4.862*10 <sup>-5</sup> [mol/m <sup>3</sup> s]
Km_g	0.93 [mol/m <sup>3</sup> ]
V_o	3.164*10 <sup>-5</sup> [mol/m <sup>3</sup> s]
Km_o	0.205[mol/m <sup>3</sup> ]

**Note:** These  $V_g$ ,  $Km_g$ ,  $V_o$ ,  $Km_o$  are the first order rate constants for glucose and oxygen respectively and they are derived from the data obtained in literature. This data is specifically for smooth muscle cells. The initial concentrations of glucose and oxygen used further while setting the Boundary conditions are also taken from the literature.

### **C.2.3. Setting the Boundary conditions:**

#### **C.2.3.1 Setting Boundary conditions for momentum balance:**

##### Subdomain Settings:

2. In the **Model Tree** > **Geom1**> Select **Incompressible Navier- Stokes Equation**.
3. Go to **Physics tab**> Click **subdomain settings**. A window will pop up.
4. In the **subdomain selection** section > select 1. Set  $\rho$  as 'rho' and  $\eta$  as 'eta'.
5. Check mark on **Flow in porous media** and set porosity as  $\epsilon_p$ : 0.85 and  $k$  as 'k'.
6. Repeat the same for 2 and 4.
7. In the **subdomain selection** section > select 3. and follow step 3. **Do not** check mark on Flow in porous media.
8. Click on **artificial diffusion** > Check mark on **Streamline diffusion** >select **GalerkinLeast-square(GLS)**.
9. Repeat step 6, 7 for subdomain 5.

##### Boundary Settings:

1. Go to **Physics tab** > click on **Boundary Settings**> **Boundary selection** section > select 11.
2. **Boundary conditions** section> **Boundary type**> select 'inlet' and **Boundary condition** > select 'velocity'.

3. **Quantity** > check mark on the option that shows all the three initial velocities  $u_0$ ,  $v_0$ ,  $w_0$ . Set **u** and **v** to 'zero' and set **w** to  $w_0$
4. **Boundary selection** section > select 24. Set **Boundary type**: 'outlet' and set **Boundary condition** as 'Pressure'.
5. Leave the rest of the Boundaries with wall and no slip condition.

### C.2.3.2. Setting Boundary conditions for mass balance:

#### Subdomain Settings:

1. **Model Tree** > Select **Convection and Diffusion(chcd)**
2. Go to **Physics tab** in the Menu bar > Click on **Subdomain Settings**. A window will pop up.
3. **Subdomain Selection** > Select 1.
4. Select tab **c1**> check mark on **D (isotropic)** and input the value as  $21.85 \cdot 10^{-10} \text{m}^2/\text{s}$  (this is the infinite diffusion coefficient of oxygen in water).
5. Set **R** as  $-V_o \cdot c_1 / (K_{m_o} + c_1)$  (the negative sign before indicates that it is reactant and being consumed). Now, Set the velocities **u** as  $u$ , **v** as  $v$  and **w** as  $w$  respectively.
6. Select tab **c2**> Check mark on **D (isotropic)** and input the values as  $9.55 \cdot 10^{-10} \text{m}^2/\text{s}$ .
7. Set **R** as  $-V_g \cdot c_2 / (K_{m_g} + c_2)$ . Now, set the velocities **u** as  $u$ , **v** as  $v$  and **w** as  $w$  respectively.
8. Repeat the same for subdomains 2,4.
9. **Subdomain Selection** > Select 3.
10. Repeat steps 1 to 7. and Set **R** as zero for oxygen and glucose in the c1 and c2 tabs .

Do the same for subdomain 5.

Boundary Settings:

1. Go to **Physics tab** in the Menu Bar > Click on **Boundary Settings**. A window will pop up.
2. In the **Boundaries tab**> Select 11. and then go to **c1** tab and set **Boundary conditions** as concentration and **c<sub>10</sub>** as 0.199 mol/m<sup>3</sup>. Go to **c2** tab> Set **Boundary condition** as concentration and **c<sub>20</sub>** as 5.5 mol/m<sup>3</sup>.
3. In the **Boundaries tab** > Select 24. Then Go to **c1** tab and set **Boundary condition** as convective flux. Go to **c2** tab > set **Boundary condition** as convective flux.
4. Set rest of the Boundaries as **Insulation/symmetry**.

Meshing:

1. In the Menu bar go to **Mesh** tab> select **Swept Mesh Parameter**. A window will pop up.
2. In the **subdomain selection** > select 1. Check mark on **Manual specification of element layers**. Select **Number of element layers** as 4. Set **element ratio** as 1. and **Distribution method** as linear.
3. Repeat the same for Sub domains 2 and 4.
4. In the **sub domain selection** > select 3. Set **number of element layers** as 8. Set **element ratio** as 1. and **Distribution method** as linear. Repeat the same for sub domain
5. Click on **OK**.

Use **Interactive Meshing** in the **Mesh** tab for more ways of meshing. First we

need to Mesh the **edges** and then the **Boundaries** from which we are planning to **sweep** the mesh for a particular subdomain. Click on **Free Mesh Parameter** in the **Mesh** tab and then mesh the **edges** and **Boundaries** before sweeping a mesh for a **subdomain**. To Mesh a particular subdomain /edge / boundary. First Select that particular tab in the **Free Mesh Parameter** window and then go to the **Model View** to select the particular subdomain/edge.boundary.

Setting Solver:

1. Go to **Solve** tab in the Menu bar. Click on **Solve Parameters** > A window will pop up.
2. In the **Analysis** section select Stationary. Select the **solver** as Stationary.
3. Go to **General** tab > **Linear system solver** : Direct(PARDISO).
4. Leave the rest as same. Click **OK**.
5. Select the solver according to the requirement.
6. Go to **Solve** tab > Click on **Solver Manager**. A window will pop up.
7. Select **initial value** tab> check mark on **Initial value evaluated using current solution**. In the **Values of variables not solved for and linearization point** section > Select **Stored Solution**.
8. Click on **Solve for** tab> Select **Incompressible Navier-Stokes(Chns)**
9. *Undo* Select for **Convection and Diffusion** and also *Undo* select for **Geom2(2D)**.
10. Click **Solve**.
11. After the Solver runs and solves for Navier Stokes equation. Click on **Solve** tab >**solver manager**. Select > **Initial value** tab. Click on **stored solution** button. Check

mark on **stored solution**. Select **solve for** tab > select **Convection and diffusion**. And then Click **Solve**.

**Post Processing the Results:**

1. Go to **Post Processing** tab in the Menu bar> Click on **Plot parameters**. A window will pop up. Select **Slice** tab.
2. Check mark on **Slice plot**.
3. **Predefined quantities** > select **concentration c1**.
4. set **x levels** : 0, **y levels** : 0 and **z levels** as 5.
5. Click **Ok**. To see the concentration profile of oxygen.
6. Similarly select c2 in the Predefined quantities to see the concentration profile of glucose. This gives us the concentration profile of oxygen and glucose on 5 planes in the axis parallel to the surface.

To get the concentration profile on a particular plane,

1. Go to **Post Processing** tab in the Menu bar> Select **Cross-section plot parameter**.
2. A window will pop up.
3. Click on **Slice** tab.
4. Check mark on **Slice plot**. Set the **predefined quantities** as concentration, c1.
5. In the **Plane Through 3 points section** : set the three points as follows:

**x0:** 0.05      0.05      -0.05

**y0:** 0.05      -0.05      0.05

**z0:** 0.001      0.001      0.001

Click OK.

**Post Processing** tab> Click on **Domain Plot Paramters**> Select **Viscous Force/unit area,x-component**. Click **OK**. This gives us the shear stress in the x direction. Similarly we can get the shear stress in the y direction.

Saving the Images from Post processing:

Go to **File tab**> Export > Click **Image**. Click **Export**.

Select the folder in which you want to store your document in 'Look in'. Give a file name. Click Export.

VITA

Mamatha Devarapalli

Candidate for the Degree of

Master of Science

Thesis: DESIGNING A BIOREACTOR FOR REGENERATION OF HIGH ASPECT  
RATIO TISSUES

Major Field: Chemical Engineering

Biographical:

Education:

Completed the requirements for the Master of Science in Chemical Engineering at Oklahoma State University, Stillwater, Oklahoma in December, 2008.

Completed the Bachelors in Technology in Chemical Engineering at Bhoj Reddy Engineering College for Women, affiliated to Jawaharlal Nehru Technology University, Hyderabad, Andhra Pradesh, India in May, 2006.

Professional Memberships:

Member of AIChE, 2008.

Name: Mamatha Devarapalli

Date of Degree: December, 2008\*

Institution: Oklahoma State University

Location: Stillwater, Oklahoma

Title of Study: DESIGNING A BIOREACTOR FOR REGENERATION OF HIGH ASPECT RATIO TISSUES

Pages in Study: 135

Candidate for the Degree of Master of Science

Major Field: Chemical Engineering

Scope and Method of Study:

Many tissues have a high aspect ratio (large surface area relative to the thickness of the matrix) and contain multiple cell types. Effect of flow-through configuration within these systems has not been studied. In these scale-up systems, non-ideal fluid distribution conditions could arise from two possible factors: channeling, and dead zones. This study utilized a circular parallel plate reactor that allows large tissue scaffolds. The objective of this study was to understand the flow distribution in a reactor for growing large tissues (10 cm diameter and 2 mm thick) *in vitro* and to evaluate the nutrient distribution with consumption for three different cell types (namely hepatocytes, smooth muscle cells and chondrocytes). Simulations were performed using CFD packages CFX 11 for flow distribution without porous structure and Comsol Multiphysics 3.4 for flow distribution with nutrient consumption in the porous structure. The flow distribution simulations were validated by doing residence time distribution experiments.

Findings and Conclusions:

1. The inlet and outlet locations affect the fluid distribution.
2. Presence of porous structure increased the non ideal flow patterns in the system.
3. Location of inlet and outlet over the porous region resulted in high shear stresses.
4. High shear stress regions were eliminated and better nutrient distribution was observed when the inlet and outlet were moved away from the porous region
5. Nutrients flow rate requirements for the cells to grow varied for different cell types

ADVISER'S APPROVAL: Sundararajan V. Madihally